THE UNIVERSITY
of EDINBURGH

Advanced Imaging to Detect Disease Burden, Activity and Progression in Coronary Artery Disease and Aortic Valve Disease

Dr Mhairi Katrina Doris

MBChB (Hons) MRCP

THE UNIVERSITY *of* EDINBURGH

A Thesis Presented for the Degree of Doctor of Philosophy

The University of Edinburgh

2020

To Mark

CONTENTS

INDEX OF TABLES

INDEX OF FIGURES

Declaration

This thesis represents research I performed at the Clinical Research Facility at the Queens Medical Research Institute, Little France Campus, the Royal Infirmary of Edinburgh, and the Department of Medicine and Clinical Imaging, Cedars Sinai Medical Center, Los Angeles, California between August 2015 and August 2019.

Research conducted in this thesis was supported by the British Heart Foundation (FS/17/79/33226) and a Cardiac Imaging Research Initiative grant from the Adelson Medical Research Foundation. The DIAMOND study was funded by a Wellcome Trust Senior Investigator Award (WT103782AIA) and an unrestricted educational grant from AstraZeneca. AstraZeneca was not involved with study design or analysis. The SALTIRE 2 study was funded by the British Heart Foundation (FS/14/78/31020).

I was directly involved in all aspects of work described in this thesis. I was Principal Investigator for the SALTIRE 2 study between October 2017-August 2019 and was primarily responsible for study conduct. I acted as co-investigator for the DIAMOND study. In keeping with the nature of collaborative research, imaging data from the Ring of Fire study described in chapter 6 was provided by Dr William Jenkins and Professor Marc Dweck. With regards to the data utilised for the remaining chapters in this thesis, I was directly involved in the concept, design, data analysis and interpretation for all studies described.

Chapters 3, 5, 6 and 7 have been published in peer-reviewed journals and, at the time of submission, chapter 4 has been accepted for publication and is currently in press.

This thesis has not been accepted in any previous applications for a degree and all sources of information have been acknowledged. The research was undertaken in accordance with the Declaration of Helsinki and the regulations of the South East Scotland Research Ethics Committee.

Mhairi Katrina Doris 5th April 2021

Abstract

Introduction

Coronary artery disease and aortic stenosis represent two important manifestations of cardiovascular disease, a dominant cause of morbidity and mortality in the UK and worldwide. In recent years, advances in modern imaging techniques have transformed our understanding of the pathophysiology of these underlying disease states, enabling the detailed characterisation of disease processes and the identification of a large number of potential therapeutic targets. To address the increasing burden of cardiovascular disease, improved identification of patients at risk of disease progression and future events is crucial. Application of advanced non-invasive imaging will be instrumental in achieving this goal and could enable improved targeting of existing or novel therapies directed against these disease processes.

The objective of this thesis was to investigate the ability of novel advanced non-invasive imaging to quantify disease burden, to measure disease activity and to assess disease progression in both coronary artery disease and aortic valve disease.

Methods and Results

The Association between Non-invasive Fractional Flow Reserve and Plaque Burden in Non-obstructive Atherosclerosis

The association between nonobstructive atherosclerosis and non-invasive fractional flow reserve derived from computed tomography (FFRCT) measured in distal coronary vessels was investigated in 155 patients undergoing computed tomography coronary angiography with greater than 25% coronary stenosis in at least one epicardial vessel. Plaque analysis was performed on all vessels with between 25-70% stenosis using dedicated software (Autoplaque, Cedars Sinai Medical Center, Los Angeles, USA). Multiple plaque components including calcified plaque (CP) volume, non-calcified plaque (NCP) volume, low density plaque (LD-NCP) volume, remodelling index (RI) and contrast density difference (CDD) were quantified. An abnormal distal vessel FFRCT (V-FFRCT) was defined as ≤0.75. Total plaque volume, calcified plaque volume, noncalcified plaque volume and low-density plaque volume were higher in vessels with an abnormal V-FFRCT compared to those with a normal V-FFRCT ($p<0.05$ for all). After adjusting for percent diameter stenosis and contrast density difference, all measures of plaque volume were independent predictors of an abnormal V-FFRCT (OR 2.09, 1.36, 1.95, 1.95 for TP, CP, NCP and LD-NCP volume, respectively; $p<0.05$ for all).

^{18}F-Fluoride Positron Emission Tomography and Progression of Coronary Calcification

In a pre-specified sub-study of a randomised controlled trial, the relationship between ^{18}F-fluoride PET activity and the progression of coronary calcification was investigated in patients with clinically stable, multivessel coronary artery disease. In 183 participants, increased ^{18}F-fluoride activity (defined as a TBRmax >1.25) correlated with change in calcium score at one year (Spearman's Rho 0.37, p<0.0001). Participants with evidence of increased ^{18}F-fluoride uptake at baseline demonstrated more rapid progression of coronary calcification at one year (change in calcium score, 97 [39-166] versus 35 [7-93] AU; p<0.0001). When individual coronary segments with increased ^{18}F-fluoride activity were compared to negative reference plaques in the same participant, segments with increased ^{18}F-fluoride uptake demonstrated progressive calcification at one year (from 95 [30-209] AU to 148 [61-289] AU; p<0.001) whereas there was no change in calcium score for reference segments (from 46 [16-113] to 49 [20-115] AU; p=0.329).

Image Optimisation and Motion Correction of Coronary PET-CT

The effect of different PET reconstruction algorithms and application of cardiac motion correction upon coronary ^{18}F-fluoride PET activity was assessed in a cohort of patients with a recent diagnosis of Acute Coronary Syndrome (n=22). Image quality was assessed using Signal-to-Noise Ratio (SNR). An optimal balance between signal intensity and noise was achieved using 24 subsets, 4 iterations, point-spread-function modelling, time of flight and 5-mm post-filtering which provided the highest median SNR. A novel cardiac motion correction method led to improved SNR of culprit

plaques (24.5[19.9-31.5]) when compared to the standard method of using PET data from the diastolic cardiac phase only (15.7[12.4-18.1]; p<0.001). Further, motion-correction led to a greater SNR difference between culprit and reference lesions (10.9 [6.3-12.6]) compared to diastolic (6.2 [3.6-10.3] p=0.001) and summed data (7.1 [4.8-11.6] p=0.001).

CT-AVC and Echocardiography in the Progression of Aortic Stenosis

In a study of participants with aortic stenosis, the reproducibility of CT calcium scoring of the aortic valve as well as its ability to detect changes in disease severity over time was assessed and compared with echocardiography, the current gold standard imaging technique in aortic stenosis. In a group of 15 participants who underwent repeat CT scanning within four weeks, quantification of aortic valve calcification by CT (CT-AVC) was reproducible (limits of agreement -12 to 10%, ICC 0.99). Peak aortic jet velocity was the most reproducible measure of aortic stenosis severity on echocardiography (limits of agreement -7 to 17%; ICC 0.96). In a second cohort of patients, progression of calcification on CT and haemodynamic progression by echocardiography was assessed and a ratio of annualised disease progression and measurement variability was generated and used to estimate numbers of patients required to detect annualised changes in disease severity on both modalities. CT-AVC demonstrated a favourable progression-to-variability ratio (Cohen's d statistic 3.12) versus echocardiography (Cohen's d statistic for peak velocity 0.71), suggesting fewer patients would be required to detect changes in disease progression.

Cardiac Motion Correction applied to PET-CT and PET-MR of the Aortic Valve

The application of cardiac motion correction was investigated in a group of participants with aortic stenosis undergoing ^{18}F-fluoride PET-CT (n=5) and PET-MR (n=1). When compared to the standard method of utilising PET data acquired during the diastolic phase only, the application of cardiac motion correction improved signal to noise ratio (48.8 vs 21.2; $p<0.05$) and tissue to background ratio (3.1 vs 2.5 $p<0.05$).

Conclusions

The application of advanced non-invasive imaging techniques can provide novel measures of disease burden, activity and progression in both coronary atherosclerosis and aortic stenosis.

Lay Summary

Within this thesis, I investigate new techniques to use scanning technology to help improve the identification of the burden, activity and progression of two leading causes of cardiovascular disease: coronary artery disease and aortic stenosis.

In this thesis, I firstly investigated the role of advanced imaging methods which can be applied to computed tomography of the heart. Computed tomography coronary angiography can provide detailed images of the blood vessels supplying blood to the heart. This enables visualisation of the artery walls and identification of different components of atherosclerosis including calcium and lipid deposits. Specialised imaging software can allow detailed measurements of the volume and composition of atherosclerotic plaques. Fractional flow reserve is used as a measure of how blocked an artery has become and provides a guide as to whether areas of narrowing in blood vessels cause reduced blood flow to the heart muscle. This is traditionally measured during an invasive angiogram, but recent technology has enabled this to be measured directly from computed tomography scans. In this thesis, I investigated whether non-invasive fractional flow reserve from Computed Tomography (FFRCT) was related to the volume and composition of atherosclerosis in blood vessels without a clear or significant narrowing. I found that diffuse atherosclerosis in blood vessels could cause an abnormal FFRCT, suggesting this may provide a measure of plaque burden and composition.

Positron Emission Tomography (PET) is a scanning technique which can measure the activity of specific disease processes following injection of targeted radioactive molecules into the body. In a study of patients with heart disease, I investigated the use of a radioactive molecule (^{18}F-sodium fluoride) which binds to areas of developing calcium within the body. In this thesis, I have found that this molecule can identify areas of activity within the walls of blood vessels in the heart which predict progression of calcium formation within one year. This may enable us to detect patients who are more at risk of disease progression and may benefit from more aggressive treatment. This may also be of value in studies investigating the role of new treatments for heart disease.

As a scanning technique, PET has a number of challenges when imaging the heart. One major challenge is motion caused by the beating of the heart during the duration of the scan, as well as movement of the lungs during each breathing cycle. This makes it difficult to localise precisely areas of activity and can lead to areas of interest becoming blurred or noisy. In this thesis, I investigated how different methods of post-processing PET images leads to variations in signal intensity and image noise and how to optimise this for imaging the heart. I also applied a motion correction technique to PET images which aimed to counteract the effects of motion caused by movement of the heart during the scan. This led to an improvement in signal intensity and reduction in image noise in both the coronary arteries and the aortic valve. These results will be useful for future studies using this scanning technology to image the heart.

Finally, I investigated the role of computed tomography in aortic stenosis. Computed tomography scanning provides the ability to quantify calcium in the aortic valve,

providing a measure of the severity of aortic stenosis. I found that this scanning technique is reproducible and is able to detect small changes in calcium load over time. The repeatability of CT calcium scoring combined with its ability to detect small increases in disease severity over time means that this imaging technique could potentially identify patients in whom aortic stenosis is progressing rapidly and, by detecting early markers of change, may also be useful in research studies investigating the role of new treatments for this condition.

In summary, the advanced imaging techniques studied in this thesis provide a means of exploring different features of coronary artery disease and aortic stenosis. This will not only help to improve our understanding of these important disease processes but has the potential to change the way in which we assess an individual patient's risk of disease progression in the future. Further studies are now needed to investigate the direct impact of these findings on patient outcomes and the role of novel treatments for these conditions.

Acknowledgements

This research was conducted under the supervision of Professor David Newby and Professor Marc Dweck at the University of Edinburgh. Throughout my PhD programme, both Professor Newby and Professor Dweck have provided invaluable advice and support, without which this thesis would not have been possible. I am incredibly grateful to have had the privilege to work with them and for the encouragement and opportunities they have provided.

During my PhD studies, I had the unique opportunity to spend a year in Los Angeles, California, working within the Cardiac Imaging Research Team at Cedars Sinai Medical Center under the supervision of Dr Daniel Berman, Dr Piotr Slomka and Dr Damini Dey. This was an exciting opportunity to work within an international collaboration and gain skills in advanced non-invasive imaging. I am extremely grateful to the team at Cedars Sinai Medical Center for their support.

I would like to thank the British Heart Foundation for supporting my research. I would also like to express thanks to the staff at the Clinical Research Imaging Centre, Edinburgh Clinical Trials Unit and the Wellcome Trust Clinical Research Facility within the Royal Infirmary of Edinburgh. I am especially grateful to Audrey White for her dedication and commitment in performing all the research echocardiograms for a number of studies included in this thesis and to Hayley Cuthbert for her tireless assistance with the SALTIRE2 study.

During the time spent working on this thesis, I have been extremely fortunate to share my research experience with a number of colleagues who have ultimately become close friends. I am particularly grateful to them for providing inspiration, friendship and great company during my days in the ‘Barn’.

Finally, I would like to thank my family. My parents who have always provided advice and guidance at every stage of my studies and career and my sister who has been a great source of support. My husband, Mark, who has not only provided guidance and encouragement throughout my studies but agreed to embark upon a temporary relocation to Los Angeles. Your unwavering support, patience and unique ability to make me laugh even during moments of stress have been instrumental in this achievement. I dedicate this thesis to you and look forward to our exciting next chapter.

Abbreviations

ACS	Acute Coronary Syndrome
AS	Aortic Stenosis
AU	Agatston Units
AVA	Aortic Valve Area
CMR	Cardiac Magnetic Resonance
CT	Computed Tomography
CT-AVC	Computed Tomography Aortic Valve Calcification
CTCA	Computed Tomography Coronary Angiography
DI	Dimensionless Index
DSE	Dobutamine Stress Echocardiography
ECG	Electrocardiogram
ECV	Extracellular volume
EF	Ejection Fraction
ESC	European Society of Cardiology
FFR	Fractional Flow Reserve
HU	Hounsfield Units
LV	Left Ventricle
LVOT	Left Ventricular Outflow Tract
MBq	Megabecquerel
PET	Positron Emission Tomography
SNR	Signal to Noise Ratio

SUV	Standardised Uptake Value
TBR	Tissue-to-background ratio
VIC	Valve Interstitial Cell

CHAPTER 1

Introduction

Including adaptations and extracts from;

Doris MK, Newby DE. Identification of early vascular calcification with 18Fsodium fluoride: potential clinical application. Expert Rev Cardiovasc Ther. 2016;14(6):691-701.

Doris MK, Newby DE. Coronary CT Angiography as a Diagnostic and Prognostic Tool: Perspectives from the SCOT-HEART Trial. Curr Cardiol Rep. 2016; 18: 18

Doris MK, Everett RJ, Shun-Shin M, Clavel MA, Dweck MR. The role of imaging in measuring disease progression and assessing novel therapies in aortic stenosis. JACC Cardiovasc Imaging. 2019;12(1):185-197.

Chapter 1 Introduction

1.1 OVERVIEW

Recent years have witnessed innovative advances in the diagnosis and management of cardiovascular disease. Despite this, predicting and anticipating events at an individual patient level remains challenging and this precludes individualised tailoring of treatment. As a consequence, cardiovascular disease remains a leading cause of death in the United Kingdom and worldwide. Technological advances in non-invasive imaging modalities have precipitated an increasing drive to utilise technology to provide a safe and efficient means of exploring the underlying disease mechanisms responsible for progression of cardiovascular disease and ultimately adverse clinical outcomes. Interest has also focused on how we may utilise technology to assess the effect of novel therapies on the progression of cardiovascular disease.

This thesis aims to investigate the role of advanced non-invasive imaging strategies in providing measures of and improving our understanding of disease burden, activity and progression in coronary atherosclerosis and aortic stenosis, two distinct leading manifestations of cardiovascular disease.

1.2 CORONARY ATHEROSCLEROSIS

1.2.1 THE VULNERABLE PLAQUE

The majority of acute ischaemic vascular events are precipitated by rupture of a vulnerable atherosclerotic plaque. In this population, events are often unheralded and occur without preceding symptoms. Our understanding of specific characteristics of

the vulnerable atherosclerotic plaque has been enhanced by retrospective pathological studies which have identified common phenotypic features of the atherosclerotic plaque most prone to rupture and trigger thrombotic events. These characteristics comprise the 'thin-cap fibroatheroma' and include a thin fibrous cap, large plaque volume, necrotic core, positive remodelling, intraplaque haemorrhage and spotty calcification. (1-4) Pathological and imaging studies have highlighted that such vulnerable lesions often do not cause significant luminal obstruction. (2) The degree of calcification of vulnerable lesions is variable, with over half exhibiting spotty or no visible calcification, and only a minority demonstrating diffuse calcification. (2) Such high-risk plaques often do not occur in isolation, and patients at greatest risk of future events often exhibit multiple high-risk lesions. (5)

Longitudinal imaging studies have demonstrated that plaque morphology may evolve over time and that high-risk plaques may heal to form more stable thick cap fibroatheroma or fibrotic plaques, possibly after periods of subclinical rupture and plaque expansion. (6, 7) Patients with chronic stable disease often exhibit symptoms as a consequence of luminal obstruction and more extensive calcification is often a feature of advanced, stable atherosclerosis. (8)

1.2.2 CALCIFICATION

Whilst historically considered a passive and degenerative pathology, vascular calcification is now recognised as a complex, dynamic and tightly regulated process that bears many similarities to skeletal bone formation. The incidence of vascular calcification rises with age, observed in up to 50% of individuals aged 40-49 (9) and over 80% of individuals over the age of 70, its presence often reflecting advanced

atherosclerosis. (10) In two-thirds of asymptomatic men and women over the age of 70, extensive calcification is found throughout multiple vascular beds. (10) However, its progression may also be accelerated in metabolic disorders including diabetes mellitus, hypercholesterolaemia and chronic renal disease. (11, 12)

Within the coronary arteries, intimal calcification is pathognomonic of atherosclerosis. The extent of coronary calcification correlates closely with atherosclerotic plaque burden and can be used as a reliable surrogate marker of coronary heart disease. (13) In patients aged 30-39 with symptomatic coronary artery disease, coronary calcification is observed in 70%. (1) Whilst the absence of visible calcification does not exclude the presence of atherosclerosis (13), individuals without coronary calcification have a low cardiovascular mortality. Conversely, the extent and severity of calcification are associated with an increased risk of adverse cardiovascular events. (14, 15)

In atherosclerosis, the initiation of vascular mineralisation is closely associated with progressive inflammation, cell death and necrosis. We hypothesise that this process may be initiated in an attempt to wall off the necrotic core, subdue inflammation, and shield the hypoxic inflamed plaque from circulating pro-inflammatory and thrombogenic mediators. A similar healing response can be observed in other conditions associated with focal, necrotic inflammation. For example, in response to the caseating granuloma in primary pulmonary tuberculosis, the body acts to contain this inflammation within the calcified Ghon focus. Similarly, in certain parasitic infections and foreign body inclusions, calcification is initiated to encapsulate these focal areas of intense inflammation.

The earliest form of mineralisation that may be identified within the vasculature exists in the form of calcified microvesicles containing hydroxyapatite: the most abundant mineralised form of calcium phosphate found in both bone and the vasculature. Hydroxyapatite initially forms as nanoparticles that exist as long crystalline structures. As these nucleate and propagate, microvesicles coalesce to form organised macrocalcific deposits. As mineralisation progresses further, large granules and organised plates of calcium form, and calcification within the vasculature adopts a form akin to lamellar bone. (16) Once initiated, vascular calcification can progress quickly, aided by the downregulation of inhibitors of mineralisation. (17, 18)

When this advanced stage is reached, the barrier between the thrombogenic plaque core and circulating blood has successfully formed. In atherosclerosis, this translates into an increase in stability of the plaque and is reflected by a lower risk of rupture and thrombosis. (2)

1.2.2.1 Microcalcification

In contrast to the stability possibly imparted by extensive calcification, the earliest stages of microcalcification are associated with intense inflammation and plaque vulnerability. The majority of ruptured plaques exhibit evidence of spotty microcalcific deposits, leading to the appreciation of microcalcification as a key pathological feature of the vulnerable plaque. (2, 4)

The association between the early stages of calcification and plaque vulnerability may be a consequence of the ongoing intense inflammation and necrosis within the plaque, before the process of calcification has succeeded in its role of shielding the necrotic core from the vascular lumen. During its initial stages, microcalcification has been

postulated to play an active role in inflammation by inducing further vascular smooth muscle cell death and release of pro-inflammatory mediators. (19)

Additionally, it has been hypothesized that early calcification may be directly implicated in plaque rupture due to its influence on mechanical stress within the intima. An abundance of high-density microvesicles containing hydroxyapatite scattered amongst the low-density lipid contents of the necrotic core may precipitate plaque rupture by increasing shear stress. (20) If calcified vesicles migrate to the thinned fibrous cap, increased mechanical stress within this vulnerable region may predispose to acute microfractures, rupture and subsequent thrombosis. (21) A recent study by Hutcheson, et al, documented an inverse relationship between collagen content and size of microcalcifications in atherosclerotic plaques, suggesting a relationship between fibrous cap degradation and microcalcification. (22)

Irrespective of the mechanism, it is evident that early microcalcification coincides with active, inflamed, vulnerable atherosclerosis. Histologically, early calcific deposits colocalize with macrophage burden, and matrix vesicles responsible for initiating mineralisation or generating microcalcification may be derived from macrophages. (17, 18, 23-25) In contrast, extensive calcification may reflect advanced, less inflamed and stable disease in which dense, organised calcium has effectively formed a barrier between the thrombogenic plaque core and circulating blood. (2, 4, 17, 26) Histological evidence has elucidated that advanced calcification is remote from areas of inflammation and macrophage accumulation (17), supporting the hypothesis that this process may indeed subdue inflammation.

1.3 IMAGING CORONARY ATHEROSCLEROSIS

Traditional diagnostic approaches have focused on identifying the presence and degree of coronary artery stenosis and downstream ischaemia. However, evidence has continued to emerge that the overall burden of disease and plaque characteristics in coronary atherosclerosis have prognostic significance. Indeed, the majority of acute coronary events are caused at arterial sites with nonobstructive disease on antecedent coronary angiography. (27) Further, it is increasingly understood that patients with evidence of high-risk plaque features or plaque progression are at risk of future events irrespective of the degree of coronary stenosis. (28, 29) For these reasons, multimodality imaging has recently focused on identifying features of the vulnerable plaque which provide targets for the researcher and clinician to develop a greater understanding of disease burden, characteristics and biological disease activity to improve risk stratification in patients with coronary artery disease. (Figure 1.1)

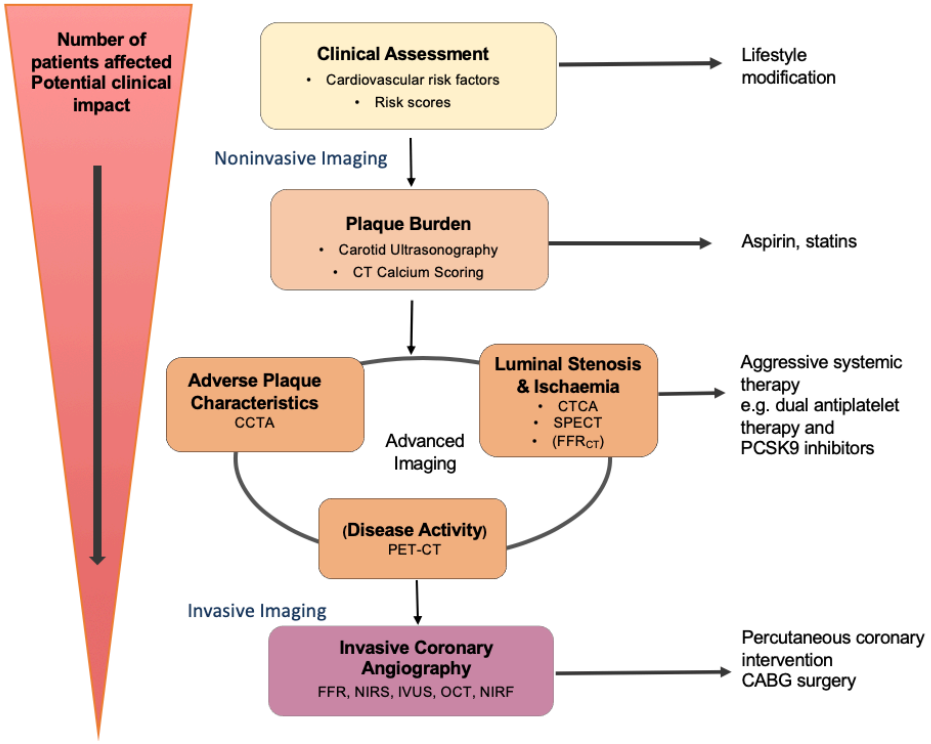

Figure 1.1 Possible approach using multi-modality imaging to stratify risk in patients with atherosclerosis.

Advances in imaging technology now allow multiple different atherosclerotic features to be assessed using both invasive and non-invasive technology. The challenge is to use these advances to improve patient risk stratification, to guide clinical management and ultimately to reduce adverse cardiovascular events. A possible future approach to patient assessment and risk stratification is presented. Initial screening with risk factor assessment and simple strategies to measure plaque burden may be used in large populations, guide lifestyle interventions and the prescription of aspirin and statins. In those with advanced plaque burden more advanced imaging using assessments of luminal stenosis, myocardial ischemia and plaque characteristics can then be used to identify those at the highest risk of future events. Combined information is likely to provide complementary results. These vulnerable patients could then be targeted with powerful yet expensive systemic therapies that are emerging (e.g. PCS-K9 inhibitors) or dual antiplatelet therapy where the potential for bleeding may be outweighed by the high cardiovascular risk. As further data emerges, the use of hybrid imaging (e.g. PET/CT) may further refine advanced non-invasive risk stratification, differentiating patients with active disease versus those with burnt out stable atheroma. Finally, in those patients being considered for revascularisation, advanced invasive imaging including FFR and other emerging approaches can be used to optimise decisions regarding percutaneous intervention (PCI) or coronary artery bypass grafting (CABG). (*Adapted from Dweck MR and Doris MK et al, Nat Rev Cardiol 2016;13(9):533-48*) (30)

1.3.1 CORONARY ARTERY CALCIUM SCORING

The quantification of coronary artery calcification on non-contrast CT provides a surrogate marker of total plaque burden. This is routinely performed using the Agatston method which applies a factor relating to maximum plaque attenuation and multiples this by the calcium area to generate a weighted sum of lesions with attenuation greater than 130 Hounsfield Units (HU). (31) The coronary calcium score, expressed in Agatston Units (AU) has demonstrated prognostic significance, with a greater burden of coronary calcification associated with adverse prognosis beyond conventional risk factors. (32, 33) Beyond the total plaque burden, additional measures including the distribution of coronary calcium, number of plaques and plaque density have been shown to add to total Agatston score in the assessment of prognosis. (34) Further, progression of calcium score on CT predicts adverse prognosis independent of the baseline calcium score. (14) The relatively low cost, availability and ease of imaging protocols without need for contrast make coronary artery calcium scanning an attractive non-invasive imaging modality for imaging coronary atherosclerosis. Modern imaging protocols now enable CT calcium scoring to be performed with a low radiation exposure (1-3 mSv). (35)

1.3.2 COMPUTED TOMOGRAPHY CORONARY ANGIOGRAPHY

Computed Tomography Coronary Angiography (CTCA) has demonstrated accuracy in identifying the presence, extent and severity of coronary artery disease compared with invasive angiography. (36, 37) The SCOTHEART study investigated the benefit of CTCA in clarifying the diagnosis of angina secondary to coronary heart disease and demonstrated that, in patients with recent onset stable chest pain, CTCA clarified the

diagnosis of angina secondary to coronary heart disease, improving diagnostic certainty in one in four patients. (38) This in turn led to positive treatment decisions whereby the identification of obstructive and nonobstructive disease guided changes to management and the initiation or cessation of preventative therapies where indicated. Subsequent follow-up analyses have demonstrated that the use of CTCA in addition to standard care reduced the risk of death from coronary heart disease or non-fatal MI at 5 years, with no difference in overall rate of invasive angiography or revascularisation. (39)

In addition to identifying the presence of obstructive or nonobstructive atherosclerosis, CTCA also provides the opportunity to directly visualise the arterial wall, highlighting plaque composition and identifying adverse features such as necrotic core, positive remodelling and spotty calcification. The presence of high-risk plaque features on CTCA, particularly if identified in combination, is associated with an increased risk of future adverse cardiac events. (28, 40, 41)

1.3.2.1 Automatic plaque quantification

While the identification of adverse plaque features on CTCA has demonstrated prognostic significance, this process is subjective, may be time-consuming and has demonstrated only fair agreement between observers. (42) The development of semi-automated software capable of identifying and quantifying the burden of high-risk plaque features on CTCA both reduces the time taken for analysis and improves reproducibility. (43, 44) Semi-automated software has demonstrated accurate quantification of noncalcified plaque when compared with intravascular ultrasound. (45) In a post-hoc analysis of the SCOTHEART study, low attenuation plaque burden

was the strongest predictor of future fatal or nonfatal myocardial infarction irrespective of cardiovascular risk score, coronary calcium score and area stenosis. (29) Patients with a low attenuation plaque burden greater than 4% were 5 times more likely to suffer a fatal or nonfatal myocardial infarction at five years. (29)

1.3.3 Fractional flow reserve derived from CT angiography (FFRCT)

In addition to the detection of high-risk plaque features on CTCA, the evolution of approaches to combine this anatomical information with physiological measures of coronary blood flow and perfusion hold promise for the future of CTCA. Recent developments in the calculation of fractional flow reserve noninvasively (FFRCT) have been highlighted in three large multicentre studies (NXT, DISCOVER-FLOW and DeFACTO) which have compared the accuracy of FFRCT with invasive FFR measurements. (46-48) A meta-analysis of the DeFACTO, NXT and DISCOVER-FLOW trials concluded that FFRCT has a pooled sensitivity similar to CTCA (0.89 versus 0.89 at per-patient analysis; 0.83 versus 0.86 at per-vessel analysis) but improves specificity in both a per-vessel and per-patient analysis (0.71 versus 0.35 at per-patient analysis; 0.78 versus 0.56 at per-vessel analysis). (49) The high negative predictive value of FFRCT has raised promise for its potential to exclude ischaemia caused by intermediate grade lesions, potentially avoiding unnecessary invasive angiography. (50) Recently, the Prospective LongitudinAl Trial of FFRCT: Outcome and Resource Impacts (PLATFORM) study has investigated the clinical use of FFRCT and the results revealed that CTCA with FFRCT did in fact lead to a marked reduction in the frequency of invasive angiography showing no obstructive coronary artery

disease. (51) This was a non-randomised study and there was no comparison with CTCA alone, and further study is therefore warranted.

1.3.4 POSITRON EMISSION TOMOGRAPHY

Positron emission tomography (PET) utilises radiolabelled tracers targeting specific molecular processes within tissues and the vasculature. Combined with anatomical information gained from computed tomography, hybrid PET-CT imaging provides a unique opportunity to identify active biological processes non-invasively. Tracers targeting many key pathological processes in cardiovascular disease have been developed, some already well established. (Table 1.1) Currently the most widely available and utilised tracer is ^{18}F-fluorodeoxyglucose (^{18}F-FDG), a glucose analogue which becomes trapped within metabolically active cells. The increased metabolic activity of macrophages compared to surrounding tissues has enabled its use as a marker of inflammation. Given its close association with inflammation, early microcalcification also serves as a suitable imaging target for the identification of high-risk vascular disease. The detection of microcalcification within the vasculature may serve as a surrogate marker for dynamic, progressive atherosclerosis and plaque vulnerability.

Table 1.1 Applications of ^{18}F-fluorodeoxyglucose and ^{18}F-sodium fluoride in cardiovascular disease.

	^{18}F-Fluorodeoxyglucose	**^{18}F-Sodium Fluoride**
Target Process	Inflammation	Microcalcification
Cellular/Molecular Target	Macrophages	Hydroxyapatite
Specificity	Poor	High
Clinical Application		
1. Atherosclerosis of Large Vessels	Increased uptake in large arteries (TBR ≥1.7) is a strong predictor of subsequent vascular events. (52)	At least one site of increased uptake observed in all patients with prior CV events. (53)
2. Coronary Artery Disease	Increased uptake in culprit plaque in 33% of patients following MI. One half of vessel territories unable to be interpreted due to myocardial uptake. TBRmax of culprit plaques 1.71 and non-culprit plaques 1.58 (p=0.34). (54, 55)	Increased uptake in culprit vessel in 93% of patients following MI. Focal uptake in 45% of patients with stable CAD. TBRmax of culprit plaques 1·66 and non-culprit plaques 1·24 (p<0·0001). (55)
3. Carotid Disease	Uptake 27% higher in symptomatic vs asymptomatic plaques. (56)	Uptake correlated with CV risk factors. (57) Increased uptake in culprit vs contralateral plaques. (58)
4. Aortic Stenosis	Increased TBR in 35% of patients with aortic stenosis (TBR>1.63). Modest rise in max TBR with severity (r=0.47, P<0.001). (59, 60)	Increased uptake in 91% of patients with aortic stenosis (TBR>1.97). Progressive rise in max TBR with severity (r=0.73, P<0.001). Uptake predicts disease progression. (60, 61)
Histology		
1. Excised Aortic Valves	Signal did not correlate with macrophage burden (CD 68 staining) [r=0.43; p=0.22], suggesting non-specific binding. (61)	Signal co-localized with regions of calcification and could also be observed in regions of evolving calcification. (60, 61)
2. Carotid Endarterectomy Specimens	Accumulation in macrophage rich areas of plaque. (56)	Focal uptake at site of plaque rupture. (55) Uptake associated with active calcification and necrosis. (55, 62)

1.3.4.1 ^{18}F-sodium fluoride

^{18}F-Sodium Fluoride was first developed in 1962 when it was introduced as a suitable radioactive tracer for the study of bone disease. (63) In the following years, its use was largely superseded by technetium-99m-diphosphonate compounds. However, the highly favourable pharmacokinetics of this tracer and increased sensitivity in the detection of skeletal metastases led to its re-emergence as a favourable scanning agent in both focal and generalised bone disease. It is currently used widely in the diagnosis of both malignant and metabolic bone disease and in the evaluation of skeletal trauma. (64-68)

In skeletal imaging, ^{18}F-sodium fluoride binds to hydroxyapatite, the major inorganic component of skeletal bone. The level of uptake and corresponding signal intensity largely depend on both blood flow (the rate limiting step) and surface area of exposed hydroxyapatite. In metabolic bone disease or malignancy, increases in regional blood flow as well as increased bone turnover lead to a greater surface area of exposed hydroxyapatite and result in increased uptake of the tracer. (65)

Following intravenous administration, ^{18}F-sodium fluoride is rapidly cleared from the plasma by diffusion through capillary beds into the extracellular compartment. When it reaches the bone surface, the exchange of the fluoride ion with the hydroxyl group in hydroxyapatite leads to the formation of fluoroapatite ($Ca_{10}(PO_4)6F_2$). Following rapid initial chemisorption, the slower incorporation of fluoroapatite with the bone matrix occurs, a process which can take days or weeks. (69)

As a result of minimal plasma protein binding, high first-pass extraction and avid irreversible association with hydroxyapatite, almost all of the injected dose is retained

by bone after a single pass of blood. This facilitates high contrast skeletal imaging just one hour following injection. (69, 70) The biological half-life of ^{18}F-sodium fluoride is 90 min. (70)

Within the vasculature, ^{18}F-sodium fluoride uptake occurs by similar mechanisms, providing a marker of calcification activity. Phosphor-imaging autoradiography has demonstrated that ^{18}F-sodium fluoride associates with regions of calcification with a high affinity and exhibits negligible non-specific binding. (62) In immunohistochemical analysis, ^{18}F-sodium fluoride co-localizes specifically to vascular calcification as opposed to upstream markers of the calcific response. (62) Within the vasculature, ^{18}F-sodium fluoride detects regions of dynamic microcalcification (<50 μm), with a proportionately smaller radioactivity signal observed in large calcific deposits and many regions of heavily calcified atherosclerotic plaque displaying no tracer uptake. (54, 62, 71) Indeed, the intensity of ^{18}F-sodium fluoride uptake has been found to be inversely correlated with calcified plaque density. (72) This feature may be explained by the finding that arterial ^{18}F-sodium fluoride is unable to penetrate through organised mineral layers in advanced macrocalcific deposits, with uptake dependent on the surface area of exposed hydroxyapatite. This hypothesis has been supported by micro-PET/micro-CT analysis of carotid endarterectomy specimens. When intact specimens were imaged following incubation with ^{18}F-sodium fluoride, increased activity was demonstrated only on the surface of macroscopic calcium deposits, with no uptake within their core. However, if specimens were sectioned prior to incubation with ^{18}F-sodium fluoride, increased tracer uptake was subsequently observed within the newly exposed regions of

macrocalcification. (62) This offers an explanation for the apparent discordance between advanced calcification and ^{18}F-sodium fluoride uptake. In large volume and flat calcified deposits, most of the hydroxyapatite is internalised and the radioactive tracer cannot penetrate through the organised mineral layers. Conversely, dispersed convex vesicles in the early stages of microcalcification provide a much larger surface area of available hydroxyapatite. (62) A clear value of this radiotracer lies in its ability to identify microcalcification as opposed to macrocalcification visible on computed tomography. Therefore, by selectively detecting regions of biologically active developing microcalcification within the vasculature and doing so with both a high affinity and sensitivity, PET imaging with ^{18}F-sodium fluoride identifies key features of plaque vulnerability and an active disease state thereby providing distinct information to computed tomography and potentially leading to a number of important cardiovascular applications. Whilst not present in all vulnerable atherosclerotic plaques, the presence of microcalcified deposits has been demonstrated in the majority of acute plaque ruptures. (2)

1.3.5 TECHNICAL CHALLENGES OF POSITRON EMISSION TOMOGRAPHY

Whilst emerging as a promising technique, many technical challenges relate to cardiac PET imaging, and overcoming these will be crucial to assist in the adoption of this technique in the research and clinical setting.

Imaging of the coronary arteries is particularly challenging due to the impact of respiratory and cardiac motion on coronary artery territories, often leading to blurring of the PET signal. Discarding the PET data obtained during systole and only using the data from end diastole effectively reduces motion but does so at the expense of

increasing noise. This can pose difficulty in distinguishing true positive lesions from background noise and leads to an average difference of only 34% in tissue-to-background ratios between positive and negative coronary plaques. (55) However, the application of innovative motion correction techniques has shown promise in reducing background noise and improving tissue-to-background ratios. (73) (Figure 1.2)

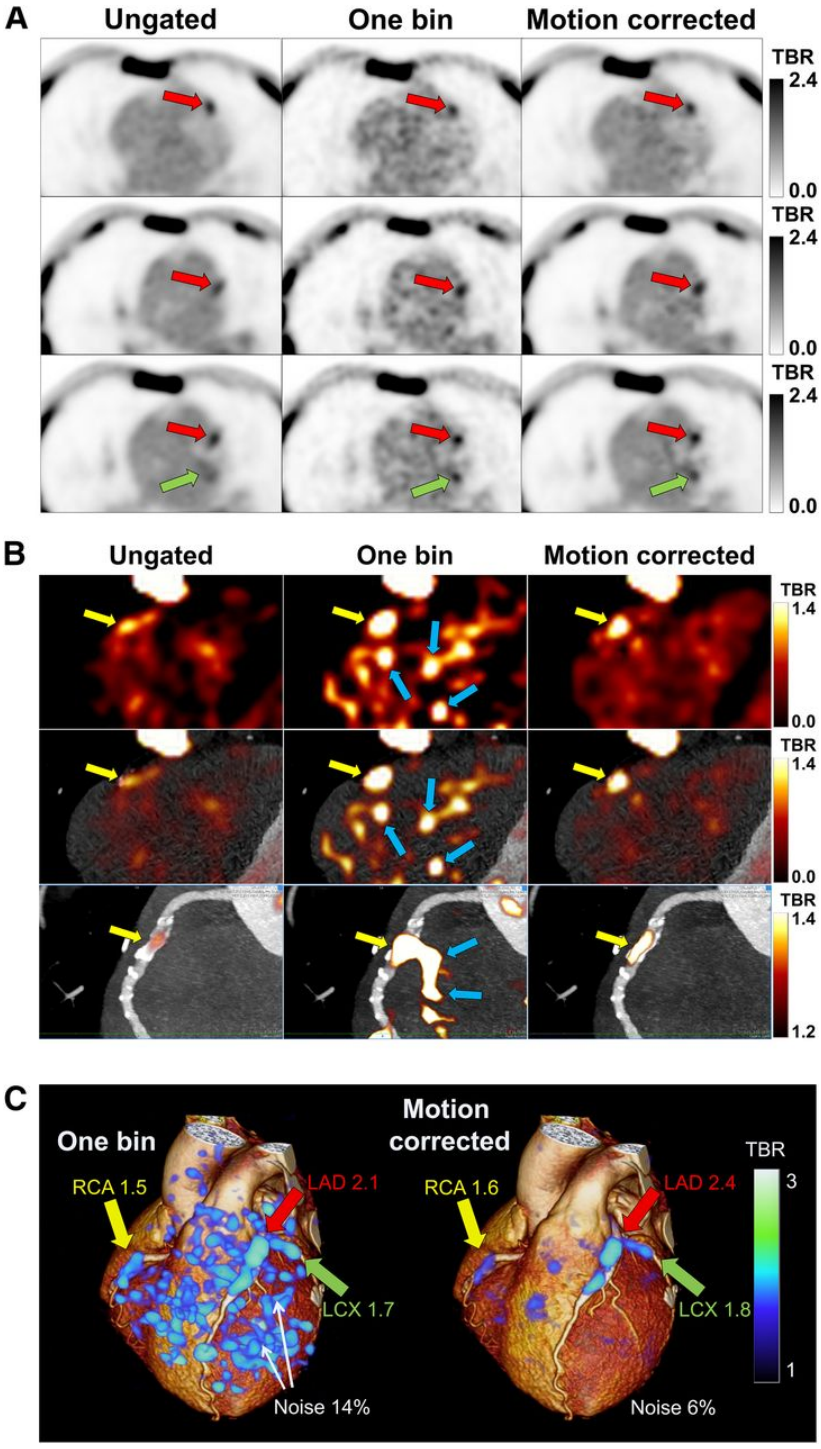

Figure 1.2 Noise reduction and TBR improvement in ^{18}F-fluoride PET images of 65-y-old man.

(A) On linear grayscale transverse slices, ^{18}F-fluoride plaque uptake is seen in left anterior descending (LAD) (red arrows) and left circumflex (LCX) (green arrows)

coronary arteries. The images show blurred lesion signal in ungated images, significant noise in 1-bin images, and high lesion signal with reduced noise in motion-corrected images. (B) On PET (top), PET-CTCA (middle), and multiplanar-reformatted PET-CTCA (bottom) images with exponential colour table and same window and level settings, vulnerable plaque is seen in right coronary artery (RCA) (yellow arrows). Low lesion signal is seen in ungated images, significant noise in 1-bin images (blue arrows), and high signal with less noise in motion-corrected images. (C) 3-dimensional rendering of 1-bin image (25% of PET counts) as in study of Joshi et al. (55) (left) and motion-corrected image (right) superimposed on rendered CTCA volume. Increased uptake is seen in RCA, LAD, and LCX coronary arteries in high-noise 1-bin image and remains clear in motion-corrected image. (Rubeaux M et al, J Nucl Med 2016;57:54-59). (74)

Another challenge exists as a consequence of the finite spatial resolution of PET imaging systems, meaning that quantitative measurements of tracer concentrations in small areas can pose difficulty. Partial volume effects may lead to blurring of the radiotracer signal, especially from small tissue structures such as the coronary arteries. (75) As measurements of tracer uptake in small volume structures become increasingly important, the potential for enhanced correction techniques may develop.

The advent of combined PET and magnetic resonance imaging, with the combination of excellent soft tissue contrast and functional imaging capabilities, holds promise in imaging of the vasculature. With the evolution of innovative motion correction techniques, this technology has the potential to enhance our understanding of the natural history of vascular calcification and its clinical consequences, thereby influencing and improving management of cardiovascular disease.

Even with such technological advances, the question will remain as to whether the identification of ^{18}F-sodium fluoride positive coronary plaques will complement existing investigative strategies and allow improved prospective identification of vulnerable patients with high-risk disease. Given the expensive cost of PET-CT

imaging and use of additional radiation, use of this technique must be found to have an incremental clinical impact above existing risk prediction models and imaging strategies prior to clinical implementation. This will require results from large prospective studies demonstrating the clinical utility and cost effectiveness of imaging the coronary arteries and vasculature.

1.4 AORTIC STENOSIS

1.4.1 BACKGROUND

Aortic stenosis (AS) affects over 7 million people aged over 75 years in Europe and North America and its prevalence is expected to triple in the next forty years. (76-78) The development of effective medical therapy is a major unmet clinical need that will require both a greater understanding of the underlying pathophysiology and the adoption of novel imaging methods to establish safety and efficacy of candidate drugs. AS is a fibrocalcific disease in which progressive deposition of lipid, collagen and calcification leads to thickening and immobility of the aortic valve leaflets, resulting in progressive valve narrowing and obstruction to left ventricular outflow. Over time, the left ventricle responds to the consequent increase in afterload by myocyte hypertrophy, extracellular expansion and ultimately myocardial fibrosis and decompensation. (79, 80)

1.4.2 THE PATHOPHYSIOLOGY OF AORTIC STENOSIS

The Valve: The *initiation phase* of AS shares many pathophysiological similarities with atherosclerosis and is dominated by inflammation, lipid infiltration and

extracellular matrix remodelling under the control of inflammatory signalling pathways. (81-85) Like atherosclerosis, the initiating insult appears to be a combination of increased mechanical and oxidative stress or reduced shear stress leading to endothelial damage and a powerful inflammatory response. As this process continues, inflammatory signalling pathways are superseded by a powerful and relentless cycle of progressive calcification, coordinated by osteoblast-like cells and governed by pro-osteogenic signalling pathways. (79, 86, 87) The accumulation of calcium within the valve during the later *propagation phase* induces further injury, thereby establishing a vicious cycle of accelerating calcification and progressive valvular obstruction.

The Myocardium: In addition to progressive valvular obstruction, AS has direct effects on the left ventricle. Progressive valve obstruction results in an increased afterload, triggering myocyte hypertrophy and compensatory wall thickening that initially preserves wall stress and maintains cardiac output. Over time, however, cellular hypertrophy progresses to myocyte death, expansion of the extracellular space and replacement fibrosis. (80, 88-91) Indeed these two processes drive left ventricular decompensation and the transition from hypertrophy to heart failure.

1.4.3 WHAT DO WE REQUIRE OF IMAGING IN AORTIC STENOSIS?

Cardiac imaging is pivotal to the management of aortic stenosis and relied upon to confirm the diagnosis and to grade stenosis severity and assess myocardial health both at baseline and over time. AS is a slowly progressive condition that advances at a variable and inconsistent rate. In order to accurately measure or predict disease progression over time, imaging tests must have sufficient reproducibility and

robustness to detect small changes in disease severity with high accuracy. In the clinical setting, this is of utmost importance when selecting the appropriate management strategy and optimal timing of intervention for the individual patient. In the research setting, these attributes are crucial in clinical trials seeking to investigate efficacy of novel therapies. Indeed, imaging biomarkers with improved repeatability and sensitivity to change will minimise sample sizes, follow-up duration and the expense of trials. Drug trials using imaging endpoints therefore desire biomarkers that maximise signal-to-noise or the *progression-to-noise ratio*: the ratio between the magnitude of average progression in a particular parameter compared to its scan-rescan repeatability (the error in measuring that parameter on two different scans). While transthoracic echocardiography has remained the gold standard method for assessing the aortic valve and myocardium and the tool of choice in the clinical setting, novel imaging techniques demonstrate potential advantages and are therefore being increasingly explored, particularly in clinical trials of novel therapies. **(**Figure 1.3**)**

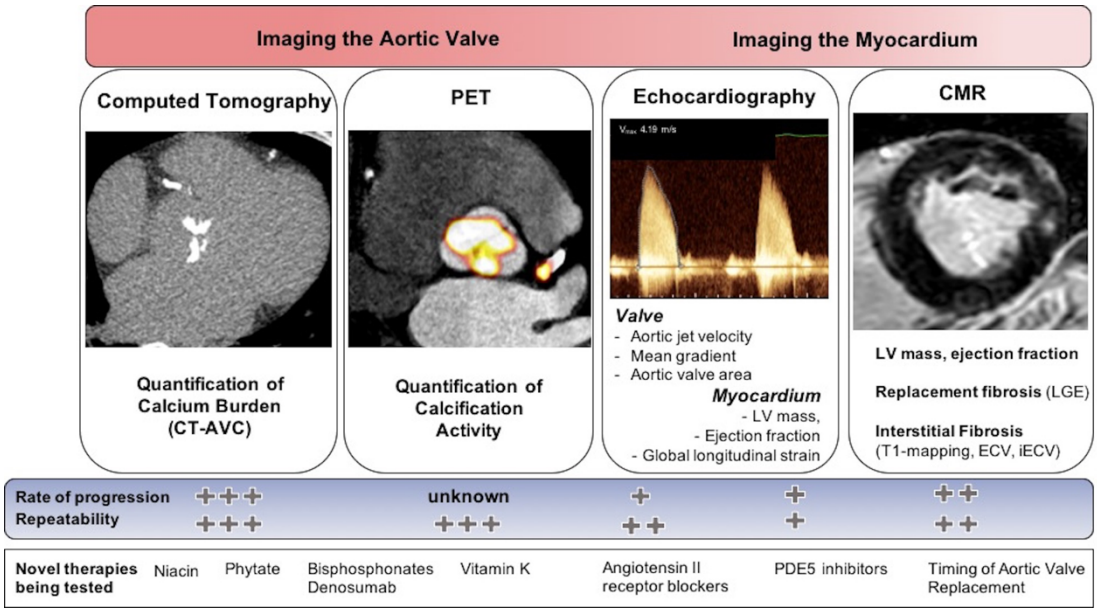

Figure 1.3. The role of imaging in aortic stenosis progression.

Non-invasive imaging provides the ability to directly image the aortic valve and consequent pathophysiological effects on the myocardium. Imaging the valve may be performed by CT to quantify aortic valve calcium load (CT-AVC), PET to measure calcification activity and/or echocardiography to assess haemodynamic severity. The response of the left ventricle may be assessed by echocardiographic measures of mass, EF and/or strain, while CMR offers additional quantification of fibrosis. The ability of these techniques to detect therapeutic efficacy depends on the scan-rescan repeatability of the test and the rate of change of the parameter being measured. These attributes are being exploited in a number of ongoing studies to investigate novel therapies for aortic stenosis.

1.4.4 ECHOCARDIOGRAPHY

While there may not be a true reference standard for AS severity, echocardiography is considered the "gold-standard" for clinical assessment. Early work in the 1970s found that Doppler ultrasound could be used to examine the jets of stenotic and regurgitant lesions. (92) This laid the groundwork for Hatle (93, 94) to demonstrate that Doppler ultrasound was highly feasible in AS and the peak jet velocity, converted into a gradient using the simplified Bernoulli equation, (95) had good agreement with invasive measurements. Otto, (96) along with many others, have since demonstrated that echocardiographic biomarkers strongly predict the need for intervention. Finally, the use of echocardiographic markers of severity as enrolment criteria in the PARTNER B trial (97) demonstrates the ability of echocardiography to select patients for beneficial therapy. Combined with the absence of radiation, widespread availability and low imaging costs, these characteristics place echocardiography as the first-line modality for screening and serial follow-up in aortic stenosis.

Although multiple echocardiographic parameters exist to assess disease severity, current guidelines recommend the assessment of severity and progression based upon peak velocity, mean gradient and aortic valve area (AVA). (98) Each of these central parameters have been found to predict outcome across multiple studies. (99-101) Aortic peak velocity remains the first line biomarker in recent guidelines [ESC/EACTS 2017], providing powerful prognostic information and superior reproducibility than other parameters. (102, 103) However, peak velocity is dependent on flow status and accurate alignment of the echocardiography probe with the jet of blood through the valve. While mean gradient is subject to the same limitations as peak

velocity, aortic valve area (AVA) is in principle less flow dependent. However, measurements of aortic valve area can represent an important source of discrepancy, particularly as a result of variations in direct measurements of the left ventricular outflow tract (LVOT). As LVOT diameter is squared to provide AVA by the continuity equation, small differences in measurement can lead to significant variation, and often an underestimation of AVA. Echocardiographic measurements therefore display considerable variability leading to inaccuracies when estimating disease progression. Moreover, echocardiographic measurements demonstrate relatively slow progression with time. As a consequence, the progression to noise ratio for most echocardiographic assessments is not favourable. (104, 105) While this is often not a major issue in clinical practice, in the research setting it means that clinical trials require relatively large numbers of patients and prolonged follow-up to detect true treatment effects. (104)

An additional limitation worth considering is that echocardiographic measures of AS often provide conflicting assessments of disease severity. Indeed, discordant echocardiographic results are seen in one quarter of patients, most often arising from a valve area <1 cm^2 suggesting severe disease, and a peak velocity <4.0 m/s or mean gradient <40 mmHg indicating moderate stenosis. (106, 107) In cases of low flow, low gradient aortic stenosis, flow can be temporarily increased to assess the true haemodynamic severity of aortic valve disease. Low dose dobutamine stress echocardiography (DSE) is often useful in this regard - with an increase in velocity with increased flow rates used to diagnose true severe AS (108) and to discriminate patients with and without contractile reserve. (109) However, a significant proportion

of patients with discordant findings are in fact found to have normal flow status, making echocardiographic results difficult to interpret.

For these reasons, interest in developing novel assessments of disease severity and progression in aortic stenosis is growing, and novel imaging techniques may complement echocardiography in adjudicating disease severity and monitoring disease progression.

1.4.5 COMPUTED TOMOGRAPHY CALCIUM SCORING

Calcification is the predominant process causing valve obstruction in AS. Quantification of the calcium burden has therefore been suggested as an alternative flow-independent method of determining disease severity. (110) This was first demonstrated using a semi-quantitative assessment on echocardiography, (110, 111) although the clinical utility of this approach has been limited by subjectivity and suboptimal reproducibility. (112) Interest has instead turned to computed tomography (CT) calcium scoring, an established clinical technique already widely used to quantify coronary arterial calcification. Using a non-contrast, ECG-gated CT acquisition and similar protocols as for coronary calcium scoring, the burden of valvular calcium can be quantified using the Agatston method, which encompasses both the area and weighted density of a given region of calcification. (Figure 1.4)

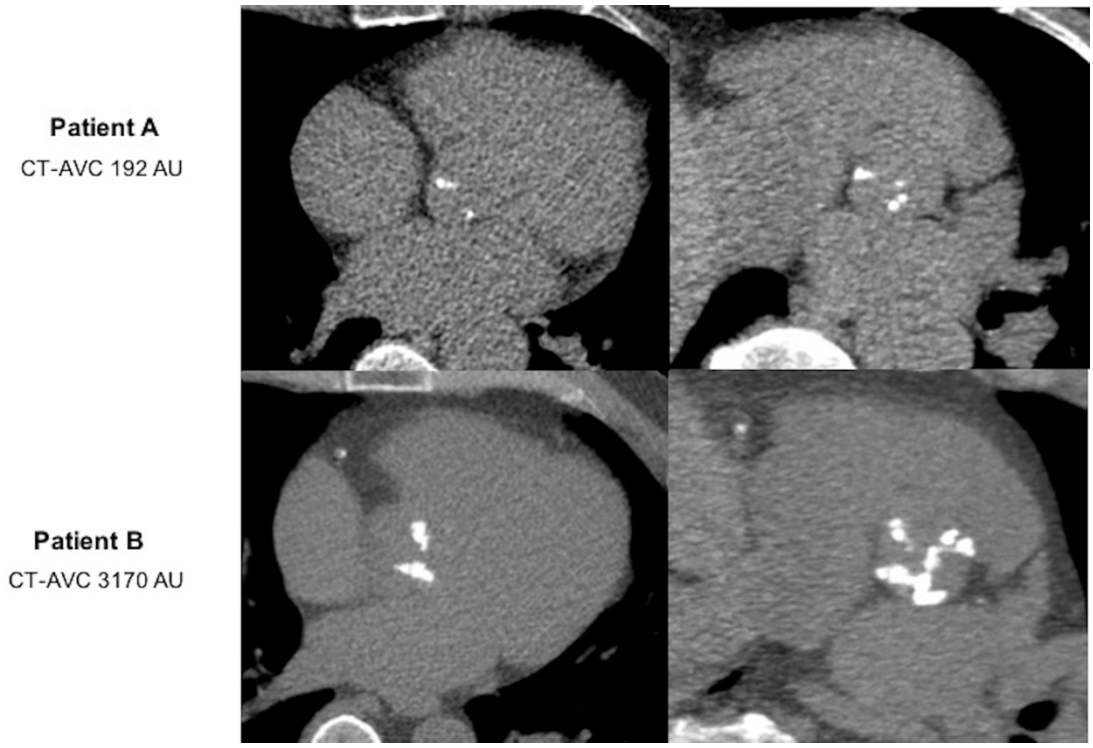

Figure 1.4. CT calcium scoring of the aortic valve.

An example of mild aortic valve calcification (Patient A, top panel) and severe calcification by CT (Patient B, bottom panel) in transverse (left) and short-axis (right) views of the valve.

Early studies of aortic valve CT calcium scoring (CT-AVC) highlighted that this could provide a complementary measure of stenosis severity, correlating moderately with haemodynamic severity on echocardiography. (112, 113) A major advance was the realisation that men and women require different calcium scores to develop severe stenosis, even when adjusted for body size or LV outflow dimensions, and therefore that sex-specific thresholds were needed to grade severity. (114) In 646 patients with normal LV systolic function, the application of calcium score thresholds of 2065 (AU) for men and 1274 (AU) for women correctly classified severe AS with a sensitivity of

≥86% and specificity of ≥79%. (106) These thresholds have been validated in a further multicentre cohort of over 900 patients, holding particular potential in adjudicating disease severity in patients with discordant echocardiography results. (115, 116)

In addition to defining severity, CT-AVC offers powerful prediction of future clinical events. (115, 116) Indeed, in recent multicentre studies, severe calcification was associated with a 3 to 4-fold increase in death or AVR, (107, 117) emerging as an independent predictor of these events after adjustment for clinical and echocardiographic parameters. CT-AVC may also provide value in measuring disease progression, improving the progression-to-noise ratio previously discussed. Quantification of calcium by CT has been shown to demonstrate excellent interobserver reproducibility and scan-rescan repeatability; with limits of agreement approximately ±70 AU and variation of approximately 4-8%, respectively. (112, 114, 118) Moreover, mean annual progression in calcium score is relatively large, ranging from approximately 141 AU/year in mild AS to 361 AU/year in severe AS. (115) Whether CT calcium scoring will be modifiable with medical therapies is yet to be determined, however its attributes have led to its adoption in the research setting as the primary efficacy end point in multiple ongoing studies investigating novel treatments for aortic stenosis. CT calcium scoring is not currently recommended for routinely tracking disease progression in the clinical arena, although recent ESC guidelines support its use in adjudicating disease severity in patients with discordant echocardiographic assessments and normal flow. (98)

1.4.6 POSITRON EMISSION TOMOGRAPHY

Positron Emission Tomography (PET) is another novel technique, the use of which is being explored in aortic stenosis. By monitoring biological processes within the body, this modality has the potential to offer important mechanistic insights into pathophysiology. Further, as a marker of disease activity and very early calcium formation, there is growing interest in using PET to detect early therapeutic effects in aortic stenosis at a stage in the process when calcium is more likely to be reversible. (Figure 1.5)

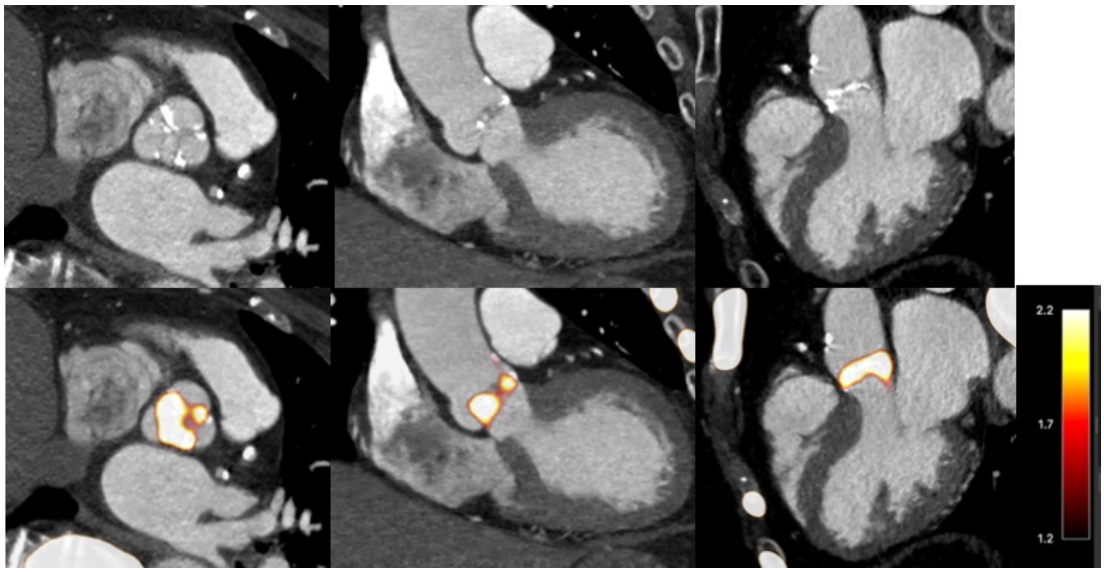

Figure 1.5. ^{18}F-fluoride PET-CT of the aortic valve.

Contrast-enhanced CT of the aortic valve (top panel) with fused ^{18}F-fluoride PET-CTA images in the same patient (bottom panel). Strong PET uptake can be localized to the aortic valve in short-axis (left), coronal (middle) and sagittal (right) views.

Radiolabelled sodium fluoride (^{18}F-fluoride) is a widely available PET tracer that can be used to measure calcification activity in the vasculature, with an affinity for

developing microcalcification. (53, 55, 61, 62) ^{18}F-fluoride activity is increased in patients with aortic valve disease compared to the healthy population, with a progressive rise in PET uptake with increasing severity of aortic stenosis (jet velocity and calcium score). (60) Furthermore, early studies have suggested that ^{18}F-fluoride activity predicts the rate of future disease progression as measured by CT-AVC and echocardiography. (61, 119) Indeed, new areas of macrocalcification appear to subsequently develop at sites of increased baseline ^{18}F-fluoride uptake, consistent with this tracer identifying developing calcification before it is visible on CT. **(**Figure 1.6**)** As a marker of disease activity, ^{18}F-fluoride therefore holds potential in detecting therapeutic effects more rapidly than conventional anatomical imaging approaches. (120) Encouragingly, excellent reproducibility of this technique has been demonstrated (ICC >0.8) and scan-rescan reproducibility has also shown good agreement with a percentage error of ±10%. (120) However, the incremental value of this modality beyond anatomical imaging modalities has yet to be shown and given the cost, availability of scanners and radiation exposure, it is unlikely to be used clinically in the near future. However, ^{18}F-fluoride PET does hold major promise in the research arena and as an end point in clinical trials of novel therapy, potentially being more sensitive to treatments effects than other imaging markers. While it remains to be determined whether the aortic valve ^{18}F-fluoride PET signal is modifiable with medical therapy, the same is true for all imaging biomarkers in the absence of an effective medical therapy for this condition. Interestingly, skeletal ^{18}F-fluoride uptake in metabolic bone disease does appear to be modifiable, demonstrating clear changes after only one month of bisphosphonate therapy. (121)

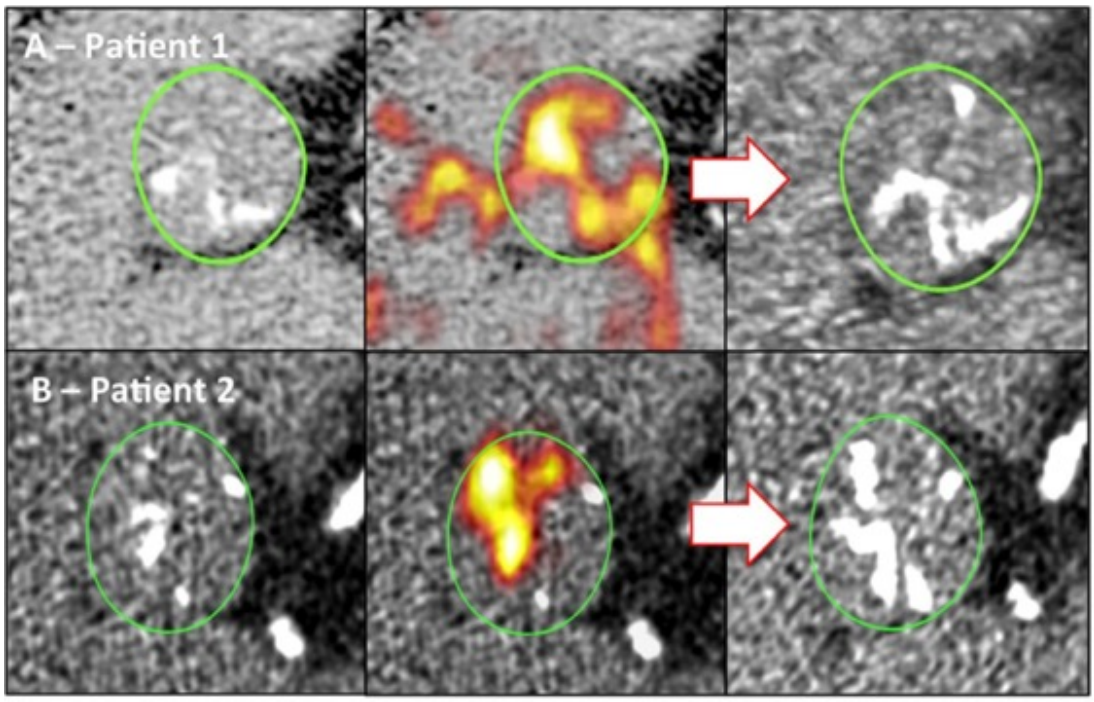

Figure 1.6 ^{18}F-Fluoride PET-CT predicts disease progression in aortic stenosis.

Baseline CT calcium score scans (left) for patients 1 (top panel, A) and 2 (bottom panel, B). Fused ^{18}F-fluoride PET-CT scans (middle) show fluoride uptake in red and yellow. Follow-up CT at 1 year (right) suggests that the baseline PET signal predicts where new macroscopic calcium, visible on the CT, is going to develop. *(Dweck M et al, Circ Cardiovasc Imaging 2014;7:371-378)* (61)

Another widely used PET tracer that has been explored in imaging of the aortic valve is ^{18}F-FDG. This glucose analogue becomes trapped in metabolically active cells and serves as a surrogate marker for macrophage burden and inflammation. In aortic stenosis, ^{18}F-FDG activity is increased in patients with aortic stenosis although in practice image interpretation is frequently challenging due to overspill of activity from the adjacent myocardium. (60, 61) Finally, the development of PET-MRI scanning platforms provides new opportunities to perform PET imaging studies at low radiation

dose and potentially allowing multiple time points to be studied in individual patients. (122)

1.4.7 THE USE OF IMAGING TO TEST DRUG EFFICACY

As yet, no medical therapy has proven effective in reducing progression of AS or improving clinical outcomes in patients with this condition. However, as our understanding of the complex pathophysiological processes underlying AS improves, novel therapeutic strategies have been developed and are under active investigation. (Table 1.2) A challenge is to identify patients in whom the progressive cycle of calcification may be reversible with effective therapy, and this may be more likely to occur early in stages of calcium formation. Most randomised trials to date have targeted patients with mild or moderate aortic stenosis and it has been suggested that patients would be more effectively treated at an earlier stage. However, as the majority of patients with aortic sclerosis do not develop aortic stenosis, identifying patients with mild aortic valve calcification who are likely to derive benefit from treatment would be challenging. Furthermore, many patients do not present until they have developed advanced disease and so developing therapies which halt disease progression in this patient group is also of great importance. Regardless of the stage of disease, it appears probable that calcification is more likely to be reversible in its earlier stages of development meaning that imaging techniques that can identify early developing microcalcification are likely to be of value.

Table 1.2. Current trials investigating the effects of novel therapies on progression of aortic stenosis.

Trial name	Trial Identifier	Therapy	Population	Imaging End Points	Primary Outcome
Early Aortic Valve Lipoprotein(s) Lowering (EaVall)	NCT02109614	Niacin vs Placebo	238 participants with aortic sclerosis or mild aortic stenosis	CT calcium score Echo	Change in CT calcium score at 2 years
Study Investigating the Effect of Drugs Used to Treat Osteoporosis on the Progression (SALTIRE2)	NCT02132026	Alendronate or Denosumab vs Placebo	150 patients with AV Vmax >2.5 m/s and grade 2-4 calcification on echo	CT calcium score Echo 18F-fluoride PET-CT	Change in CT calcium score at 2 years
PCSK9 Inhibitors in the Progression of Aortic Stenosis	NCT03051360	PCSK9 inhibitor vs placebo	140 patients with mild to moderate AS	CT calcium score Echo 18F-fluoride PET-CT	Change in calcium score and 18F-NaF PET activity at 2 years
Bicuspid Aortic Valve Stenosis and the Effect of Vitamin K2 on Calcium Metabolism on 18F-NaF PET/MRI (BASIK2)	NCT02917525	Vitamin K2 vs Placebo	44 patients with a bicuspid aortic valve and mild-moderate calcification on echo	CT calcium score Echo 18F-fluoride PET-MRI	Change in 18F-NaF PET activity at 6 months
Value of oral phytate in the prevention of progression of cardiovascular calcifications (CALCIFICA)	NCT01000233	Phytine vs Placebo	250 patients with grade 2 or 3 aortic valve calcification on echo	CT calcium score	CT calcium score at 2 years
Aortic Stenosis and Phosphodiesterase Type 5 inhibition (ASPEN)	NCT01275339	Tadalafil vs Placebo	moderate to severe AS (AVA <1.5cm)	MRI Echo	Change in LV mass at 6 months Change in diastolic function on Echo Change in LV longitudinal strain on echo
A Study Evaluating the Effects of Ataciguat (HMR 1766) on Aortic Valve Calcification	NCT02481258	Ataciguat (HMR1766) vs Placebo	35 patients with AVA between 1-2 cm2 and calcium score greater than 300AU + EF>50%.	CT calcium score Echo	Change in CT calcium score at 6 and 12 months

1.4.7.1 Lipid-lowering strategies

While statin therapy has failed to slow disease progression in three randomized trials (123-125), the question remains as to whether alternative lipid-lowering approaches could be successful, potentially at earlier stages of the disease. One promising therapeutic target is lipoprotein(a), a cholesterol-rich plasma lipoprotein containing an LDL particle with apolipoprotein B100 bound to apolipoprotein(a). (126) Lipoprotein(a) has been recognized as a powerful cardiovascular risk factor (126), and a recent genome-wide association study has implicated a single-nucleotide polymorphism in the Lp(a) locus to the development of the disease. (127)

The growing evidence that Lp(a) plays a causal role in the development and also perhaps the progression of AS (128, 129) has led to great enthusiasm in exploring this as a therapeutic target. One potential therapeutic agent is Niacin, which has been shown to lower Lp(a) in a dose-dependent manner. Whether extended-release Niacin can reduce the progression of aortic valve disease is currently under investigation as part of the Early Aortic Valve Lipoprotein(s) Lowering (EaVall) study (NCT 02109614). This pilot study will randomise over 200 patients with elevated Lp(a) and mild aortic valve disease to extended-release Niacin or placebo with a primary outcome of change in CT-AVC at two years. (129)

1.4.7.2 Anti-calcific therapies

Calcification is a key target for novel therapies in AS given its central role in driving progressive valvular obstruction. An important concern, however, is how best to reduce calcification activity in the valve while maintaining bone health in elderly patients with AS who are at risk of osteoporosis and fractures. One potential option is to use treatments licensed for osteoporosis, such as bisphosphonates or RANKL-

inhibitors, which not only improve bone health but have demonstrated the ability to reduce vascular calcification. (130) In addition to reducing bone resorption and thereby reducing circulating calcium and phosphate, bisphosphonates have been shown to reduce local production of inflammatory cytokines, inhibit release of matrix metalloproteinases and stimulate macrophage apoptosis. (131, 132) Pre-clinical studies have demonstrated that bisphosphonate therapy reduces valvular calcification in animal models. (133, 134) The monoclonal antibody to RANKL, denosumab, acts by preventing the interaction between RANKL and RANK, a cytokine which plays an important role in up-regulating pro-osteogenic mediators and inducing osteoblastic transformation of valve interstitial cells (VICs). Whether these therapies reduce the progression of valvular calcification has yet to be determined and is currently being investigated in a randomized placebo-controlled trial (SALTIRE II NCT02132026). This blinded study is using change in CT calcium score at two years as the primary efficacy end point. However, measures of calcification activity by PET-CT will also be performed at baseline and one year, in addition to serial echocardiography every six months. (135)

Another potential anti-calcific therapy under investigation is Vitamin K. Vitamin K is required for activation of Matrix Gla Protein (MGP), a potent inhibitor of vascular calcification synthesised by vascular smooth muscle cells. In the aortic valve, MGP acts by blocking the binding of BMP-2 to its receptor, thereby preventing BMP-mediated differentiation of VICs to pro-osteogenic cells. MGP also inhibits growth of microcalcification crystals by binding directly to hydroxyapatite and stabilising circulating calcifying protein particles. (136) Reduced expression of MGP has been

demonstrated in calcific aortic valves. (137) The BASIK2 randomized trial will investigate the effect of vitamin K2 in 44 patients with bicuspid aortic valve disease (NCT02917525). The primary outcome of the study is the change in ^{18}F-fluoride PET signal on PET-MRI at six months. (136)

1.4.7.3 Anti-fibrotic strategies

Therapies targeting the remodelling response of the left ventricle have also gained interest. While the RIAS trial of ACE-inhibitor therapy showed a small positive effect on LV mass, a small and underpowered study did not demonstrate an effect of eplerenone on LV mass progression. (138) Further work in this field is required particularly to investigate the effects of novel therapies on myocardial fibrosis (139), with hope that more aggressive inhibition of the RAAS system and or novel anti-fibrotic therapies may prove more effective. (140-142)

1.5 THESIS AIMS AND HYPOTHESES

The overall aim of this thesis is to explore advanced imaging approaches to detect the burden, activity and progression of disease in coronary artery disease and aortic stenosis. This objective can be divided into four component parts. The first is to explore the role of advanced imaging technology with novel quantitative plaque measures on fractional flow reserve derived from computed tomography angiography to investigate the relationship between plaque burden, plaque characteristics and non-invasive fractional flow reserve. The second is to investigate whether uptake of the radiotracer ^{18}F-fluoride may predict progression of coronary calcification. The third objective is to investigate technical improvements to PET imaging of disease activity including a novel motion correction method to assess whether application of these may improve the utility of this novel imaging method in both coronary atherosclerosis and aortic valve disease. Lastly, this thesis aims to investigate the role of CT quantification of the burden of aortic valve calcification in the assessment of aortic stenosis and disease progression.

The following hypotheses will be tested;

i. Quantitative measures of atherosclerosis burden in coronary epicardial vessels with non-obstructive stenosis may predict abnormal CT-derived fractional flow reserve across the whole coronary vessel (Chapter 3).
ii. Uptake of the radiotracer ^{18}F-fluoride in coronary vessels may predict progression of coronary calcification in patients with clinically stable coronary artery disease (Chapter 4).

iii. Application of a novel motion-correction method to coronary PET-CT will improve quantification of ^{18}F-fluoride uptake and disease activity (Chapter 5).

iv. Measurement of aortic valve calcification burden by computed tomography is a reproducible technique and may provide value in the assessment of disease progression in aortic stenosis (Chapter 6).

v. Application of a novel cardiac motion correction method to both PET-CT and PET-MRI of the aortic valve is feasible and will improve signal quantification and assessment of disease activity (Chapter 7).

CHAPTER 2

Methodology

Chapter 2 Methodology

2.1 SUMMARY

Data for chapter 3 were produced from a prospective observational cohort of patients who underwent computed tomography coronary angiography at Cedars Sinai Medical Center, Los Angeles, USA. Data for chapter 4 were produced as a pre-specified sub-study of the Dual antiplatelet therapy to Inhibit coronary Atherosclerosis and MyOcardial injury in patients with Necrotic high-risk coronary plaque Disease (DIAMOND) prospective randomised controlled trial (ClinicalTrials.gov identifier: NCT02110303). Data for chapter 5 were derived from a prospective observational cohort of patients with acute coronary syndrome recruited from Cedars-Sinai Medical Center in Los Angeles, USA. Data for chapter 6 were derived from sub-studies of the Role of Active Valvular Calcification and Inflammation in patients with Aortic Stenosis ('Ring of Fire') study (ClinicalTrials.gov identifier: NCT01358513) and the ongoing Study Investigating the effect of Drugs Used to Treat Osteoporosis on the Progression of Calcific Aortic Stenosis (SALTIRE 2) randomised controlled trial (ClinicalTrials.gov identifier: NCT02132026) for which I was the Principal Investigator between October 2017-August 2019. Data for chapter 7 were produced from the SALTIRE 2 study and a patient recruited as part of an ongoing research study at Cedars Sinai Medical Center in Los Angeles, USA. Specific study designs and methodology are described in detail in each relevant chapter.

2.2 PATIENT COHORTS

2.2.1 FFRCT AND PLAQUE BURDEN POPULATION

The study population for chapter 3 included patients who underwent Computed Tomography Coronary Angiography (CTCA) at Cedars Sinai Medical Center for clinical reasons and provided written informed consent at the time of scanning for data to be used for research purposes. Participants were recruited between February-October 2016. Patients were included if there was evidence of at least 25% stenosis in one major epicardial vessel. Patients with prior coronary stent implantation, coronary artery bypass surgery or inadequate CTCA image quality were excluded. The Chief Investigator for this study was Dr Daniel Berman.

2.2.2 DIAMOND TRIAL POPULATION

The Dual antiplatelet therapy to Inhibit coronary Atherosclerosis and MyOcardial injury in patients with Necrotic high-risk coronary plaque Disease (DIAMOND) study (NCT02110303) was a double-blind randomised controlled trial of an investigational medicinal product (CTIMP) which aimed to investigate whether ticagrelor therapy reduces high-sensitivity troponin I in patients with established coronary disease and high-risk plaque. The primary results of this study have recently been reported. (143)

The study population comprised patients aged ≥40 years with clinically stable established multivessel coronary artery disease. Multivessel disease was defined as at least two major epicardial vessels with any combination of either (a) >50% luminal stenosis, or (b) previous revascularisation by percutaneous coronary intervention or

coronary artery bypass graft surgery. Patients were excluded if they had been diagnosed with an acute coronary syndrome within the preceding 12 months or had undergone revascularisation within the preceding 3 months. Full eligibility criteria are provided in Table 2.1. Participants were recruited from the Royal Infirmary of Edinburgh, UK and underwent combined Positron Emission Tomography and Computed Tomography Coronary Angiography (PET-CTCA) and non-contrast CT imaging at the Clinical Research Imaging Centre at the Royal Infirmary of Edinburgh. For the pre-specified sub-study, participants without follow-up imaging and those in whom interval revascularisation was performed in a new vessel were excluded, leaving 183 participants included in the analysis of a total of 220 recruited. The Chief Investigator for this study was Professor Newby.

Table 2.1. Inclusion and exclusion criteria for the DIAMOND study

Inclusion Criteria
For inclusion in the study subjects should fulfil the following criteria: 1. Patients aged ≥40 years with angiographically proven multivessel coronary artery disease defined as at least two major epicardial vessels with any combination of either (a) >50% luminal stenosis, or (b) previous revascularization (percutaneous coronary intervention or coronary artery bypass graft surgery). 2. Provision of informed consent prior to any study specific procedures 3. Receiving aspirin
Exclusion Criteria
Subjects should not enter the study if any of the following exclusion criteria are fulfilled: 1. An acute coronary syndrome within the last 12 months 2. An indication for dual anti-platelet therapy, such as drug eluting stent 3. Receiving thienopyridine therapy such as clopidogrel or prasugrel 4. Percutaneous coronary intervention or coronary artery bypass graft surgery within the last 3 months 5. Inability or unwilling to give informed consent 6. Women who are pregnant, breastfeeding or of child-bearing potential (women who have experienced menarche, are pre-menopausal and have not been sterilised) will not be enrolled into the trial 7. Known hypersensitivity to ticagrelor or one of its excipients 8. Active pathological bleeding or bleeding diathesis 9. Significant thrombocytopenia: platelets <100 x 10^9 /L 10. History of intracranial haemorrhage 11. Moderate to severe liver impairments (Child's Grade B or C) 12. Maintenance therapy with strong CYP3A4 inhibitors, such as ketoconazole, nefazodone, ritonavir, indinavir, atazanavir, or clarithromycin 13. Major intercurrent illness of life expectancy <1 year 14. Renal dysfunction (eGFR ≤30 mL/min/1.73m^2) 15. Contraindication to iodinated contrast agents 16. Planned coronary revascularization or major non-cardiac surgery in the next 12 months 17. Maintenance therapy with simvastatin or lovastatin at doses greater than 40mg daily 18. Receiving oral anticoagulants including warfarin, rivaroxaban, dabigatran or apixaban

2.2.3 CEDARS-SINAI ACS POPULATION

This study population comprised patients who were recruited from Cedars Sinai Medical Center, Los Angeles, USA, following presentation with an acute coronary syndrome and with angiographic evidence of >50% luminal stenosis in one or more coronary arteries. Participants were recruited between December 2015 and June 2016. All participants underwent a comprehensive baseline clinical assessment followed by combined PET-CTA at the Mark Taper Cardiac Imaging Center, Cedars Sinai Medical Center. The Chief Investigator for this study was Dr Daniel Berman.

2.2.4 SALTIRE 2 TRIAL POPULATION

SALTIRE 2 is a prospective, double-blinded randomised controlled clinical trial investigating the effects of alendronic acid and denosumab on the progression of aortic stenosis. (NCT01358513). The study has recruited 150 individuals aged over the age of 50 years with aortic stenosis (defined as peak aortic jet velocity >2.5 m/s and grade 2-4 calcification on echocardiography). Exclusion criteria included hypocalcaemia, known allergy or intolerance to alendronate of denosumab, life expectancy <2 years or planned aortic valve surgery in the next six months. Full eligibility criteria are shown in Table 2.2. Participants from this population were included in the echocardiography cohort in chapter 6 and in the PET-CT cohort of chapter 7. Prior to commencement of the main study, a sub-study was performed to investigate reproducibility of ^{18}F-Fluoride PET-CT imaging methodologies and, for this purpose, a subgroup of participants was invited to attend for two ^{18}F-Fluoride PET-CTCA and CT calcium scans within 4 weeks. The calcium scoring data from this population are

analysed in chapter 6. The Chief Investigator for this study was Professor David Newby.

Table 2.2. Inclusion and exclusion criteria for the SALTIRE2 study.

Inclusion Criteria
For inclusion in the study subjects should fulfil the following criteria: 1. Age >50years 2. Peak aortic jet velocity >2.5m/s on Doppler echocardiography 3. Grade 2-4 calcification of the aortic valve on echocardiography
Exclusion Criteria
Subjects should not enter the study if any of the following exclusion criteria are fulfilled: 1. Anticipated or planned aortic valve surgery in the next 6 months 2. Life expectancy <2years 3. Inability to undergo scanning 4. Treatment for osteoporosis with bisphosphonates or denosumab 5. Long-term corticosteroid use 6. Abnormalities of the oesophagus or conditions which delay oesophageal/gastric emptying 7. Inability to sit or stand for at least 30 minutes 8. Known allergy or intolerance to alendronate or denosumab, or any of their excipients 9. Hypocalcaemia 10. Regular calcium supplementation 11. Dental extraction within 6 months 12. History of osteonecrosis of the jaw 13. Major or untreated cancers 14. Poor dental hygiene 15. Women of childbearing potential who have experienced menarche, are pre-menopausal, have not been sterilised or who are currently pregnant 16. Women who are breastfeeding 17. Renal failure (estimated glomerular filtration rate <30ml/min) 18. Allergy or contraindication to iodinated contrast 19. Inability or unwilling to give informed consent 20. Likelihood of noncompliance to treatment allocation or study protocol

2.2.5 RING OF FIRE TRIAL POPULATION

The Ring of Fire study was a prospective clinical study which recruited patients aged over 50 years with mild, moderate and severe aortic stenosis. Participants underwent echocardiography, ^{18}F-Fluoride PET-CT and ^{18}F-FDG PET-CT at baseline with follow-up echocardiography and/or non-contrast Computed Tomography performed at one and two years. The primary results of this study have already been reported. (60) For the purposes of this sub-study, the echocardiography and calcium scoring data from the PET-CT scans were analysed. The Chief Investigator for this study was Professor David Newby.

2.2.6 AORTIC VALVE MOTION CORRECTION POPULATION

This study population consisted of five patients recruited as part of the SALTIRE 2 study as previously described and one patient recruited from Cedars Sinai Medical Center who underwent a single PET-MRI scan as part of an ongoing observational study investigating the role of hybrid imaging in cardiovascular disease. The Chief Investigator for this study was Dr Daniel Berman.

2.3 ECHOCARDIOGRAPHY

Echocardiography utilises ultrasound to gain detailed information about cardiac structure and function and is the gold standard clinical tool for the diagnosis and monitoring of aortic stenosis.

2.3.1 IMAGE ACQUISITION AND ANALYSIS

Transthoracic echocardiography was performed by an experienced and accredited echocardiographer (Audrey White) using a pre-specified standardised protocol aligning with European Society of Echocardiography guidelines. (144) All scans were performed in the same room on a single dedicated echocardiography machine (Phillips Affinity 70 Ultrasound System) with participants in the supine and left lateral positions.

Images were acquired in the parasternal long and short axis views, apical 4 and 5-chamber views, subcostal and suprasternal views. Structural dimensions of the right and left ventricles, atria, left ventricular outflow tract and aortic root were measured. Left ventricular systolic function was estimated by visual assessment and confirmed using Simpson's biplane measurement where possible. Left ventricular diastolic function was also assessed using mitral valve pulsed wave and tissue Doppler. All valves were analysed by using visual assessment, colour flow, continuous wave and pulsed wave Doppler.

The severity of aortic valve disease was graded according to the European Society of Echocardiography Guidelines. (98) Peak aortic jet velocity was obtained from multiple acoustic windows using continuous wave Doppler ensuring careful patient positioning and a pencil probe to assess the right parasternal window.

Pulsed wave and continuous wave Doppler were used to measure peak transvalvular velocity and mean gradient using multiple acoustic windows and ensuring careful patient positioning. Continuous wave Doppler measurements were repeated at the

suprasternal notch, apex and right parasternal edge using a pencil probe. An average of three measurements was obtained in participants in sinus rhythm, and an average of five measurements from patients in atrial fibrillation. Aortic valve area was calculated using the continuity equation. The degree of aortic valve calcification was also assessed using a semi-quantitative scale previously described. (110) This scale comprised scores of 1-4; 1, no calcification; 2, mildly calcified with small isolated spots; 3, moderately calcified with multiple larger spots and 4, heavily calcified with extensive thickening of all cusps. (110) All research echocardiograms were performed by the same echocardiographer to minimise measurement variability, particularly with measurement of aortic valve area which has been shown to be high, with the exception of reproducibility assessments performed in chapter 6. (145)

2.4 CTCA, FFRCT AND PLAQUE QUANTIFICATION

Computed tomography coronary angiography (CTCA) provides detailed 3-dimensional images of cardiac anatomy. The use of iodinated contrast increases the difference in CT attenuation between target tissues and surrounding structures, improving image enhancement. With modern scanning protocols, detailed anatomical and morphological information can be gained and the development of automated software for plaque quantification as well as techniques to combine this with non-invasive fractional flow reserve provides the opportunity to gain detailed anatomical and functional information from a single scan.

2.4.1 IMAGE ACQUISITION

Computed Tomography Coronary Angiography was performed on a dual source CT scanner (Somatom, Siemens Medical Solutions, Forchheim, Germany). Unless contra-indicated, oral and/or intravenous beta blockade was administered to achieve a resting heart rate ≤70bpm prior to scanning. Sublingual nitroglycerin (0.4 or 0.8mg) was administered immediately prior to image acquisition. Where possible, images were acquired using prospective ECG-gating following the administration of intravenous contrast (Omnipaque or Visipaque, GE Healthcare, New Jersey). Images were acquired using retrospective ECG- gating with dose modulation if heart rate control was suboptimal. Scanning parameters included: tube voltage of 120 or 100 kVp (the latter used in patients with weight <200 pounds or BMI < 30 kg/m²), 0.6-mm slice thickness, 0.3-mm slice increment, 250-mm field-of-view, and 512 × 512 matrix.

CTCA images were transferred to an external core laboratory for calculation of FFRCT, which was performed as previously described (*Heartflow, Inc; Redwood City, USA*). (146) Briefly, computational fluid dynamics is applied to an anatomic model of the coronary arteries and using a mathematical model of coronary physiology to generate a non-invasive measure of fractional flow reserve. (146)

2.4.2 IMAGE ANALYSIS

Coronary artery plaque quantification was performed using semi-automated software (Autoplaque, Cedars Sinai Medical Center, Los Angeles, USA) by four trained observers who were blinded to the CTCA and FFRCT results. Proximal and distal limits of coronary arteries were manually defined, and coronary artery centrelines were

extracted using a semiautomated method. A circular region of interest was delimited in the proximal ascending aorta to define reference blood pool attenuation. The coronary vessel lumen, wall and plaque components including calcified plaque, non-calcified plaque and low-attenuation plaque were automatically identified using scan-specific thresholds. Manual adjustments were made by the operator as required. Plaque quantification using this technique has previously demonstrated excellent intra-observer, inter-observer and scan-rescan reproducibility (Spearman's Rho 0.87-0.99). (43, 44)

2.5 CT CALCIUM SCORING

Computed tomography (CT) uses X-rays to generate cross-sectional images of the body due to the differences in photon attenuation of different tissue classes. Attenuation coefficients can be transformed to Hounsfield Units (HU) which provides a quantitative scale to measure radiodensity. Calcification can be quantified on CT by the widely used Agatston method. (31) This applies a density threshold of 130 HU and an area threshold of $\geq 1 mm^2$ to create a score by applying an arbitrary weighted density score for each range of Hounsfield Units as follows; 1 for 130-199 HU; 2 for 200-299 HU; 3 for 300-399 HU and 4 for ≥400 HU. The Agatston score is then generated by multiplying the calcium density score by the area to provide a total score in Agatston Units (AU). (31)

2.5.1 CORONARY CALCIUM SCORING

Coronary calcification was quantified using dedicated analysis software (Vitrea Advanced, Vital Images, Minnetonka, USA). All analyses were performed in the

transverse plane. Calcium was quantified from the origin of the right coronary artery and left main stem to include each of the three main epicardial arteries (right coronary artery, left coronary artery and left circumflex artery) and their main branches. Coronary stents were excluded from analysis. Reproducibility of this technique has previously been described. (147, 148)

2.5.2 AORTIC VALVE CALCIUM SCORING

Aortic valve calcification was quantified using dedicated analysis software (Vitrea Advanced, Vital Images, Minnetonka, USA) in the transverse plane. Calcium was quantified from the base of the valve to the superior border of the valve before the ascending aorta. In cases in which confluent calcium extended into the ascending aorta, the origin of the left coronary artery was set as the most rostral slice beyond which further calcium was excluded. Efforts were made to exclude calcium from nearby structures such as the mitral valve annulus and coronary arteries. (Figure 2.1)

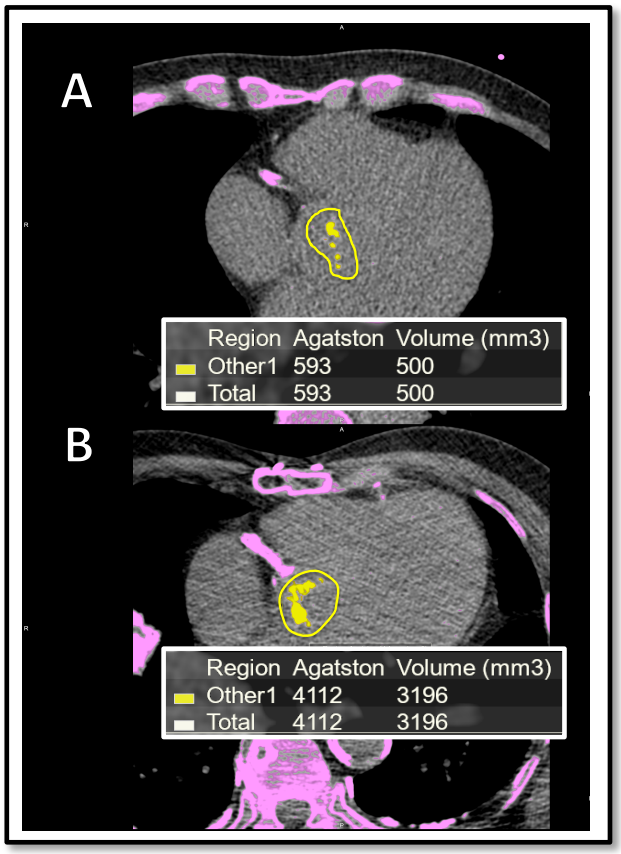

Figure 2.1. Computed Tomography calcium scoring of the aortic valve.

Computed Tomography calcium scoring performed on contiguous slices of the aortic valve in the transverse plane. Examples from patients with mild (A) and severe (B) aortic stenosis are shown. All calcium is highlighted in pink. Contours are then drawn around calcium in the aortic valve which then turns yellow once selected. An overall score in Agatston Units and a calcium volume are then generated.

2.6 PET-CT

Combined Positron Emission Tomography Computed Tomography (PET-CT) provides a unique insight into disease activity in cardiovascular disease. Following intravenous injection, radioactive ligands targeted against a specific disease process

accumulate and can provide a map of disease activity within the body which can be localised by anatomical information gained from computed tomography.

2.6.1 IMAGE ACQUISITION AND RECONSTRUCTION

The radiotracer ^{18}F-fluoride was produced by the radiopharmaceutical department and Edinburgh Clinical Research Imaging Centre and underwent quality control checks prior to its use for scanning. Participants were administered a target dose of 250 MBq ^{18}F-fluoride (in those undergoing coronary PET-CT) or 125 MBq ^{18}F-fluoride (in those undergoing PET-CT of the aortic valve) intravenously and rested in a lead-lined uptake room for sixty minutes. Dynamic imaging has demonstrated that sixty minutes circulating time provides peak radiotracer and target association and optimal contrast between plasma and vascular tissues. (62) Prior to the scan, participants were requested to empty their bladder in designated toilets. In the absence of any contraindications, patients were administered oral or intravenous beta-blockade to achieve a resting heart rate <65 bpm. For coronary imaging, participants were administered 400micrograms sublingual glyceryl trinitrate immediately prior to image acquisition unless contraindicated.

All imaging was performed on a hybrid scanner (for participants in Edinburgh - 64-multidetector Biograph mCT, Siemens Medical Systems, Erlangen, Germany and for participants in Los Angeles - GE Discovery 710) in a single bed position. An attenuation correction CT scan was performed prior to thirty minutes ECG-gated PET in list mode. This was immediately followed by ECG-gated non-contrast CT calcium scanning and contrast-enhanced CTCA at end expiration. CTCA was acquired in the diastolic phase with prospective ECG gating where possible, but wider scanning

windows or retrospective gating were employed in cases where the resting heart rate remained suboptimal.

PET data were reconstructed into four cardiac gates and the diastolic phase (gate 3, corresponding to 50-75% of the R-R interval) was used for primary analysis. For chapters 4 and 7, PET images were reconstructed using an Ordered Subsets Expectation Maximisation (OSEM) algorithm applying time of flight and point-spread function modelling (Siemens Ultra-HD) with the following parameters; 2 iterations, 21 subsets, 256x256 matrix size and 5mm Gaussian smoothing). Corrections were applied for attenuation, dead time, scatter and random coincidences. For chapter 5, different methods of image reconstruction were employed, and these are described fully in the respective chapter.

Cardiac motion correction was performed to compensate for coronary arterial motion during each phase of the cardiac cycle. Registration of all gates of PET data was performed using anatomical data from CTCA and aligning all PET gates with the end-diastolic position. Coronary artery centrelines were first extracted using semi-automated software (Autoplaque, Cedars Sinai Medical Centre) and the centreline co-ordinates were transferred to the PET data to extract 3-dimensional volumes of interest defined by a 20mm radius around each centreline. A diffeomorphic mass-preserving image registration algorithm was applied to align all gates of PET data with the end-diastolic phase, creating a new static image volume which utilised all PET counts. This technique has been shown to reduce image noise and improve discrimination of culprit coronary plaques. (149, 150) An overview of the motion-correction technique is shown in Figure 2.2.

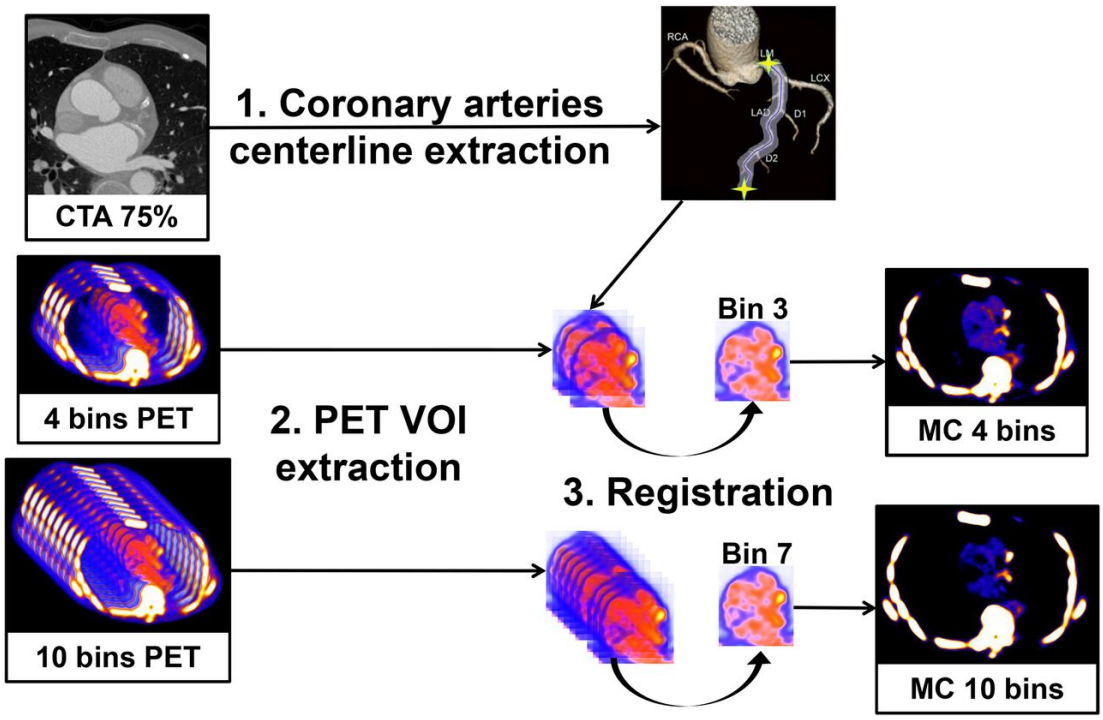

Figure 2.2. Overview of the motion correction method.

(1) Coronary artery centrelines are extracted from CTCA in end-diastolic phase using CTCA analysis software. **(2)** Volumes of interest surrounding coronary arteries are extracted from 4- and 10-bin PET data using previously extracted CTCA centrelines. **(3)** All bins of data are registered to the common end-diastolic reference bin (bins 3 and 7 for 4- and 10-bin data, respectively) by nonlinear level-set registration restricted to coronary regions. Then, registered VOIs are inserted back into their original PET volumes, and all registered PET images are summed into a single volume to obtain motion-corrected 4- and 10-bin data. MC = motion-corrected; VOI = volume of interest. (*Rubeaux M et al, J Nucl Med 2016;57:54-59*) (74)

2.6.2 IMAGE ANALYSIS

2.6.2.1 Coronary artery PET

Careful co-registration of PET and CTCA was performed in three anatomical planes

(transverse, sagittal and coronal) using anatomical structures on the contrast-enhanced

CT, including the ascending and descending aorta and myocardium to align the PET data with the cardiac chambers.

Coronary artery plaques were deemed positive if there was focal radiotracer accumulation which co-localised to an atherosclerotic plaque on coronary CT angiography and followed the course of the coronary artery >5 mm in transverse, sagittal and orthogonal views. Where visual uptake was identified, semi-quantitative analysis was performed by drawing 2-dimensional regions of interest on the transverse images and quantifying the maximum standardised uptake value (SUVmax) for that lesion. In each participant, SUVmax was also quantified in a proximal coronary atherosclerotic plaque without visual evidence of radiotracer localisation as a reference. Background blood pool activity was quantified by measuring activity in the right atrium within 2-cm radius regions of interest on three consecutive slices. Tissue-to-background ratios (TBRs) were calculated by dividing plaque SUVmax values by mean average SUV values in the right atrium. Coronary plaques were considered PET-positive in the presence of focal radiotracer uptake localised to a plaque with a tissue-background ratio greater than 1.25, as described previously. (55) Image analysis was performed using an OsiriX workstation (OsiriX version 3.5.1 64-bit; OsiriX Imaging Software, Geneva, Switzerland) or FusionQuant software (Cedars Sinai Medical Center, Los Angeles, California).

2.6.2.2 Aortic valve PET

As described for coronary PET analysis, careful co-registration of PET and CTCA was performed in three anatomical planes (transverse, sagittal and coronal) using anatomical structures on the contrast-enhanced CT, including the ascending and

descending aorta and myocardium to align the PET data with the CT. The fused images were reoriented into the plane of the aortic valve to create an *en-face* image of the aortic valve. Three dimensional regions of interest were drawn around the aortic valve at the area of the most diseased segment by creating a three-dimensional polygon with a height of 6mm. A three-dimensional region of interest measuring $2mm^3$ was created in the right atrium at the level of the right coronary ostia to measure background blood pool activity. Tissue to background ratios (TBRs) were calculated by dividing the valve SUVmean by the SUVmean of the right atrium (TBRmean) and SUVmax of the aortic valve by the SUVmean of the right atrium (TBRmax). Image analysis was performed using FusionQuant software (Cedars Sinai Medical Center, Los Angeles, California).

2.7 PET-MRI

The combination of PET imaging with magnetic resonance (MR) imaging in hybrid PET-MR platforms provides some advantages over PET-CT. PET and MR data can be acquired simultaneously enabling accurate co-registration and with much lower radiation doses. Further, magnetic resonance imaging may provide detailed tissue characterisation and functional imaging.

2.7.1 IMAGE ACQUISITION AND RECONSTRUCTION

Combined PET-MR imaging was performed on a hybrid scanner (Biograph mMR scanner, Siemens, Erlangen, Germany). The participant was injected with 212 MBq ^{18}F-sodium fluoride and rested in a quiet environment. MR image acquisition began 20 minutes later and included standard short axis cine views to evaluate left ventricular

function, contrast-enhanced MR angiography acquired in diastole and late gadolinium enhancement imaging for assessment of midwall fibrosis or myocardial scar. PET acquisition began sixty minutes following radiotracer injection and was acquired in list mode simultaneously with MR acquisition for sixty minutes.

2.7.2 IMAGE ANALYSIS

Image analysis of PET-MR was performed as described for PET-CT.

2.8 ETHICAL CONSIDERATIONS

All studies were approved by the local review board. For research conducted at Cedars Sinai Medical Center, the studies were approved by the Institutional Review Board (IRB). For studies conducted in Edinburgh, research was approved by the Research and Development Department within the University of Edinburgh and the South-East Scotland Ethics Committee. The SALTIRE 2 study and the DIAMOND study were each a Clinical Trial of an Investigational Medicinal Product (CTIMP) and were therefore approved by the Medicines and Healthcare products Regulatory Agency (MHRA). Studies performed in Edinburgh were also approved by the United Kingdom Administration of Radiation Substances Advisory Committee.

All study participants provided written informed consent prior to taking part in any study procedures.

2.9 STATISTICAL ANALYSIS

Details of specific statistical methods are described fully in each individual results chapter. Statistical analyses were performed using SPSS statistics (IBM, versions 22 and 23), Stata software version 13 (StataCorp, College Station, TX, USA) and R version 3.5.0 (R Foundation for Statistical Computing, Vienna, Austria). Continuous variables were assessed for normality using Shapiro Wilks test and expressed as mean ± standard deviation or median [interquartile range] as appropriate. Correlations between continuous variables were assessed with Pearson's R or Spearman's Rho subject to normality of the relevant variables. Statistical significance was considered as a two-tailed $p<0.05$.

CHAPTER 3

Non-invasive Fractional Flow Reserve and Coronary Plaque Burden

Published in:

Doris MK*, Otaki Y*, Arnson Y, Tamarappoo B, Goeller M, Gransar H, Wang F, Hayes S, Friedman J, Thomson L, Slomka P, Dey D, Berman D. Non-invasive fractional flow reserve in vessels without severe obstructive stenosis is associated with coronary plaque burden. *J Cardiovasc Comput Tomogr* 2018;12(5):379-384

**Equal contribution as first author*

Chapter 3 Non-invasive Fractional Flow Reserve and Coronary Plaque Burden

3.1 SUMMARY

Background

Non-invasive fractional flow reserve derived from coronary CT angiography (FFRCT) has been shown to be predictive of lesion-specific ischaemia as assessed by invasive fractional flow reserve (FFR). However, in practice, clinicians are often faced with an abnormal distal FFRCT in the absence of a discrete obstructive lesion. Using quantitative plaque analysis, we sought to determine the relationship between an abnormal whole vessel FFRCT (V-FFRCT) and quantitative measures of whole vessel atherosclerosis in coronary arteries without obstructive stenosis.

Methods

FFRCT was measured in 155 consecutive patients undergoing coronary CTA with ≥25% but less than 70% stenosis in at least one major epicardial vessel. Semi-automated software was used to quantify plaque volumes (total plaque [TP], calcified plaque [CP], non-calcified plaque [NCP], low-density non-calcified plaque [LD-NCP]), remodelling index [RI], maximal contrast density difference [CDD] and percent diameter stenosis [%DS]. Abnormal V-FFRCT was defined as a minimum value of ≤0.75 across the vessel.

Results

Vessels with abnormal V-FFRCT had higher per-vessel TP (554 vs 331 mm^3), CP (59 vs 25 mm^3), NCP (429 vs 295 mm^3), LD-NCP (65 vs 35 mm^3) volume and maximum CDD (21 vs 14%) than those with normal V-FFRCT (median, $p<0.05$ for all). Using a multivariate analysis to adjust for CDD and %DS, all measures of plaque volume were predictive of abnormal V-FFRCT (OR 2.09, 1.36, 1.95, 1.95 for TP, CP, NCP and LD-NCP volume, respectively; $p<0.05$ for all).

Conclusions

Abnormal V-FFRCT in vessels without obstructive stenosis is associated with multiple markers of diffuse non-obstructive atherosclerosis, independent of stenosis severity. Whole vessel FFRCT may represent a novel measure of diffuse coronary plaque burden.

3.2 INTRODUCTION

The emergence of non-invasive FFR, derived from coronary computed tomography angiography (FFRCT), has been an important advance in combining detailed information regarding anatomy and physiology using coronary CT angiography (CTA) in a single standard examination, with no need for repeat contrast injection, additional radiation, or pharmacologic stress.

FFRCT has been demonstrated to predict invasive FFR (46-48) and improve diagnostic specificity in the detection of hemodynamically significant coronary lesions compared to coronary computed tomography angiography (CTA) alone. (46)

Quantitative plaque analysis from coronary CTA can allow the measurement of plaque volume and composition in specific lesions and whole vessels, providing detailed information about plaque burden and adverse plaque characteristics. Such methods have been used to investigate the impact of adverse plaque characteristics on FFRCT and myocardial ischaemia, demonstrating that the presence of large plaque volume and adverse plaque characteristics, such as positive remodelling and a lipid core, can allow the identification of ischaemia-inducing lesions, independent of the degree of stenosis. (151-153) In clinical practice, we have observed that FFRCT often becomes abnormal in only the distal portion of vessels. The significance of this finding and its relationship to diffuse epicardial disease is unknown. We hypothesized that whole vessel FFRCT (V-FFRCT) may reflect whole vessel plaque burden in vessels without severe stenosis.

3.3 METHODS

3.3.1 STUDY POPULATION

One hundred and fifty-five patients who underwent clinically indicated coronary CTA at Cedars Sinai Medical Centre between February and October 2016 with at least 25% stenosis in one major epicardial vessel were included. FFRCT was calculated as previously described *(Heartflow, Inc; Redwood City, CA, USA)*. (146) Patients with prior coronary stent implantation, coronary artery bypass surgery or inadequate CTA image quality for FFRCT processing were excluded from the analysis**.** The study protocol was approved by the Cedars-Sinai Institutional Review Board and all patients provided written informed consent.

3.3.2 CORONARY COMPUTED TOMOGRAPHY ANGIOGRAPHY ACQUISITION

Coronary CTA was performed on a dual-source CT scanner (Somatom, Siemens Medical Solutions, Forchheim, Germany). When necessary, oral and/or intravenous metoprolol was administered to achieve a target heart rate of ≤70 beats/min (bpm). (154) Immediately prior to scanning, 0.4 or 0.8 mg of sublingual nitroglycerin (ScielePharma, Alpharetta, Georgia) was administered. Images were acquired with prospective ECG-gating following the administration of 85ml intravenous contrast (Omnipaque or Visipaque, GE Healthcare, Princeton, New Jersey). In the event of suboptimal heart rate control, images were acquired using helical scanning with dose modulation. Scanning parameters included: tube voltage of 120 or 100 kVp (the latter

used in patients with weight <200 pounds or BMI < 30 kg/m^2), 0.6-mm slice thickness, 0.3-mm slice increment, 250-mm field-of-view, and 512 × 512 matrix.

3.3.3 QUANTITATIVE CORONARY PLAQUE ANALYSIS

Coronary segments ≥2 mm with visible plaque were analysed along the entire length of the coronary arteries using semi-automated software (AutoPlaque version 9.7, Cedars-Sinai Medical Center, Los Angeles, CA, USA). Four experienced readers (Y.O, M.D, Y.A and B.K.T) who were blinded to the coronary CTA findings and FFRCT values analysed 365 vessels with visible coronary plaque using multiplanar coronary CTA images. Percent diameter stenosis (%DS) was calculated by dividing the narrowest lumen diameter by the mean of two non-diseased reference points. Scan-specific thresholds for non-calcified plaque (NCP) and calcified plaque (CP) were automatically generated. Low-density non-CP (LD-NCP) was defined as plaque with attenuation <30 Hounsfield units. Plaque components were quantified within the manually designated areas using adaptive algorithms. (45) Remodelling index was determined as the ratio of maximum vessel area to that at the proximal normal reference point. (155) Plaque length (in mm) was the length of the diseased vessel as computed in AutoPlaque. Contrast density difference across the lesion was computed as follows: the luminal contrast density, defined as attenuation per unit area, similar to area gradient, (156) was computed over 1-mm cross sections of the arterial segment. The contrast density difference was defined as the maximum percent difference in contrast density compared to a proximal reference cross section without atherosclerotic disease. Manual adjustments of vessel contours were made if necessary. For each artery, whole vessel plaque volume measurements were obtained

by the sum of plaque volumes in each segment of the three major epicardial coronary vessels (left anterior descending, left circumflex and right coronary arteries).

Plaque analysis was performed on a per-vessel basis after excluding vessels with severe obstructive stenosis (%DS ≥70), as the V-FFRCT values would be expected to be dominated by the presence of obstructive stenosis in these patients. The time required for whole vessel quantitative plaque analysis was approximately 10 minutes per vessel.

3.3.4 COMPUTATION OF FRACTIONAL FLOW RESERVE DERIVED FROM CORONARY COMPUTED TOMOGRAPHY ANGIOGRAPHY

Computation of FFRCT was performed centrally by independent blinded analysts (software version 1.4). The FFRCT computation process has previously been described in detail. (46, 146) Briefly, non-invasive fractional flow reserve (FFRCT) applies computational fluid dynamics to calculate the drop in coronary pressure across a stenosis as a ratio to pressure in a non-diseased artery, thereby acting as a surrogate measure of ischaemia.

In each subject, FFRCT measurements were computed throughout the coronary tree. The distal minimum values for each entire coronary vessel (V-FFRCT) were included in the analysis. A whole vessel FFRCT ≤0.75 was considered abnormal. If the FFRCT could not be calculated due to small vessel calibre or poor image quality, the vessel was excluded from analysis. A case example illustrating quantitative plaque analysis and V-FFRCT measurements is shown in Figure 3.1.

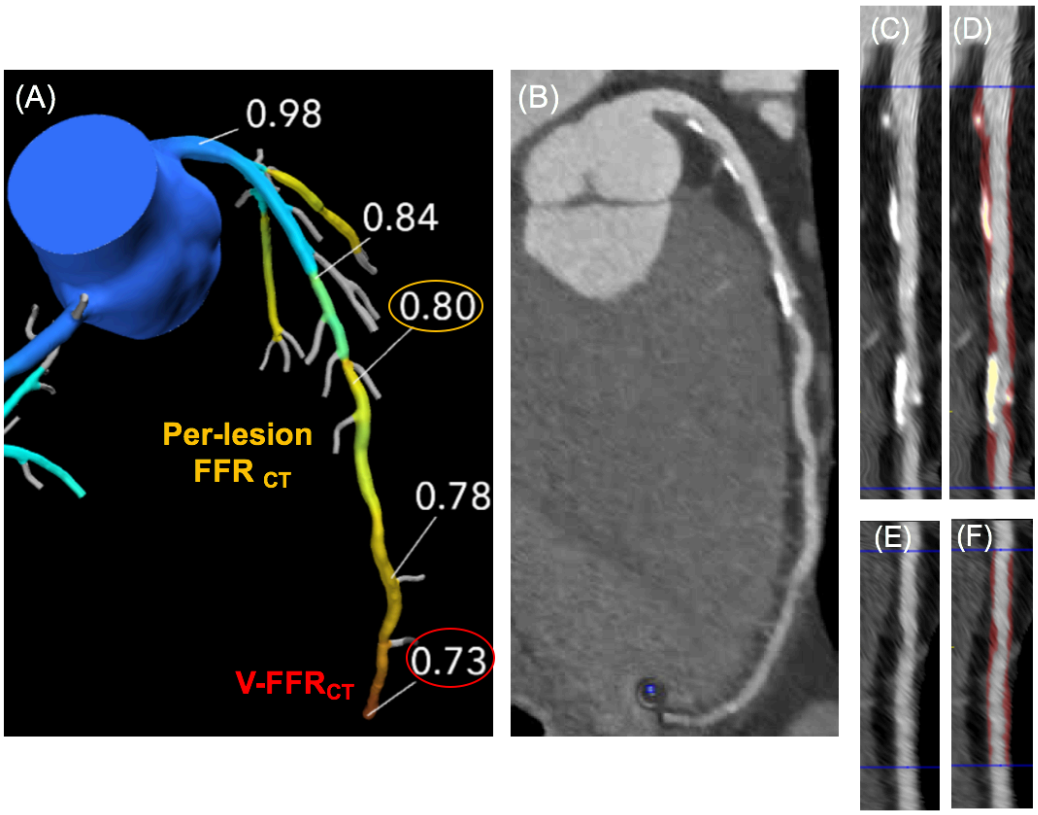

Figure 3.1 A case example of a 52 year old asymptomatic male with risk factors for coronary artery disease.

CTCA demonstrates diffuse plaque in the proximal to distal portions of the left anterior descending coronary artery (LAD) (A). FFRCT was computed in the LAD and the results demonstrate an FFRCT value of 0.80 across the region of maximal stenosis and a distal V-FFRCT value (whole vessel FFRCT) of 0.73 (B). Quantitative plaque analysis was performed using AutoPlaque (C & D: proximal to mid LAD and E & F: mid to distal LAD) and demonstrated total non-calcified plaque (760 mm^3, red), total calcified plaque (67mm^3, yellow), total low-density non-calcified plaque (48 mm^3), maximum remodelling index 1.6, maximum contrast density difference 30% and maximum diameter stenosis 47%.

3.3.5 STATISTICAL ANALYSIS

Continuous variables were presented as mean +/- standard deviation (SD) or median (interquartile range) as appropriate, after being assessed for normality using the Shapiro-Wilks test. Categorical variables were expressed as numbers and percentages. Quantitative plaque parameters across >2 groups were compared using the Kruskal-Wallis test; categorical variables were compared across groups using Pearson Chi-square test or Fisher Exact test for cell counts < 6. The relationship between plaque volume (TP, CP, NCP and LD-NCP) and abnormal V-FFRCT was evaluated after adjusting for contrast density difference, and diameter stenosis, using logistic regression analysis. To account for collinearity in measurements of plaque volume, different multivariate models were used to assess the relationship between V-FFRCT and TP, CP, NCP and LD-NCP. Four different multivariable analyses were performed using logistic regression adjusted for CDD and diameter stenosis to investigate the association between abnormal V-FFRCT and TP, CP, NCP and LD-NCP volumes, respectively. Because up to three coronary arteries were examined per patient, intraclass coefficients were calculated to assess the within-patient correlations, as previously described. (157) For logistic regression analyses, the standard errors were then adjusted using the clustered sandwich estimator to take into account the within-group correlations of up to 3 coronary arteries per patient. (158) Statistical analyses were performed with Stata software version 13 (StataCorp, College Station, TX, USA) and SPSS version 22 (IBM Corp, USA). Two-sided P-values <0.05 were considered statistically significant.

3.4 RESULTS

3.4.1 PATIENT CHARACTERISTICS AND VESSELS ANALYSED

Baseline characteristics of the study population are shown in Table 3.1. From a total of 465 vessels in 155 patients, 168 vessels were excluded from the analysis. This included 100 vessels with no visible plaque, 54 vessels with quantitative diameter stenosis >70%, and 25 vessels in which FFR_{CT} could not be processed due to small vessel calibre. Of the remaining 297 vessels included in the analysis, 122 (41%) comprised the left anterior descending coronary artery, 80 (27%) the left circumflex coronary artery, and 95 (32%) the right coronary artery.

Table 3.1. Baseline characteristics.

Baseline Characteristics	
Number of patients	155
Age, years (mean ± SD)	66±10
Male, n (%)	113 (73)
Body mass index, kg/m^2 (mean ± SD)	27±5
Risk factors and history of coronary artery disease	
Diabetes, n (%)	27 (17)
Hypertension, n (%)	81 (52)
Hyperlipidaemia, n (%)	110 (71)
Current smoker, n (%)	11 (7)
Previous myocardial infarction, n (%)	2 (1)
Symptoms	
Typical angina, n (%)	8 (5)
Atypical angina, n (%)	12 (8)
Nonanginal chest pain, n (%)	45 (29)
Shortness of breath, n (%)	72 (46)
Asymptomatic, n (%)	55 (35)

SD= standard deviation

3.4.2 RELATIONSHIP BETWEEN QUANTITATIVE DIAMETER STENOSIS AND V-FFRCT

There were 32 vessels with abnormal V-FFRCT and 265 vessels with normal V-FFRCT. The quantitative diameter stenosis was significantly higher in vessels with abnormal V-FFRCT than in vessels with normal V-FFRCT (diameter stenosis [median, IQR]: 40%, 26-47% in abnormal V-FFRCT vs. 26%, 14-37% in normal V-FFR_{CT}, p=0.003, Figure 3.2). There was no difference in the frequency of vessels with

50-69% stenosis between the groups with normal and abnormal V-FFRCT (16% in abnormal V-FFRCT vs. 12% in normal V-FFRCT, p=0.61).

3.4.3 Relationship between plaque characteristics and V-FFRCT

Total plaque volume, CP volume, NCP volume, and LD-NCP volume were higher in vessels with abnormal V-FFRCT than in vessels with normal V-FFRCT ($p<0.005$ for all). Moreover, vessels with abnormal V-FFRCT had higher maximal CDD and plaque length compared to vessels with normal V-FFRCT ($p<0.005$ for both, Figure 3.2). There was no significant difference in remodelling index between vessels with normal and abnormal V-FFRCT (Figure 3.2).

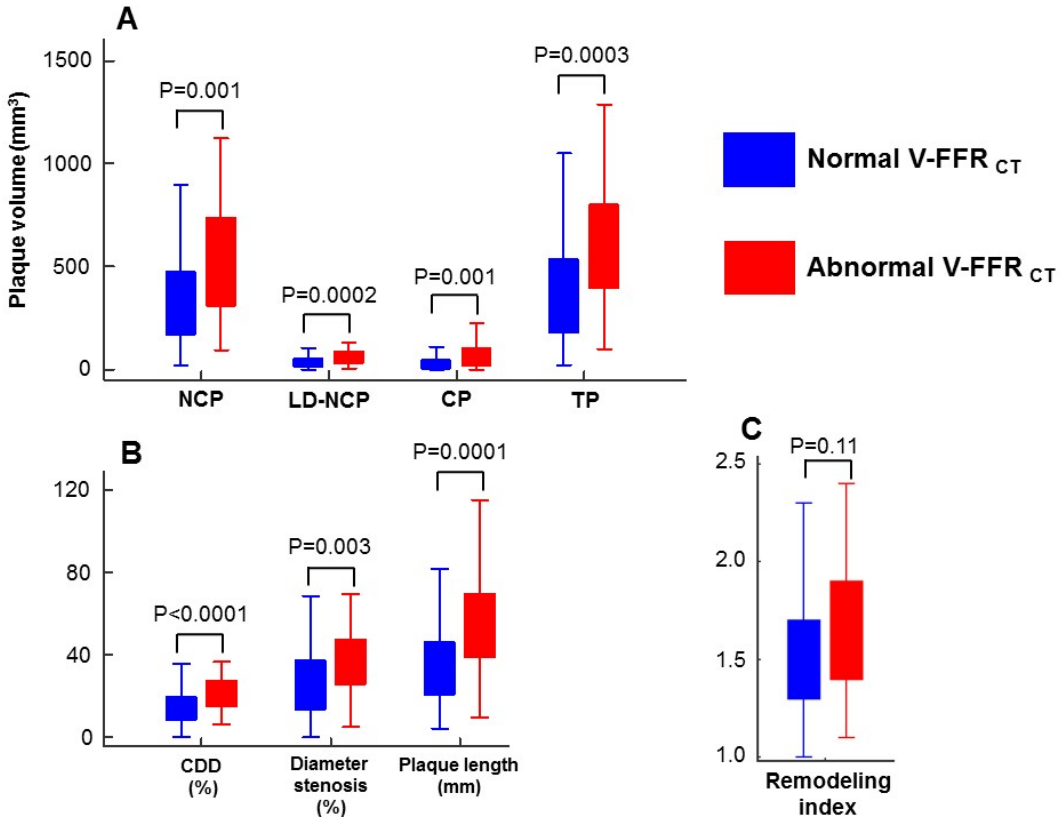

Figure 3.2. Differences in coronary plaque volume (A), contrast density difference, diameter stenosis and plaque length (B) and remodelling index (C) between vessels with normal and abnormal V-FFRCT.

Distributions of plaque volume and plaque subcomponents boxes indicate quartiles, and whiskers display adjacent values. V-FFRCT: whole vessel FFRCT, NCP: non-calcified plaque, LD-NCP: low-density non-calcified plaque, CP: calcified plaque, TP: total plaque, CDD: contrast density difference.

3.4.4 PLAQUE CHARACTERISTICS TO PREDICT ABNORMAL V-FFRCT

In univariate analysis to predict abnormal V-FFRCT, all measures of plaque volume (TP, CP, NCP, and LD-NCP), CDD, plaque length and diameter stenosis were independent predictors of an impaired V-FFRCT (Table 3.2). In multivariate analysis adjusting for CDD and diameter stenosis, the results demonstrated a significant association between abnormal V-FFRCT and log-transformed TP, CP, NCP and LD-NCP volumes (Odds ratio of TP volume: 2.09, 95% CI: 1.09 to 4.01, p=0.03, odds ratio for CP volume: 1.36, 95% CI: 1.01 to 1.84, p=0.04, odds ratio of NCP volume: 1.95, 95% CI: 1.02 to 3.75, p=0.04, odds ratio of LD-NCP volume: 1.95, 95%CI: 1.06 to 3.57, p=0.03, Table 3.3 Model 1-4). CDD was a significant predictor of an abnormal V-FFRCT in all multivariate models (Table 3.3 Model 1-4).

Table 3.2 Univariate logistic regression analysis of quantitative plaque features for ischaemia based on impaired whole vessel FFRCT.

	Odds ratio (95% CI)	P value
TP volume	2.03 (1.32-3.10)	0.001
CP volume	1.36 (1.11-1.67)	0.004
NCP volume	1.93 (1.26-2.94)	0.002
LD-NCP volume	2.00 (1.35-2.96)	0.001
Contrast density difference	3.35 (1.76-6.35)	<0.001
Diameter stenosis	1.03 (1.01-1.05)	0.006
Remodelling index	7.16 (0.99-51.50)	0.05
Plaque length	2.31 (1.40-3.79)	0.001

TP=total plaque, CP=calcified plaque, NCP=non-calcified plaque, LD-NCP= low-density-non-calcified plaque, CI=confidence interval

Table 3.3. Multivariate logistic regression analysis of quantitative plaque features for ischaemia based on impaired whole vessel FFRCT (297 vessels with stenosis <70% and 259 vessels with <50% stenosis).

	Maximum Diameter Stenosis <70% (n=297)		**Maximum Diameter Stenosis <50% (n=259)**	
	Odds Ratio (95% CI)	**P Value**	**Odds Ratio (95% CI)**	**P Value**
Model 1				
Total Plaque Volume	2.09 (1.09-4.01)	0.03	2.89 (1.26-6.63)	0.01
Contrast Density Difference	4.65 (1.77-12.22)	0.002	4.44 (1.46-13.44)	0.008
Diameter stenosis	…	0.29	1.70 (0.76-3.80)	0.20
Model 2				
Calcified Plaque Volume	1.36 (1.01-1.84)	0.04	1.67 (1.14-2.46)	0.009
Contrast Density Difference	3.90 (1.45-10.47)	0.007	4.11 (1.36-12.39)	0.01
Diameter Stenosis	1.56 (0.85-2.89)	0.15	2.11 (0.91-4.87)	0.08
Model 3				
Non-Calcified Plaque volume	1.95 (1.02-3.75)	0.04	2.40 (1.06-5.45)	0.04
Contrast Density Difference	4.82 (1.84-12.64)	0.001	4.63 (1.55-13.85)	0.006
Diameter Stenosis	**…**	0.29	1.72 (0.77-3.82)	0.18
Model 4				
Low Density Non-Calcified Plaque Volume	1.95 (1.06-3.57)	0.03	2.72 (1.33-5.58)	0.006
Contrast Density Difference	3.86 (1.46-10.22)	0.006	3.64 (1.27-10.43)	0.02
Diameter Stenosis	**…**	0.33	…	0.21

3.4.5 ASSOCIATION BETWEEN PLAQUE CHARACTERISTICS AND ABNORMAL V-FFRCT IN VESSELS WITH <50% STENOSIS

In vessels with a maximum diameter stenosis <50% (n=259), there were 27 vessels with abnormal V-FFRCT and 232 vessels with normal V-FFRCT. Multivariate analysis was performed using four models, as described above, to investigate the association between plaque volumes (TP, CP, NCP and LD-NCP) and abnormal V-FFRCT adjusting for CDD and diameter stenosis.

In vessels with a maximum diameter stenosis of less than 50%, the results also demonstrated a significant association between abnormal V-FFRCT and log-transformed TP, CP, NCP and LD-NCP volumes (Odds ratio for TP volume: 2.89, 95% CI: 1.26 to 6.63, p=0.01, odds ratio for CP volume: 1.67, 95% CI: 1.14 to 2.46, p=0.009, odds ratio of NCP volume: 2.40, 95% CI: 1.06 to 5.45, p=0.04, and odds ratio of LD-NCP volume: 2.72, 95%CI: 1.33 to 5.58, p=0.006, Table 3.3 Model 1-4). CDD remained a significant predictor for an abnormal V-FFRCT in all four multivariate models (Table 3.3 Model 1-4).

3.5 DISCUSSION

Lesion-specific measures of non-invasive fractional flow reserve have been demonstrated to correlate well with invasive FFR and predict lesion-specific ischemia. In practice, however, an FFRCT value which drops only distally or exhibits a gradual decline across the length of a vessel is often observed, the relevance of which is unclear. Using semi-automated quantitative plaque analysis, we have shown that plaque volume and characteristics quantified on a per-vessel basis predict an abnormal FFRCT, suggesting that an abnormal V-FFRCT may reflect diffuse epicardial atherosclerosis.

A previous study has investigated the influence of diffuse non-obstructive atherosclerosis on distal FFR measured invasively and demonstrated that vessels with diffuse but angiographically insignificant disease exhibit a gradual and progressive decline in FFR across the length of the vessel. (159) This continuous drop in pressure on FFR was observed in half of the vessels with luminal irregularities but no visual stenosis on invasive angiography, while there was no distal decline in FFR in vessels without evidence of disease. Our results add further support to the finding that an impaired whole vessel fractional flow reserve may reflect diffuse atherosclerosis. Further, we have expanded these findings by evaluating plaque characteristics on CT and performing detailed plaque quantification. In our results, non-calcified plaque volume and low-density non-calcified plaque volume, a CT-identified surrogate measure of lipid core, were independent predictors of an impaired distal FFRCT. Indeed, both non-calcified plaque volume and low-density non-calcified plaque volume were stronger predictors of abnormal V-FFRCT than calcified plaque volume.

This relationship persisted even when all vessels with greater than 50% stenosis were excluded from analysis.

Recent studies have highlighted that lesion-specific plaque characteristics can influence fractional flow reserve, and lipid density has consistently been identified as a strong predictor of flow in lesion-specific analyses. (152, 160, 161) This relationship was extended to entire vessels in our study as demonstrated in our results which revealed lipid density to be an independent predictor of an abnormal whole vessel FFRCT in vessels without obstructive stenosis. This suggests that distal FFRCT may be reflective of the presence of, not only diffuse disease, but also adverse plaque features.

Previous studies have utilized intravascular ultrasound (IVUS) imaging to demonstrate that, in the early stages of atherosclerosis, endothelial dysfunction leads to abnormal endothelial reactivity and, even in minimal atherosclerosis, the presence of local endothelial dysfunction is closely associated with high-risk plaque characteristics including the presence of a lipid core. (162) The pathophysiological explanation for this finding is considered to be a consequence of the pro-inflammatory and oxidative effect exerted by the necrotic core which results in reduced nitric oxide bioavailability and an increase in local vasoconstriction by mediators such as isoprostane. (163, 164) It may therefore be hypothesized that an abnormal V-FFRCT relates to impaired vascular reactivity across the length of the vessel, although further studies are required to confirm this.

Our findings regarding the relationship between quantitative whole vessel plaque characteristics and whole vessel FFRCT are similar to relationships observed with

segmental plaque characteristics and lesion specific FFRCT. In patients with intermediate grade stenosis, we have previously shown that plaque burden on a per-patient basis is predictive of an abnormal invasive FFR. (152) In a study of 56 patients undergoing invasive coronary angiography and invasive FFR, total plaque burden was a significant predictor of impaired invasive FFR (Odds Ratio [OR] 1.15, P=0.007). (152) Further, in a study examining the relationship between plaque features and FFR, percent aggregate plaque volume (defined as the aggregate plaque volume divided by the total vessel volume) provided incremental prediction of ischaemia by invasive FFR when added to adverse plaque characteristics and CTA-measured stenosis. (161)

Another recent study examined the effects of diffuse atherosclerosis and, specifically, lesion length in all grades of stenosis and demonstrated that diffuse disease, as measured by lesion length, was an independent predictor of invasive FFR. (165) Our report, however, is the first to our knowledge to assess the impact of quantitative plaque volume, burden and composition in vessels with <70% stenosis on whole vessel FFRCT and suggests that distal whole vessel FFRCT is reflective of whole vessel plaque burden.

We excluded severe stenosis in our analysis because we expected an individual stenosis to impact on the distal FFRCT value. Nonetheless, even with this exclusion, the maximum contrast density difference was predictive of abnormal V-FFRCT. Of importance, this relationship was observed even when vessels with 50-69% stenosis were excluded. This highlights that the abnormal distal V-FFRCT values were not observed only as a direct consequence of a single proximal obstructive lesion.

Further, we adopted a threshold of less than or equal to 0.75 as indicative of an abnormal V-FFRCT. While this is lower than invasive FFR and FFRCT thresholds used in prior lesion-specific studies (160, 166), we wished to employ a value which would more reliably discriminate an abnormal distal pressure reserve. (167)

3.5.1 LIMITATIONS

While we have identified that diffuse non-obstructive disease and the presence of high-risk plaque characteristics predict an abnormal distal FFRCT, the relationship between abnormal V-FFRCT and tissue ischemia has not yet been documented. Future studies should consider the relationship between abnormal V-FFRCT and non-invasive measures of coronary flow or ischaemia, such as coronary flow reserve. Coronary flow reserve (CFR), measured by PET perfusion imaging, provides an integrated analysis of myocardial perfusion and the haemodynamic effects of both epicardial atherosclerosis and microvascular dysfunction in combination and could provide insight in this regard, particularly as a means of further understanding the relationship between microvascular dysfunction and non-obstructive coronary atherosclerosis in patients manifesting evidence of myocardial ischaemia without significant epicardial coronary stenosis.

3.6 CONCLUSION

Abnormal V-FFRCT in vessels without obstructive stenosis is associated with multiple markers of diffuse non-obstructive atherosclerosis, independent of stenosis severity. Whole vessel FFRCT may represent a novel measure of diffuse coronary plaque burden.

CHAPTER 4

Coronary ^{18}F-Fluoride Uptake and Progression of Coronary Artery Calcification

Published in;

Doris MK, Meah MN, Moss AJ, Andrews JPM, Bing R, Gillen R, Weir N, Syed M, Daghem M, Shah A, Williams MC, Beek EJR, Forsyth L, Dweck MR, Newby DE, Adamson PD. Coronary ^{18}F-Fluoride Uptake and Progression of Coronary Artery Calcification. Circulation Cardiovascular Imaging, 2020 (in press)

Chapter 4 Coronary ^{18}F-Fluoride Uptake and Progression of Coronary Artery Calcification

4.1 SUMMARY

Background

Positron emission tomography (PET) using ^{18}F-sodium fluoride (^{18}F-fluoride) to detect microcalcification may provide insight into disease activity in coronary atherosclerosis. This study aimed to investigate the relationship between ^{18}F-fluoride uptake and progression of coronary calcification in patients with clinically stable coronary artery disease.

Methods

Patients with established multivessel coronary atherosclerosis underwent ^{18}F-fluoride PET-computed tomography (CT) angiography and CT calcium scoring, with repeat CT angiography and calcium scoring at one year. Coronary PET uptake was analysed qualitatively and semi-quantitatively in diseased vessels by measuring maximum tissue-to-background ratio (TBRmax). Coronary calcification was quantified by measuring calcium score, mass and volume.

Results

In a total of 183 participants (median age 66 years, 80% male), 116 (63%) patients had increased ^{18}F-fluoride uptake in at least one vessel. Individuals with increased ^{18}F-fluoride uptake demonstrated more rapid progression of calcification compared to those without uptake (change in calcium score, 97 [39-166] versus 35 [7-93] AU;

p<0.0001). Indeed, the calcium score only increased in coronary segments with increased ^{18}F-fluoride uptake (from 95 [30-209] AU to 148 [61-289] AU; p<0.001) and remained unchanged in segments without ^{18}F-fluoride uptake (from 46 [16-113] to 49 [20-115] AU; p=0.329). Baseline coronary ^{18}F-fluoride TBRmax correlated with one-year change in calcium score, calcium volume and calcium mass (Spearman's ρ = 0.37, 0.38 and 0.46 respectively; p<0.0001 for all). At the segmental level, baseline ^{18}F-fluoride activity was an independent predictor of calcium score at 12 months (p<0.001). However, at the patient level, this was not independent of age, sex and baseline calcium score (p=0.50).

Conclusions

Coronary ^{18}F-fluoride uptake identifies both patients and individual coronary segments with more rapid progression of coronary calcification, providing important insights into disease activity within the coronary circulation. At the individual patient level, total calcium score remains an important marker of disease burden and progression.

4.2 INTRODUCTION

Atherosclerotic calcification is a complex pathophysiological process central to the development of advanced coronary artery plaques. Macroscopic coronary artery calcification can be quantified using computed tomography, serving as an important surrogate measure of atherosclerotic plaque burden and providing powerful prognostic information beyond traditional risk factors. (41, 168, 169) Furthermore, progression of coronary macrocalcification is associated with an increased risk of adverse cardiovascular events and all-cause mortality. (14, 32, 170)

The positron-emitting radiotracer ^{18}F-sodium fluoride (^{18}F-fluoride), commonly used to detect pathological metabolic activity in the skeletal system (66, 171), can provide important insights into calcification activity within the cardiovascular system. ^{18}F-Fluoride binds to hydroxyapatite in proportion to the surface area of exposed crystal, such that it binds preferentially to areas of newly developing microcalcification where the surface area is many fold higher than large macroscopic deposits. (62) Microcalcification is a key healing response in atherosclerotic plaque (62), closely associated with necrotic inflammation and high-risk disease, but ultimately leading to downstream coronary macrocalcification and plaque stabilisation. ^{18}F-Fluoride PET-CT therefore has the potential to act as a marker of disease activity in the coronary vasculature by targeting a biologically important stage of the disease. (17) Indeed, *ex vivo* studies have confirmed the exquisite sensitivity of ^{18}F-fluoride for early microcalcific deposits and its association with high-risk plaque features including macrophage infiltration and necrosis in atherosclerosis. (55, 172, 173)

Based on these principles, we hypothesised that coronary ^{18}F-fluoride PET-CT should predict the future progression of coronary macrocalcification detected on CT. We therefore prospectively investigated the relationship between *in vivo* coronary ^{18}F-fluoride uptake and the progression of coronary arterial calcification in patients with clinically stable coronary artery disease.

4.3 METHODS

4.3.1 STUDY DESIGN

This study is a pre-specified analysis of an investigator-initiated double-blind randomized controlled trial conducted at a single centre in Edinburgh, UK. (55) The study was approved by the local institutional review board, the Scottish Research Ethics Committee (REC reference: 14/SS/0089), Medicines and Healthcare products Regulatory Agency, and the United Kingdom (UK) Administration of Radiation Substances Advisory Committee. The study was performed in accordance with the Declaration of Helsinki and all patients provided written informed consent prior to any study procedures.

4.3.2 STUDY POPULATION

Patients with clinically stable multivessel coronary artery disease were recruited prospectively from the Edinburgh Heart Centre, UK, between March 2015 and March 2017. Patients were included if aged over forty years and with evidence of angiographically proven multivessel coronary artery disease, defined as at least two major epicardial vessels with any combination of either (a) >50% luminal stenosis, or (b) previous revascularization (percutaneous coronary intervention or coronary artery bypass graft surgery). Patients were excluded in the event of coronary revascularisation within the preceding 3 months or acute coronary syndrome within the previous 12 months. Patients were randomized (1:1) to receive ticagrelor or placebo in addition to aspirin therapy and the primary goal of the original study was to determine whether ticagrelor therapy, in addition to aspirin, reduces high-sensitivity

troponin I concentration in participants with high-risk coronary plaque. The primary study results have been previously reported. (143)

4.3.3 STUDY PROCEDURES

All participants underwent a baseline clinical assessment and combined ^{18}F-fluoride PET-CT scanning with the acquisition of a contrast-enhanced CT coronary angiogram and non-contrast CT for calcium scoring. Prior to scanning, participants with a resting heart rate >65 beats/min were administered oral beta-blockade (50-100 mg metoprolol) unless contraindicated. All participants were administered a target dose of 250 MBq intravenous ^{18}F-fluoride and rested in a quiet environment. Sixty minutes following injection, PET acquisition was performed on a hybrid PET-CT scanner (64-multidetector Biograph mCT, Siemens Medical Systems, Erlangen, Germany). Attenuation correction CT scans were performed prior to the acquisition of ECG-gated list-mode PET data using a single 30-min bed position centred on the heart. Finally, an ECG-gated coronary CT angiogram was performed in mid-diastole during held expiration following sublingual glyceryl trinitrate. Repeat coronary CT angiography and calcium scoring was performed using the same imaging protocol and on the same scanner at one year.

4.3.4 IMAGE ANALYSIS

Calcium scoring

Non-contrast CT images for calcium scoring were reconstructed in the transverse plane with 3-mm slice width and 1.5-mm increment. Coronary calcium was quantified on both a per-participant and per-segment level by an experienced observer using

dedicated software (Vitrea Advanced, Toshiba Systems). Calcification was quantified as calcium score (AU), calcium volume (mm^3) and calcium mass (mg). Calcium score was derived using the Agatston method. (31) To calculate calcium mass, a calibration factor was derived using a phantom to calculate equivalent water diameter, adjusted for body-mass index and lateral diameter and applied at a specified X-ray tube voltage (Table 4.1). (174) Coronary stents were excluded from the per-patient analysis by only including calcium proximal or distal to the border of the stented segment. For the per-segment analysis, only segments without stenting were selected as representative positive and negative segments.

Table 4.1. Calcium mass score calibration table.

Minimum and maximum equivalent water diameter (Dw) values were calculated from CT images of a phantom with and without an obese expansion ring. Body mass index (BMI) and lateral diameter were calculated from Dw as previously described. (174) Linear interpolation of calibration factor and anthropomorphic measurements was used between maximum and minimum values.

Equivalent water diameter Dw (mm)	Body-mass index	Lateral dimension (coronal) (mm)	Calibration factor at specified tube kilovoltage 120 kV
205	8.5	324	0.777
210	9.8	332	0.780
215	11.0	340	0.783
220	12.2	349	0.786
225	13.4	357	0.789
230	14.6	365	0.792
235	15.9	373	0.795
240	17.1	381	0.798
240	17.1	381	0.798
245	18.3	390	0.801
250	19.5	398	0.804
255	20.7	406	0.807
260	22.0	414	0.810
265	23.2	422	0.813
270	24.4	431	0.816
275	25.6	439	0.819
280	26.8	447	0.822
285	28.0	455	0.825
290	29.3	463	0.828
295	30.5	472	0.831
300	31.7	480	0.834
305	32.9	488	0.837
310	34.1	496	0.840
315	35.4	504	0.843
317	35.9	508	0.844

Coronary CT Angiography image analysis

Visual assessment of CT-defined high-risk plaque characteristics was performed by trained observers. The presence or absence of five plaque characteristics (positive remodelling, low attenuation plaque, the napkin ring sign, spotty calcification and punctate calcification) was documented on a segmental basis using a 15-segment model. (175) Positive remodelling was defined as a vessel diameter of 10% greater than a reference segment proximal to the plaque. (40) Low attenuation plaque was defined as a focal area of plaque with an attenuation density of <30 Hounsfield units. (176) Spotty calcification was defined as focal areas of arterial calcification with a maximum diameter <3mm. The 'napkin ring' side was defined as a central area of low attenuation plaque surrounded by a rim of high attenuation, as described previously. (177)

Coronary artery plaque quantification was performed on all non-stented segments with visible atherosclerotic plaque by a trained observer using semi-automated software (Autoplaque, Cedars Sinai Medical Center, Los Angeles, USA). Plaque components including remodelling index, calcified plaque, non-calcified plaque and low-attenuation plaque volume were quantified using scan-specific thresholds referencing blood pool attenuation from a circular region of interest created in the proximal ascending aorta. Manual adjustments were made as required. This technique has previously demonstrated excellent intra-observer, inter-observer and scan-rescan reproducibility. (43, 44)

Positron Emission Tomography image analysis

Positron emission tomography images were reconstructed in diastole (50-75% of the R-R interval, 2 iterations, 21 subsets, 5-mm Gaussian smoothing, Siemens Ultra-HD algorithm) and fused with contrast enhanced CT coronary angiography. Images were co-registered on three anatomical planes and qualitative and semi-quantitative analysis of coronary ^{18}F-fluoride uptake was performed by experienced observers. Coronary ^{18}F-fluoride PET-CT analysis and reproducibility have been reported previously. (174) In brief, visual assessment for increased coronary ^{18}F-fluoride uptake was performed on both a per-participant and per-segment level and deemed positive if there was focal radiotracer accumulation which co-localised to an atherosclerotic plaque on coronary CT angiography and followed the course of the coronary artery >5 mm in transverse, sagittal and orthogonal views. Where visual uptake was identified, semi-quantitative analysis was performed by drawing 2-dimensional regions of interest on the transverse images and quantifying the maximum standardised uptake value (SUVmax) for that lesion. In each participant, SUVmax was also quantified in a proximal coronary atherosclerotic plaque without visual evidence of radiotracer localisation as a reference. Background blood pool activity was quantified by measuring activity in the right atrium within 2-cm radius regions of interest on three consecutive slices. Tissue-to-background ratios were calculated by dividing plaque SUVmax values by mean average SUV values in the right atrium. Coronary plaques were considered PET-positive in the presence of focal radiotracer uptake localised to a plaque with a tissue-background ratio greater than 1.25, as described previously. (55) For the purpose of the per-segment analysis, participants were only included if there were both a PET-

positive and PET-negative plaque which was not stented (Figure 4.1). Participants in which the only PET-positive or PET-negative plaque was stented were excluded from per-segment analysis. Image analysis was performed using an OsiriX workstation (OsiriX version 3.5.1 64-bit; OsiriX Imaging Software, Geneva, Switzerland).

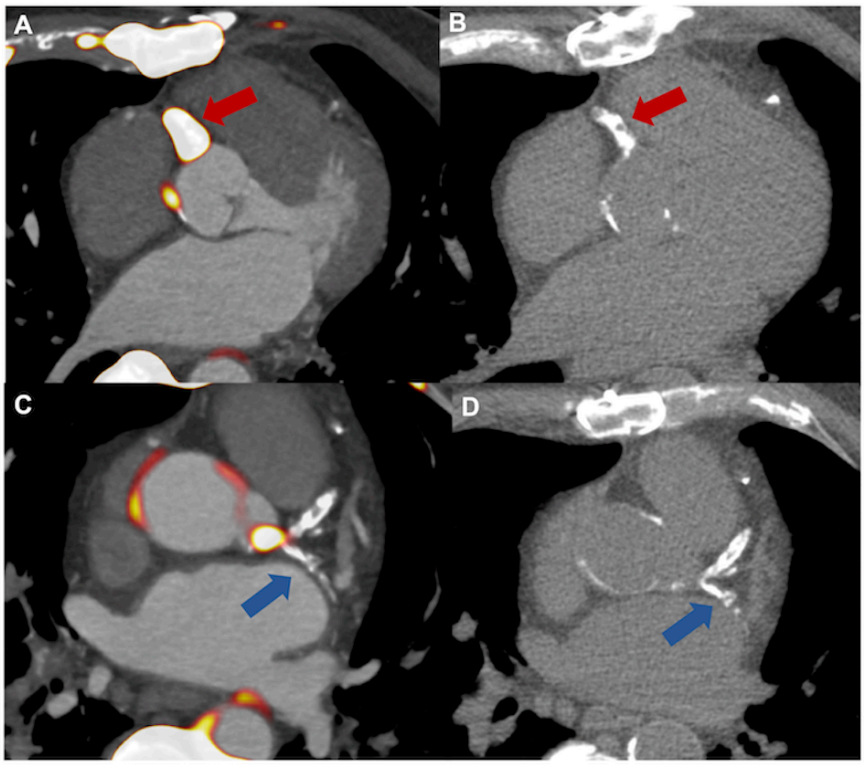

Figure 4.1. An example of per-segment PET-CTA and CT calcium scoring image analysis.

In this participant, the PET-positive segment was selected as the proximal right coronary artery which demonstrated increased ^{18}F-fluoride activity (A, red arrow). At baseline, the calcium score of this segment was 496 AU (B) and subsequently increased to 944 AU at 12 months. In this participant, the proximal left circumflex artery was selected as the PET-negative reference lesion (C, blue arrow). At baseline, the calcium score in this segment was 496 AU and subsequently increased to 616 AU at 12 months.

4.3.5 STATISTICAL ANALYSIS

Categorical variables are reported as number (%) and continuous variables as mean ± standard deviation for parametric or median [interquartile range] for non-parametric data. Continuous unpaired variables were compared using Student's T-test or the Mann Whitney U test where appropriate and paired variables compared using Student's *t*-test or the Wilcoxon matched-pairs signed-ranks test, dependent on normality. Categorical variables were compared using Chi Square tests. Logarithmic transformation (Ln[x+1]) was used to achieve normality of continuous variables. Two-tailed Pearson's correlation analysis was performed to investigate the relationship between continuous variables where normally distributed. Non-parametric continuous variables were compared using Spearman's rank correlation. To investigate the relationship between ^{18}F-fluoride activity and progression of coronary calcification at the patient level, linear regression was used with log transformation of the dependent variable. To investigate at the per-segment level, a linear mixed model was used with the participant as a random effect to adjust for repeated measurements within individuals. Using calcium mass at 12 months as the dependent variable, analysis of variance (ANOVA) was then used to compare two mixed models; model one using calcium mass at baseline, and model two using baseline calcium and segmental TBR as independent variables. Statistical analysis was undertaken using IBM SPSS Statistics 23 and R version 3.5.0 (R Foundation for Statistical Computing, Vienna, Austria). Statistical significance was considered as a two-sided p value <0.05.

4.4 RESULTS

4.4.1 BASELINE CHARACTERISTICS

A total of 185 participants underwent combined PET-CT angiography and CT calcium scoring at baseline and follow-up (mean age 65±8, 80% male; Figure 4.2). For the purposes of this analysis, we excluded participants who underwent coronary revascularisation during the course of the trial with implantation of a coronary stent within a previously unstented coronary segment (n=2). Coronary revascularisation decisions were made by the attending clinician independent of the research study team or knowledge of the PET-CT scan findings. Of the participants who underwent percutaneous coronary intervention, both had evidence of increased ^{18}F-fluoride activity. One participant underwent stenting to the left anterior descending artery and left circumflex artery, and the other underwent stenting to the left anterior descending artery. All three lesions showed obstructive stenosis on baseline san (70-99% stenosis) and two of three had high-risk plaque features (positive remodelling and spotty calcification). In the remaining eligible participants (n=183), there was a high prevalence of cardiovascular risk factors, of which 69% (n=126) had a history of acute coronary syndrome, 81% (n=148) of participants had previous percutaneous coronary intervention and the majority 96% (n=175) were on statin therapy (Table 4.2).

Of the 183 participants included in this analysis, 63% (n=116) patients had evidence of increased ^{18}F-fluoride uptake in at least one vessel (*PET-positive*). The PET-positive cohort was predominantly male (89%, n=103 *versus* 64%, n=43; p<0.001), with a

higher prevalence of prior coronary artery bypass graft surgery (28%, n=33 versus 6%, n=4; $p<0.001$).

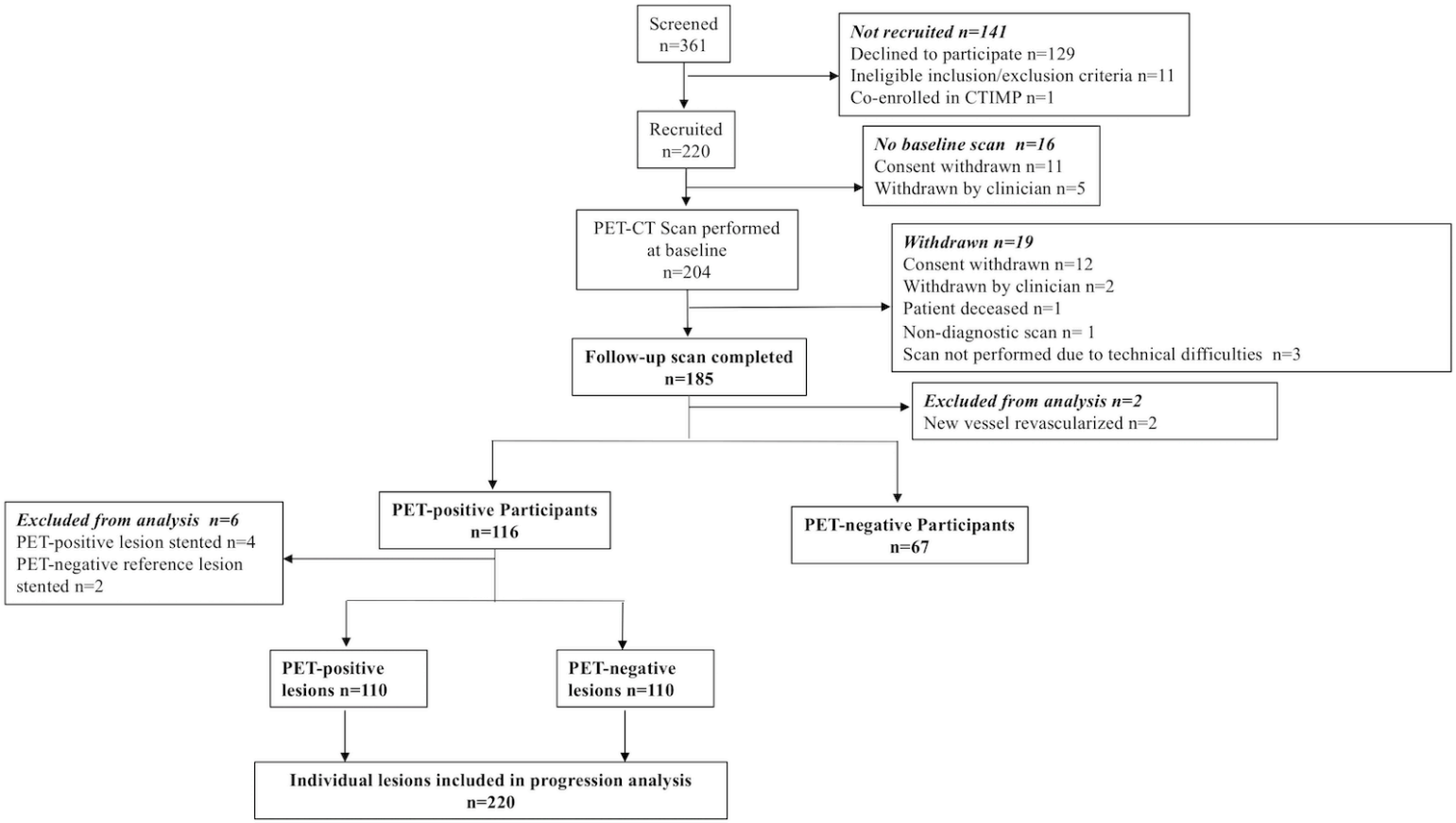

Figure 4.2 Consort diagram.

Table 4.2. Baseline characteristics.

	All patients n=183	**PET positive n=116**	**PET negative n=67**	**P value**
Male gender	146 (80)	103 (89)	43 (64)	**<0.001**
Age, years	66[59-71]	67[61-73]	65[57-70]	**0.02**
BMI (kg/m^2)	29.5	29.3	29.9	0.35
Medical History				
Current Smoker	24 (13)	12 (10)	12 (18)	0.14
History of acute coronary syndrome	126 (69)	80 (69)	46 (69)	0.97
Percutaneous Coronary Intervention	148 (81)	93 (80)	56 (84)	0.48
Coronary Artery Bypass Grafting	37 (20)	33 (28)	4 (6)	**<0.001**
Hypertension	101 (55)	65 (56)	36 (54)	0.76
Hypercholesterolaemia	177 (97)	112 (97)	65 (97)	1.0
Diabetes Mellitus	32 (17)	22 (19)	10 (15)	0.58
Prior Stroke/Transient Ischemic Attack	4 (2)	3 (3)	1 (1)	1.0
Medications				
Aspirin	183 (100)	116 (100)	67 (100)	
Statin	175 (96)	110 (95)	65 (97)	0.71
Beta-Blocker	124 (68)	78 (67)	46 (69)	0.84
Angiotensin Converting Enzyme Inhibitor/Angiotensin II Receptor Blocker	138 (75)	86 (74)	52 (78)	0.60
Biochemistry				
Haemoglobin, g/dL	14.0±1.2	14.0±1.2	14.0±1.3	0.87
Creatinine, µmmol/L	80 ± 13	80±12	80 ± 13	0.89
Total Cholesterol, mg/dL	162±39	162±39	159±31	0.33
High density lipoprotein, mg/dL	46±12	46±12	43±12	0.46
Low density lipoprotein, mg/dL	85±31	89±31	81±27	0.14
Triglycerides, mg/dL	151±89	1.7±1.2	1.7±0.8	0.79

4.4.2 BASELINE ^{18}F-FLUORIDE ACTIVITY AND PER-PARTICIPANT CALCIUM BURDEN

Participants with increased coronary ^{18}F-fluoride uptake had higher baseline calcium scores (524 [242 to 1091] versus 136 [55 to 361] AU; $p<0.001$), higher calcium mass (99 [46 to 212] versus 24 [11 to 69] mg; $p<0.0001$), and higher calcium volume (491 [247 to 984] versus 131 [64 to 343] mm^3; $p<0.0001$) compared to those without increased ^{18}F-fluoride uptake (Table 4.3). The proportion of PET-positive participants rose with increasing baseline calcium score (Figure 4.3). Thirty-eight participants had a total calcium score >1000 Agatston units at baseline and, of these, thirty-five (92%) had evidence of increased ^{18}F-fluoride uptake in at least one vessel.

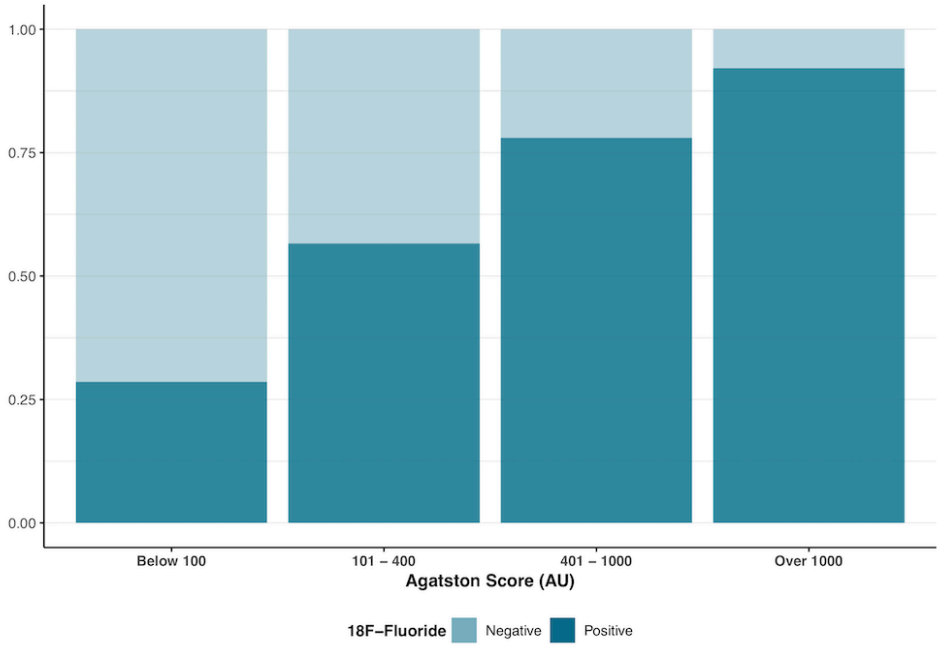

Figure 4.3. The proportion of ^{18}F-fluoride positive and negative participants with increasing baseline total calcium score.

Increased overall disease burden is associated with an increased frequency of ^{18}F-fluoride activity.

Table 4.3. Progression of calcification in participants with evidence of increased ^{18}F-fluoride uptake compared to those without uptake.

	All patients (n=183)	PET positive (n=116)	PET negative (N=67)	P value
BASELINE				
Total Agatston Score (AU)	378 [107-823]	524 [242-1091]	136 [55-361]	**p<0.001**
Calcium Volume (mm^3)	352 [131-771]	491 [247-984]	131 [64-343]	**p<0.001**
Calcium Mass (mg)	70 [23-153]	99 [46-212]	24 [11-69]	**p<0.001**
FOLLOW-UP				
Total Agatston Score (AU)	476 [173-1045]	660 [292-1216]	165 [61-461]	**p<0.001**
Calcium Volume (mm^3)	417 [167-887]	611 [313-1041]	149 [68-407]	**p<0.001**
Calcium Mass (mg)	89 [32-195]	129 [58-241]	32 [11-81]	**p<0.001**
PROGRESSION				
Change in Calcium Score (AU)	70 [22-143]	97 [39-166]	35 [7-93]	**p<0.001**
Change in Calcium Volume (mm^3)	60 [16-121]	82 [29-149]	33 [3-82]	**p<0.001**
Change in Calcium Mass (mg)	14 [4-35]	22 [7-42]	6 [1-20]	**p<0.001**

PET – positron emission tomography. PET positive and PET negative denote the presence or absence of ^{18}F-fluoride uptake

4.4.3 ^{18}F-FLUORIDE UPTAKE AND PLAQUE CHARACTERISTICS

Sixty (52%) of the PET-positive participants and 37 (55%) of the PET-negative participants had at least one high-risk plaque feature on CT coronary angiography. There was no difference in the median number of high-risk plaque features per patient in PET-positive (1.0 [0.0-2.3]) compared with PET-negative (1.0 [0.0-3.0]) participants (Table 4.4). Nine participants were excluded from quantitative plaque analysis due to suboptimal image quality. On quantitative plaque analysis in the remaining 174 participants, total plaque volume, non-calcified plaque volume and calcified plaque volume were higher in PET-positive participants at baseline and at one-year follow-up (Table 4.5).

Table 4.4. CT-defined plaque characteristics in PET-positive and PET-negative participants

Plaque Characteristic	**Overall (N=183)**	**PET positive (n=116)**	**PET negative (n=67)**
Number of positively remodelled plaques			
0	112 (61%)	70 (60%)	42 (63%)
1	41 (22%)	25 (22%)	16 (24%)
2	23 (13%)	14 (12%)	9 (13%)
3	5 (2.7%)	5 (4.3%)	0 (0%)
4	1 (0.5%)	1 (0.9%)	0 (0%)
5+	1 (0.5%)	1 (0.9%)	0 (0%)
Number of low attenuation plaques			
0	164 (90%)	104 (90%)	60 (90%)
1	17 (9.3%)	10 (8.6%)	7 (10%)
2	2 (1.1%)	2 (1.7%)	0 (0%)
Number of plaques with the napkin ring sign	4 (2.2%)	3 (2.6%)	1 (1.5%)
Number of plaques with spotty calcification			
0	116 (63%)	79 (68%)	37 (55%)
1	34 (19%)	21 (18%)	13 (19%)
2	16 (8.7%)	8 (6.9%)	8 (12%)
3	12 (6.6%)	4 (3.4%)	8 (12%)
4	4 (2.2%)	4 (3.4%)	0 (0%)
5+	1 (0.5%)	0 (0%)	1 (!.5%)
Number of plaques with punctate calcification			
0	179 (98%)	114 (98%)	65 (97%)
1	2 (1.1%)	0 (0%)	2 (3.0%)
2	2 (1.1%)	2 (1.7%)	0 (0%)
Total number of HRP per patient	1.00 [0.00-3.00]	1.00 [0.00-2.25]	1.00 [0.00-3.00]

Data presented as n (%) and median [IQR]. HRP; high-risk plaque.

Table 4.5. Quantitative plaque features in PET-positive and PET-negative participants

	All patients (n=174)	PET positive (n=110)	PET negative (n=64)	P value
BASELINE				
Total Plaque Volume (mm^3)	1361 [1033-1994]	1551 [1122-2080]	1142 [905-1488]	**<0.0001**
Non-Calcified Plaque Volume (mm^3)	1274 [953-1692]	1459 [1063-1819]	1118 [873-1443]	**0.001**
Calcified Plaque Volume (mm^3)	89 [34-224]	154 [62-285]	37 [7-78]	**<0.0001**
Low Density Non-Calcified Plaque Volume (mm^3)	87 [43-168]	91 [54-154]	78 [35-169]	0.485
Remodelling Index	1.5 [1.4-1.7]	1.5 [1.4-1.8]	1.4 [1.3-1.6]	**0.020**
FOLLOW-UP				
Total Plaque Volume (mm^3)	1493 [1097-2062]	1639 [1282-2298]	1270 [969-1600]	**<0.0001**
Non-Calcified Plaque Volume (mm^3)	1366 [1032-1831]	1492 [1099-1977]	1228 [936-1561]	**0.005**
Calcified Plaque Volume (mm^3)	109 [38-223]	161 [79-300]	43 [13-79]	**<0.0001**
Low Density Non-Calcified Plaque Volume (mm^3)	91 [48-157]	84 [49-153]	104 [41-161]	0.829
Remodelling Index	1.5 [1.3-1.7]	1.5 [1.3-1.7]	1.4 [1.3-1.6]	0.438
PROGRESSION				
Change in Total Plaque Volume (mm^3)	93[-92-270]	90 [-104-296]	93 [-82-255]	0.776
Change in Non-Calcified Plaque Volume (mm^3)	87[-92-230]	75 [-113-233]	108 [-72-227]	0.708
Change in Calcified Plaque Volume (mm^3)	4 [-13-37]	14 [-12-47]	1 [-15-17]	**0.02**
Change in Low Density Non-Calcified Plaque Volume (mm^3)	2[-20-28]	1 [-23-26]	3 [-16-32]	0.558

4.4.4 ^{18}F-FLUORIDE UPTAKE AND PROGRESSION OF CALCIFICATION ON A PER-PATIENT LEVEL

The median increase in calcium score, calcium mass and calcium volume were higher in PET-positive compared to PET-negative participants ($p<0.001$ for all; Table 4.3). Change in total calcified plaque volume on CT coronary angiography was also higher in PET-positive participants. There was no difference in change in non-calcified plaque, low-density plaque or total plaque volume (Table 4.5). Per-patient TBRmax correlated with change in calcium score (Spearman's $\rho = 0.37$), calcium mass ($\rho = 0.46$) and calcium volume ($\rho = 0.38$; $p<0.001$ for all; Table 4.6). There was a weak positive correlation between baseline TBRmax and change in total calcified plaque volume (Spearman's Rho 0.165; $p=0.029$; Table 4.6).

After adjusting for age, sex and baseline calcium score, baseline ^{18}F-fluoride activity was not an independent predictor of calcium score at 12 months when investigated at the patient level ($p=0.50$).

Table 4.6. Correlation between baseline maximum Tissue-to-Background Ratios (TBRmax) and progression of calcification.

	Number of participants	**TBRmax Correlation Coefficient (Spearman's Rho)**	**P value**
Calcium burden on non-contrast CT			
Change in total calcium burden (AU/year)	183	0.371	**<0.001**
Change in total calcium volume (mm^3/year)	183	0.379	**<0.001**
Change in total calcium mass (mg/year)	183	0.456	**<0.001**
Quantitative plaque characteristics on CT coronary angiography			
Change in total plaque volume (mm^3/year)	174	0.054	0.476
Change in non-calcified plaque volume (mm^3/year)	174	-0.001	0.990
Change in low attenuation plaque volume (mm^3/year)	174	-0.011	0.884
Change in calcified plaque volume (mm^3/year)	174	0.165	**0.029**

4.4.5 PER-SEGMENT ^{18}F-FLUORIDE ACTIVITY AND PROGRESSION OF CALCIFICATION

Calcification in individual coronary segments with evidence of ^{18}F-fluoride uptake was compared to a proximal reference segment with atherosclerotic plaque but without increased ^{18}F-fluoride uptake within the same individual (Figure 4.4). Six participants in whom the only PET-positive lesion or only PET-negative lesion was stented were excluded from analysis. Amongst the remaining PET-positive participants (n=110), lesions with ^{18}F-fluoride uptake had a higher calcium score, calcium mass and volume at baseline than PET-negative reference lesions in the same individuals ($p<0.001$ for all; Table 4.7). There was no difference in baseline average calcium density or change in average calcium density between PET-positive and PET-negative lesions (Table 4.8).

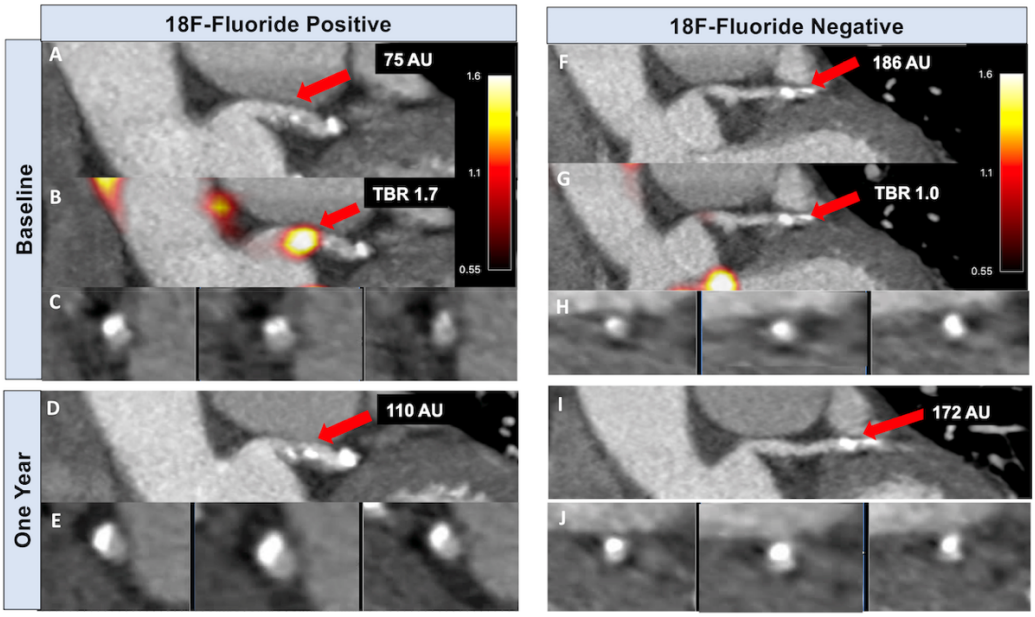

Figure 4.4. ^{18}F-Fluoride activity predicts progression of coronary arterial calcification.

^{18}F-Fluoride activity predicts progression of coronary arterial calcification. In an ^{18}F-fluoride PET positive lesion (A-E), contrast-enhanced CT coronary angiography (A) and fused PET-CT (B) demonstrate ^{18}F-fluoride uptake in the left main stem (LMS) at baseline overlying a mixed plaque shown on coronal view (A) and cross-section (C). Repeat CT coronary angiography at one year demonstrates progression of calcification in this segment with a higher calcium score (D) and dense calcium visible on cross section (E). (Calcium score 75AU at baseline, TBRmax 1.7, calcium score 110AU at one year). In the same patient, a calcified plaque in a proximal obtuse marginal branch without evidence of increased ^{18}F-fluoride activity is shown on coronal (F, G) and cross-section views (H). This plaque does not demonstrate progression in calcium score at one year (I, J). (Calcium score 186AU at baseline, TBRmax 1.0, calcium score 172AU at one year).

Table 4.7. Progression of calcification at a segmental level in coronary arterial segments with and without increased ^{18}F-fluoride uptake.

	All patients (n=110)	PET positive plaques (n=110)	PET negative plaques (N=110)	P value
BASELINE				
Total Agatston Score (AU)	548 [260-1130]	95 [30-209]	46 [16-113]	**<0.001**
Calcium Volume (mm^3)	519 [276-1014]	106 [37-185]	47 [21-95]	**<0.001**
Calcium Mass (mg)	101 [51-222]	19 [6-40]	9 [4-21]	**<0.001**
FOLLOW-UP				
Total Agatston Score (AU)	679 [346-1257]	148 [61-289]	49 [20-115]	**<0.001**
Calcium Volume (mm^3)	651 [330-1094]	129 [62-226]	44 [21-103]	**<0.001**
Calcium Mass (mg)	131 [62-242]	28 [11-55]	9 [4-23]	**<0.001**
PROGRESSION				
Change in Calcium Score (AU)	104 [45-170]	39 [20-70]	2 [-7-11]	**<0.001**
Change in Calcium Volume (mm^3)	86 [35-154]	30 [14-53]	1 [-8-8]	**<0.001**
Change in Calcium Mass (mg)	23 [10-44]	7 [4-14]	0.62 [-0.8-2.1]	**<0.001**

PET – positron emission tomography. PET positive and PET negative denote the presence or absence of ^{18}F-fluoride uptake

Table 4.8. Average calcium density in PET-positive and PET-negative segments.

	All patients (n=110)	PET positive (n=110)	PET negative (N=110)	P value
BASELINE				
Average Density (mg/mm^3)	0.20 [0.18-0.23]	0.20 [0.16-0.23]	0.19 [0.16-0.22]	0.15
FOLLOW-UP				
Average Density (mg/mm^3)	0.21 [0.18-0.23]	0.21 [0.18-0.23]	0.19 [0.17-0.23]	**0.046**
PROGRESSION				
Change in Average Density (mg/mm^3)	0.009 [0.002-0.018]	0.01 [-0.003-0.03]	0.01 [-0.01-0.03]	0.102

In PET-positive segments, there was an increase in calcium score (from 95 [30 to 209] to 148 [61 to 289] AU), calcium mass (from 19 [6 to 40] to 28 [11 to 55] mg) and calcium volume (from 106 [37 to 185] to 129 [62 to 226] mm^3; p<0.001 for all). In PET-negative reference segments, there was no change in calcium score (from 46 [16 to 113] to 49 [20 to 115] AU; p=0.329) and calcium volume (from 46 to 44 mm^3, p=0.666), although there was a small increase in calcium mass (from 9.1 to 9.2 mg; p=0.017; Figure 4.5). Similarly, changes in calcification were greater in PET-positive plaques compared to PET-negative plaques for the calcium score (39 [20 to 70] versus 2 [-7 to 11] AU), calcium mass (7 [4 to 14] versus 0.6 [-0.8 to 2.1] mg) and calcium volume (30 [14 to 53] versus 1 [-8 to 8] mm^3; p<0.001 for all). When segmental calcium mass and calcium score were measured as a ratio of follow-up to baseline, the calcium mass and calcium score ratio were each higher in PET-positive segments (Figure 4.6).

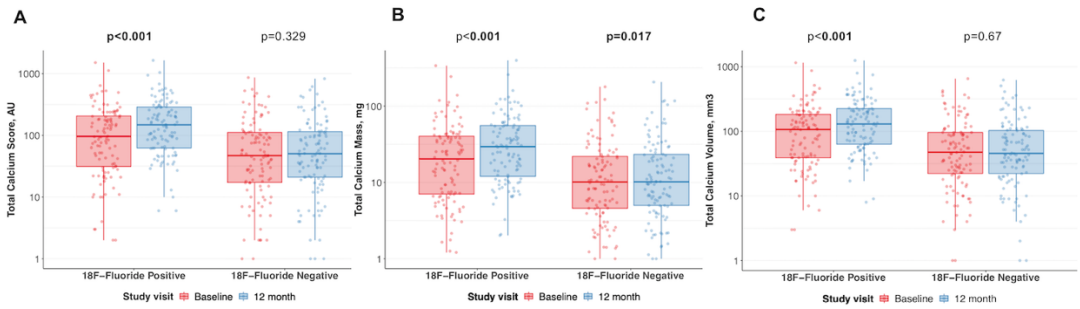

Figure 4.5. The relationship between baseline ^{18}F-fluoride activity and coronary calcification at one year.

Panels A-C display the change in calcium score (A), mass (B) and volume (C) in ^{18}F-fluoride positive versus negative lesions over twelve months. Median and interquartile range displayed.

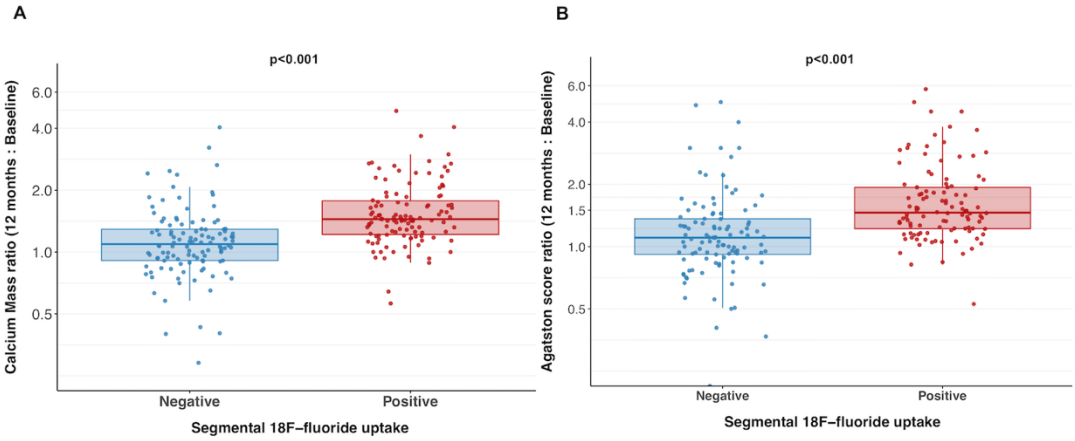

Figure 4.6. Ratio of calcification at follow-up to baseline.

Ratio of follow-up total calcium mass (A) and Agatston score (B) to baseline in individual PET-positive and PET-negative segments in participants with at least one PET-positive lesion.

When the relationship between ^{18}F-fluoride activity and progression of calcification was investigated at the segmental level, baseline TBRmax was an independent predictor of 12-month calcium mass when adjusting for baseline calcium mass (beta 0.67 Standard Error 0.06), Agatston score (beta 0.60 SE 0.09) or volume (beta 0.52 SE 0.07) and the repeated within individual measurements ($p<0.001$ for all).

4.5 DISCUSSION

In this pre-specified sub-study of a randomized controlled trial, we have demonstrated that increased ^{18}F-fluoride uptake is associated with more rapid progression of coronary atherosclerotic calcification. This finding was consistent across a range of measures of calcification and whether this was considered on a per-patient or per-segment basis. However, when considering total calcification burden at the patient level, baseline calcium score remained a powerful predictor of calcification progression. These findings nonetheless support ^{18}F-fluoride PET as a marker of increased disease activity and active mineralization within coronary atherosclerotic plaques.

Calcification plays a complex role in the development and progression of atherosclerosis. Hydroxyapatite deposition is heralded by intense inflammation, cell death and necrosis which precipitate the formation of calcifying matrix vesicles and leads to the earliest microscopic deposits of calcium which are not visible on conventional anatomical imaging modalities. (17, 20, 172) As well as reflecting the pro-inflammatory environment, microcalcification may also be directly implicated in plaque rupture as a consequence of destabilisation of the plaque's fibrous cap. (178) As microcalcific deposits coalesce to form larger macroscopic structures, plaque stability improves - a feature reflected by the observation that heavily calcified plaques are less prone to rupture or precipitate acute coronary events. (2, 179) Thus, while advanced macrocalcification may be considered a marker of plaque stability and inert disease, the earlier stages of calcium deposition are associated with increased inflammation and plaque vulnerability. (20, 180)

The precise natural history of calcification activity remains poorly understood. Indeed, the process of calcification does not progress in a linear manner and, while the earliest microcalcific deposits are associated with intense inflammation (17), it is likely that active calcification may accelerate during the process of plaque healing. This observation is concordant with prior randomized trials that have observed a pro-calcific effect of statins due to phenotypic transformation of low attenuation material to calcified plaque. (178) While computed tomography can provide quantitative measures of total plaque burden, it does not provide insight into the underlying biological disease process or disease activity, hence the rationale for utilizing targeted radiotracers.

^{18}F-Fluoride preferentially binds developing microcalcification (178), with uptake therefore potentially reflecting the earlier and more unstable stages of atherosclerotic mineralisation. Here, we have confirmed that increased ^{18}F-fluoride uptake provides an assessment of calcification activity within the coronary arteries, with uptake predicting progression in macroscopic calcium measured in individual plaques on CT, similar to previous results in the aortic valve and mitral valve annulus. (61, 181) Indeed, while calcium scores remained static in lesions without uptake, there was progression of calcification in plaques with increased ^{18}F-fluoride uptake, with an approximately 50% increase in median calcium score and calcium mass in as little as 12 months. Furthermore, the median change in calcium score in individual lesions with ^{18}F-fluoride uptake was almost twenty times greater than the change in calcium score in those without uptake. In individual coronary lesions, this finding remained even following adjustment for baseline calcium mass.

While the temporal nature of ^{18}F-fluoride activity remains unknown, it is possible that ^{18}F-fluoride uptake may increase as the atheromatous plaque begins to stabilise. Previous reports have highlighted that, while coronary ^{18}F-fluoride uptake can be localised to culprit plaques in the majority of patients following acute myocardial infarction, quantitative PET activity, as measured by tissue-to-background ratio, is higher in patients with stable coronary artery disease compared to immediately following acute myocardial infarction. (55) In a recent post-hoc analysis of nearly 300 patients with established coronary artery disease, increased ^{18}F-fluoride activity was an independent predictor of fatal and non-fatal myocardial infarction. Quantification of coronary microcalcification activity, a novel marker of ^{18}F-fluoride uptake, demonstrated powerful prediction of future adverse events leading to a 7-fold increased risk of fatal or nonfatal myocardial infarction in participants with elevated coronary microcalcification activity. (182)

In the present study, we have for the first time linked coronary ^{18}F-fluoride activity to progression in coronary atherosclerotic calcification. The main hypothesis for this study was to investigate the relationship between ^{18}F-fluoride activity and calcification progression. However, we also investigated the relationship between PET activity and other morphological features of atherosclerosis, including low attenuation plaque, non-calcified plaque and total plaque volume. We have demonstrated that total plaque volume and non-calcified plaque volume are higher in patients with increased ^{18}F-fluoride activity. The presence of increased ^{18}F-fluoride activity was also associated with a greater change in total calcified plaque volume.

The study highlights the high frequency of increased ^{18}F-fluoride activity in patients with established multivessel coronary artery disease, with two-thirds of patients having evidence of increased activity in at least one vessel. The prevalence of increased ^{18}F-fluoride uptake is similar to previous reports in clinically stable patients. (54, 55) Previous studies have reported that over one third of patients with calcium scores greater than 1000 do not have evidence of increased ^{18}F-fluoride activity. (54) In this study, we have shown that the majority of patients (92%) with calcium scores greater than 1000 had evidence of increased ^{18}F-fluoride uptake in at least one vessel, suggesting ongoing calcification activity. Indeed, an increasing disease burden was associated with an increase in the proportion of patients with evidence of increased PET activity in at least one vessel. This may reflect the underlying study population whom were largely high risk, with the majority (70%) having prior acute coronary syndrome and over 80% having previous coronary revascularisation.

We recognise that there are some limitations to our study. PET-CT imaging was performed in a single centre with experience in coronary PET-CT, and we need to explore the generalisability of our findings across multiple centres with different scanners. The high prevalence of previous percutaneous coronary intervention and stenting precluded calcium scoring assessment from at least one arterial segment in many patients. We mitigated for this by excluding those participants who underwent revascularisation in a previously untreated arterial segment prior to the follow-up scan, ensuring the calcium burden on the follow-up scan was not underestimated. Although scan-rescan reproducibility of CT calcium mass and volume within individual plaques has not been reported, repeatability and variability of CT calcium scoring protocols

has been demonstrated to be less than 20%. (147) Furthermore, our scans were all performed on a single imaging system with the same scanning protocol and reconstruction protocol, thereby minimising interscan variability. Lastly, our population represents a high-risk patient group with advanced disease and the majority having had a previous acute coronary event. Hence, these results may not be applicable to all patients with known or suspected coronary disease and future studies in different risk groups would be welcomed. While recent data have highlighted the predictive value of ^{18}F-fluoride activity in cardiovascular risk stratification, ultimately, prospective studies investigating the relationship between coronary ^{18}F-fluoride uptake and cardiovascular events will determine the prognostic utility of this novel imaging method and observational studies in this field are ongoing (PREFFIR NCT02278211).

4.6 CONCLUSION

In conclusion, increased coronary ^{18}F-fluoride uptake is associated with more rapid progression of coronary calcification at one year in patients with clinically stable multivessel coronary artery disease. In individual diseased segments, this association is independent of baseline calcium score, but at the patient level this finding is not independent of baseline calcium burden. ^{18}F-Fluoride uptake provides new insights into disease activity and progression of coronary atherosclerosis.

CHAPTER 5

Optimisation of Reconstruction and Quantification of Motion-Corrected Coronary PET-CT

Published in:

Doris MK, Otaki Y, Krishman SK, Kwiecinski J, Rubeaux M, Alessio A, Pan T, Cadet S, Dey D, Dweck MR, Newby DE, Berman DS, Slomka PJ. Optimization of reconstruction and quantification of motion-corrected coronary PET-CT. *J Nucl Cardiol*. 2020;27(2):494-504

Chapter 5 Optimisation of Reconstruction and Quantification of Motion-Corrected Coronary PET-CT

5.1 SUMMARY

Background

Although coronary PET has shown initial promise in the detection of high-risk atherosclerosis, there remains a need to optimize imaging techniques to improve quantification and overcome challenges faced by motion. We investigated the impact of different reconstruction and quantification methods in ^{18}F-Sodium Fluoride (^{18}F-fluoride) PET in patients presenting with acute coronary syndrome (ACS). Further, we applied a cardiac motion-correction method in the same group of patients and investigated whether this led to improvements in PET quantification.

Methods

Twenty-two patients underwent ^{18}F-fluoride PET within 22 days of ACS. Optimal reconstruction parameters were determined in a subgroup of 6 patients. Subsequently, motion-correction by diffeomorphic mass-preserving anatomy-guided registration within vessels automatically defined by computed tomography angiography was performed on ECG-gated data of all patients forming motion-frozen images from all cardiac gates. Tracer uptake was quantified in culprit and reference lesions by computing signal-to-noise ratio (SNR) in diastolic, summed and motion-corrected images.

Results

PET reconstruction using 24 subsets, 4 iterations, point-spread-function modelling, time of flight and 5-mm post-filtering provided the highest median SNR (31.5) compared to 4 iterations 0-mm (22.5), 8 iterations 0-mm (21.1) and 8 iterations 5-mm (25.6; $p<0.05$ for all). In all subjects, motion-correction improved SNR of culprit lesions (n=33) (24.5 [19.9-31.5]) when compared to diastolic (15.7 [12.4-18.1]; $p<0.001$) and summed data (22.1 [18.9-29.2]; $p=<0.001$). Further, motion-correction led to a greater SNR difference between culprit and reference lesions (10.9 [6.3-12.6]) compared to diastolic (6.2 [3.6-10.3] p=0.001) and summed data (7.1 [4.8-11.6] p=0.001).

Conclusions

The number of iterations and extent of post-filtering in ^{18}F-fluoride PET reconstruction has marked effects on quantification and should be considered when using coronary PET. Cardiac motion-correction improves discrimination between culprit and reference lesions.

5.2 INTRODUCTION

Positron emission tomography (PET) using ^{18}F Sodium Fluoride (^{18}F-fluoride) has emerged as a promising non-invasive imaging modality to potentially identify high-risk and ruptured coronary atherosclerotic plaques. (55, 183-185) However, imaging of the coronary arteries faces many challenges. First, the small calibre of coronary vessels combined with their tortuous course means that optimizing spatial resolution is of great importance. Second, the impact of motion from cardiac contraction, respiration and patient movement can degrade visual quality and PET quantification, highlighting the need for sophisticated methods to overcome these limitations.

To compensate for the effects of motion, prior coronary PET-CT studies have analysed data from the end-diastolic phase of the cardiac cycle (with 4-bin gating), utilizing only one quarter of PET counts and effectively discarding the remainder. While a useful initial strategy, this method leads to markedly increased noise and potentially additional difficulty in distinguishing active plaques from noise-related artefact. Indeed, in an initial study, the difference in target-to-background ratio between positive and negative plaques was small (approx. 33%), which may be a result of both noise and signal blurring due to motion. (55)

Recently, we have demonstrated that a novel cardiac motion-correction method, using a diffeomorphic mass-preserving anatomy-guided registration technique, improves PET quantification when applied to original image data from a single imaging site. (149) However, there is a need to optimize and standardize imaging and quantification

methods between centres to minimize variation and enable comparison in multicentre studies.

In this analysis, we evaluated a series of ^{18}F-fluoride coronary measurements with respect to the optimal reconstruction and motion-correction techniques. We aimed to investigate the influence of reconstruction protocols on image quality (judged both visually and quantitatively) in a subgroup of patients who presented with acute coronary syndrome. Secondly, we utilized the optimal reconstruction in a larger group of patients with acute coronary syndrome and evaluated the subsequent improvement in signal quantification gained by the application of our novel motion-correction method, now integrated within image analysis software to help streamline this process.

5.3 METHODS

5.3.1 STUDY POPULATION

Patients with a diagnosis of ACS and who underwent invasive coronary angiography were recruited from Cedars-Sinai Medical Center between December 2015-June 2016 (n=22). All patients underwent a comprehensive baseline clinical assessment, including evaluation of their cardiovascular risk factor profile. The study was approved by the Institutional Review Board and all patients provided written informed consent.

5.3.2 IMAGING PROTOCOLS AND PET RECONSTRUCTION

All patients were administered a target dose of 250 MBq of 18F-fluoride and rested in a quiet environment. After 60 minutes, image acquisition began on a hybrid PET-CT scanner (GE Discovery 710). Following the acquisition of a non-contrast CT attenuation correction scan, PET acquisition was performed in list mode for 30 minutes. Finally, coronary computed tomography angiography (CTA) was performed at end-expiration immediately following PET acquisition.

ECG-gated PET images were reconstructed using 4 and 10 cardiac bins. A standard ordered subset expectation maximization (OSEM) algorithm was used with time of flight and resolution recovery. Four different reconstruction algorithms were applied in a subgroup of 6 patients; 4 iterations with 0-mm post-filtering, 4 iterations with 5-mm post-filtering, 8 iterations with 0-mm post-filtering and 8 iterations with 5-mm post-filtering. For each subject, 24 subsets and a 256x256 matrix size with a 20x20 cm field of view were used in each reconstruction algorithm.

Following determination of the reconstruction parameters that provided the highest image quality and signal-to-noise ratio (SNR), the impact of time of flight and resolution recovery was then evaluated. PET images were then reconstructed for the remaining patients using the optimal parameters of those evaluated.

5.3.3 MOTION CORRECTION

We applied a novel motion-correction method that aimed to compensate for coronary artery motion by aligning all gates to the end-diastolic position. First, anatomical data was extracted from coronary CTA by applying a vessel tracking method implemented in dedicated software (Autoplaque 2.0, Cedars-Sinai Medical Center). Second, a diffeomorphic mass-preserving image registration algorithm (demons) was used to align 10 gates of PET data with the position of the end-diastolic gate. (149, 186) This algorithm allowed non-linear transformations with a regularization function, facilitating smoother transitions between regions and gates than the originally proposed level-set method. (150) The algorithm was fully automated and implemented in dedicated image analysis software developed at Cedars-Sinai (*FusionQuant* 1.0) using ITK image processing library. (187) After motion-correction, the 10 gates were summed back together to build a motion-free image containing counts from the entire duration of PET acquisition.

5.3.4 IMAGE ANALYSIS

Image analysis was performed using dedicated software (*FusionQuant* 1.0 Cedars-Sinai Medical Center, Los Angeles). Images from the four different reconstructions for each patient were presented to an experienced observer (MKD) in a blinded fashion

and a visual quality score was assigned to each reconstruction (score 1-4, 1 representing the highest image quality and 4 the most difficult to interpret). For each scan, fused PET-CTA images were co-registered, and the same registration was applied to diastolic, summed and motion-corrected images.

For quantitative PET analysis, activity was measured by delimiting 3-dimensional spherical volumes of interest on coronary artery plaques. Lesions were considered PET-positive if there was visual focal tracer uptake in a plaque which followed the course of the vessel over more than one slice and was visible on more than one of four gates including the end-diastolic gate. Reference lesions without visual PET-uptake (i.e. PET-negative) were measured in coronary vessels at the same segment or proximal to the PET-positive lesions. Quantitative plaque volume was measured for all PET-positive and reference PET-negative lesions, which were present in epicardial vessels with a calibre >2mm and had not been stented prior to imaging, excluding those with poor image quality. This was performed using semi-quantitative software (*AutoPlaque* version 2.0, Cedars Sinai Medical Center).

Background blood-pool activity was measured by delimiting $3cm^2$ regions of interest in the right atrium on three consecutive slices from the level of the lowest pulmonary vein insertion. Image noise was defined as the mean standard deviation of blood-pool activity. SNR was defined as the plaque maximal SUV inside the spherical region centred around the plaque (SUVmax) divided by noise. Tissue-to-Background Ratio (TBR) was defined as the SUVmax divided by the mean background blood-pool activity. For each image, PET registration and regions of interest were saved using the original image, and the same regions of interest were measured in the diastolic,

summed and motion corrected images. Semi-automated software (Autoplaque version 2.0, Cedars-Sinai Medical Center) was used to quantify total plaque volume of coronary arterial plaques for PET-positive and PET-negative reference lesions after excluding those with stents and poor image quality (n=28).

5.3.5 STATISTICAL ANALYSIS

Continuous data is expressed as mean (standard deviation) or median [interquartile range] as appropriate. Data was tested for normality using Shapiro-Wilk test. Parametric data were compared using student's T-test and non-parametric data compared using Wilcoxon Rank-Sum test as appropriate. A two-sided p value <0.05 was considered statistically significant. Statistical analyses were performed using GraphPad Prism (version 7, GraphPad software Inc) and SPSS (version 22, IBM, USA) software.

5.4 RESULTS

5.4.1 BASELINE CHARACTERISTICS

Twenty-two patients were recruited 22 days within diagnosis of acute coronary syndrome (Table 5.1). All patients underwent PET-CT following invasive angiography with a mean duration of 8.7±4.8 days between angiography and PET-CT. Culprit lesions were identified on invasive angiography in 17 of the 22 patients. In one patient, the culprit vessel was a prior bypass graft and this patient was excluded from further motion-correction analysis. Of the remaining 21 patients, 10 (48%) had multi-vessel disease on invasive angiography with at least one additional major epicardial vessel demonstrating >50% stenosis. Nineteen patients underwent percutaneous revascularization and two underwent coronary artery bypass grafting. Seven patients (33%) underwent revascularization of more than one vessel. Seventeen (81%) patients had at least one PET-positive lesion. Of these patients, 16 demonstrated focal tracer uptake in a culprit vessel which was treated at the time of invasive angiography. The remaining patient had a PET-positive lesion in the mid right coronary artery, in which chronic total occlusion was demonstrated on invasive angiography. There was no significant difference in total plaque volume between PET-positive and PET-negative lesions (305[233, 369] versus 235[231, 387] mm^3; p=0.70).

Table 5.1. Baseline characteristics.

Variable	Value	SD/Percent
Age in years, SD	62.4	11.2
Men (n), (%)	20	91
BMI (Kg,m^2), SD	27.6	5.7
Heart rate (beats per minute), SD	64.0	10.9
Systolic blood pressure (mmHg), SD	128.4	17.1
Diastolic blood pressure (mmHg), SD	72.1	11.2
Cardiovascular History (n), %		
Previous Myocardial Infarction	5	23
CVA/TIA	0	0
Previous PCI	5	23
Previous CABG	1	5
Risk Factors (n), %		
Smoking	10	45
Diabetes	5	23
Hypertension	16	73
Hypercholesterolemia	14	64
Serum Biochemistry (mg/dl), SD		
Cholesterol	152.4	34.0
HDL	42.4	13.8
LDL	87.3	27.2
Triglyceride	136.3	82.6
Creatinine	1.1	1.0
Medications (n), %		
Aspirin, %	19	86
Clopidogrel, %	12	55
Statin, %	18	82
Beta Blocker, %	15	68
ACEI/ARB, %	9	41
Calcium Channel Blockers, %	4	18
Oral Nitrates	4	18

ACEI, angiotensin-converting enzyme inhibitors; ARB, angiotensin receptor blocker; BMI, body mass index; CABG, coronary artery bypass grafting; CVA, cerebrovascular accident; HDL, high-density lipoprotein; LDL, low-density lipoprotein; PCI, percutaneous coronary intervention; TIA, transient ischaemic attack

5.4.2 RECONSTRUCTION SUBGROUP

A subgroup of six patients was selected to assess the optimal reconstruction parameters needed to improve the balance between PET quantification and noise. When evaluating visual quality, use of 8 iterations and 0-mm post-filtering led to consistently poorer image quality (score of 4 in 6/6 patients) with difficulty in image interpretation due to noise, whereas the highest visual image quality was consistently observed in the reconstruction using 4 iterations and 5-mm post-filtering with time of flight and resolution recovery (score of 1 in 6/6 patients) (Figure 5.1). The reconstruction using 4 iterations and 0-mm post-filtering scored 2 in two cases and 3 in four of six cases and, similarly, the reconstruction using 8 iterations and 5-mm post-filtering scored 2 in four cases and 3 in two of the six cases.

After motion-correction, the median signal-to-noise ratio was higher in the reconstruction using 4 iterations 5-mm (31.5 [19.5-33.9]) versus 4 iterations 0-mm (22.5 [16.7-26.8]), 8 iterations 0-mm (21.1 [16.1-22.5]), and 8 iterations 5-mm (25.6 [17.2-27.0]) ($p<0.05$ for all). Conversely, TBR was consistently higher in the reconstruction method using 8 iterations and 0-mm post-filtering in the diastolic (4.3 [3.0-7.0]), summed (2.9 [2.5-3.4] and motion-corrected (3.1 [2.8-3.9]) data. In the motion-corrected images, this reconstruction method generated higher TBR values (3.1 [2.8-3.9]) compared to 4 iterations 5-mm (1.8 [1.6-1.9]), 4 iterations 0-mm (2.2 [2.1-2.5]) and 8 iterations 5-mm (2.0 [1.9-2.2]) ($p=0.005$ for all; Figure 5.2).

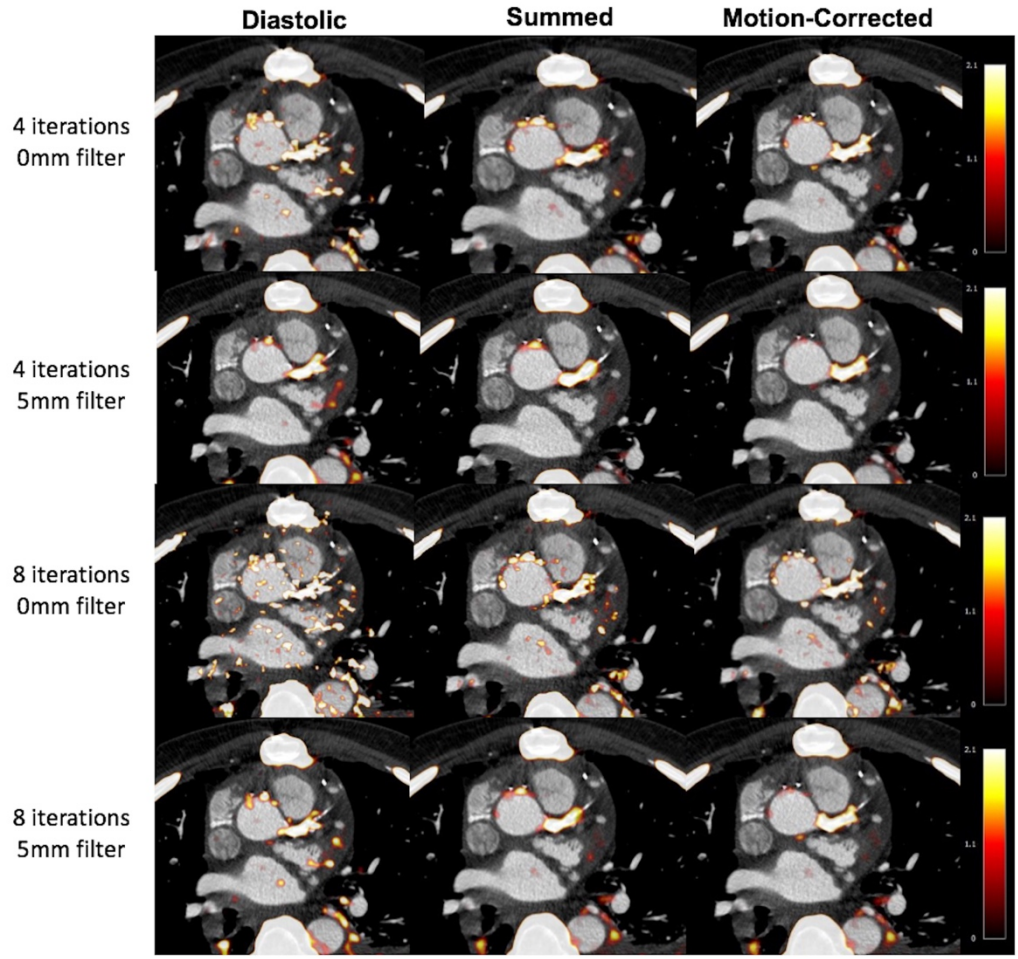

Figure 5.1. The impact of different PET reconstructions on visual image quality in diastolic and motion-corrected images in a patient with a positive culprit lesion in the left main coronary artery.

The PET reconstruction using 4 iterations and 5-mm post-filtering was considered to provide superior image quality (TBR=1.92 for motion-corrected image).

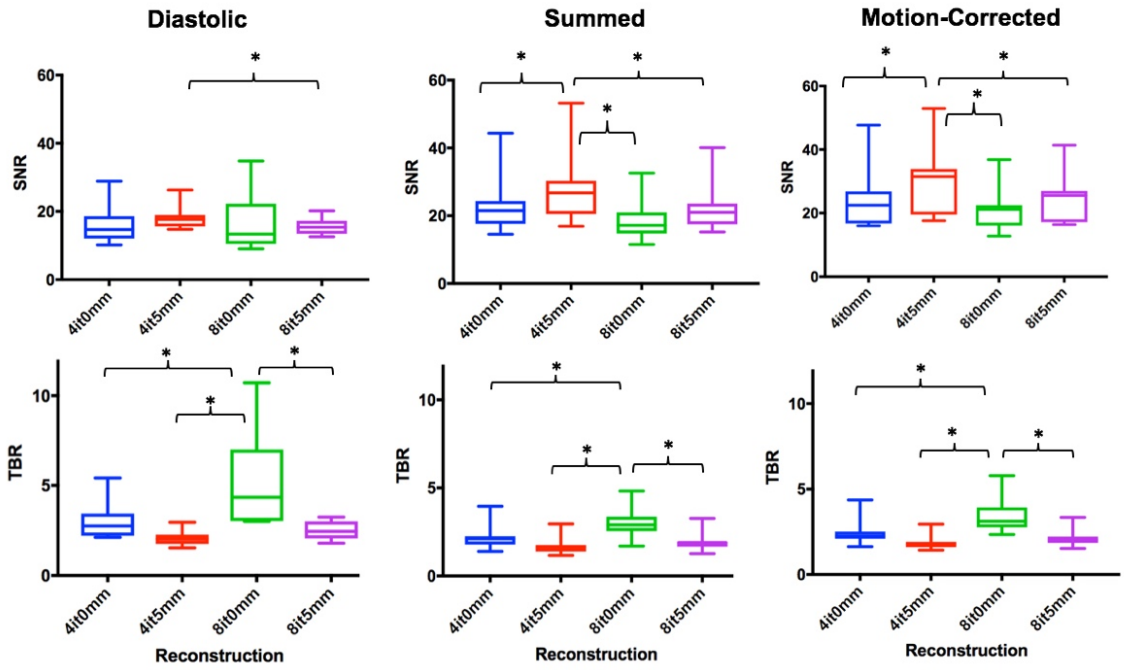

Figure 5.2. Signal-to-Noise Ratio (SNR) and Tissue-to-Background Ratio (TBR) in diastolic, summed and motion-corrected images for each reconstruction.

In the diastolic, summed and motion-corrected images, median SNR was highest when PET data was reconstructed using 4 iterations and 5mm post-filtering. Conversely, TBR was highest when more iterations were used without applying post-filtering (*$p<0.01$).

5.4.3 TIME OF FLIGHT AND RESOLUTION RECOVERY

Following selection of the reconstruction which provided superior SNR, the influence of time of flight and resolution recovery was assessed in the same subgroup (Figure 5.3). In the diastolic data, there was a trend but no significant difference in SNR with and without time of flight and resolution recovery (17.7 [15.6-19.0] versus 11.6 [10.1-14.5]; p=0.074). In the summed data, SNR improved with the use of time of flight and resolution recovery (15.4 [13.3-19.3] versus 26.8 [20.5-30.3]; p=0.007). Similarly, following motion-correction, SNR was greater when time of flight and resolution recovery were implemented (31.5 [19.5-33.9] versus 17.0 [11.7-22.2]; p=0.005). (Figure 5.4)

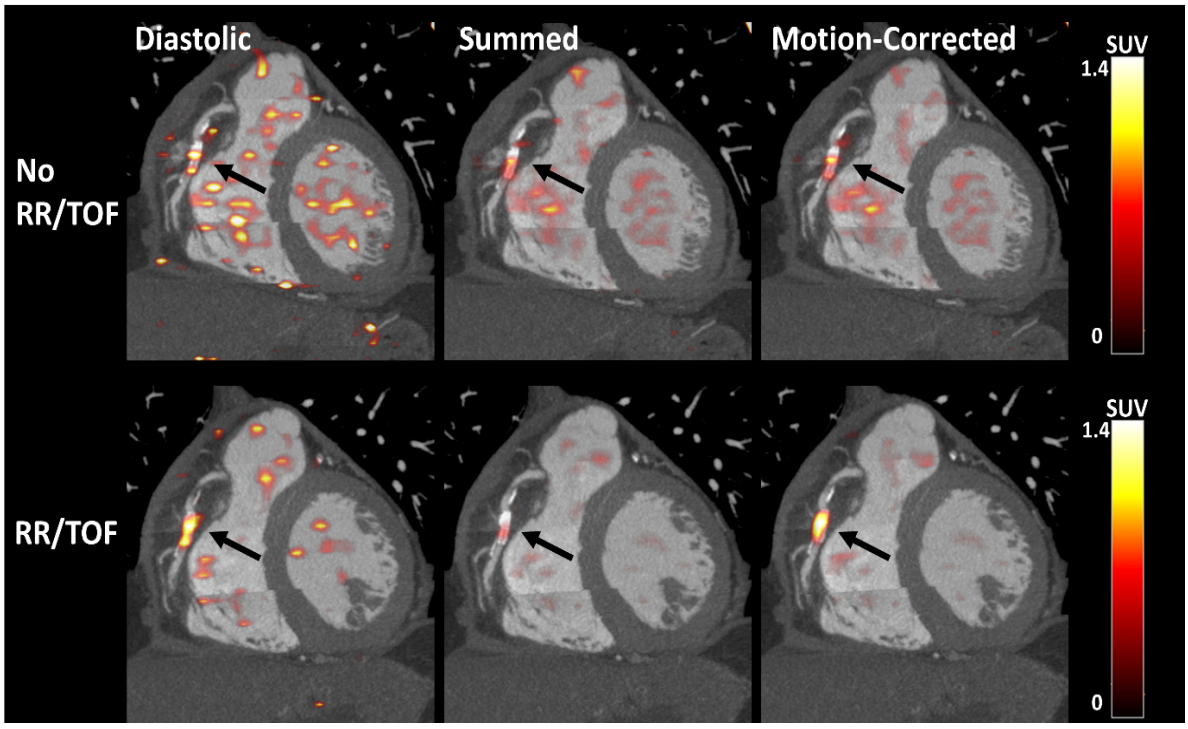

Figure 5.3. The impact of Time of Flight (TOF) and Resolution Recovery (RR).

The impact of Time of Flight (TOF) and Resolution Recovery (RR) on Signal to Noise Ratio (SNR) in diastolic, summed and motion-corrected images in a patient with a PET-positive plaque in the mid right coronary artery. In the summed and motion-corrected images, median SNR was higher with TOF and RR ($p<0.01$).

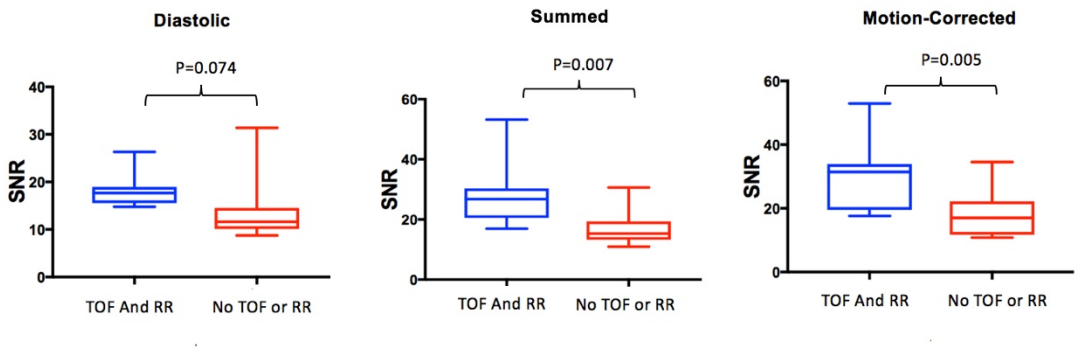

Figure 5.4. The effect of Time of Flight (TOF) and Resolution Recovery (RR) on SNR.

SNR improved following TOF and RR, summed (27 versus 15; p=0.007) and motion-corrected (32 vs 17 versus 32; p=0.005) data.

When assessing TBR in reconstructions with and without the use of time of flight and resolution recovery, there was no difference in the diastolic data with compared to without these features (2.02 [1.75-2.27] versus 2.04 [1.81-2.72]; p=0.878). However, following the application of motion-correction, TBR was higher in the motion-corrected data with time of flight and resolution recovery (1.79 [1.60-1.75] versus 1.59 [1.46-1.73]; p=0.005).

5.4.4 MOTION CORRECTION

A representative example of the extent of coronary artery motion in the right coronary artery is shown in Figure 5.5. The effects of motion-correction on visual image quality is shown in Figure 5.6.

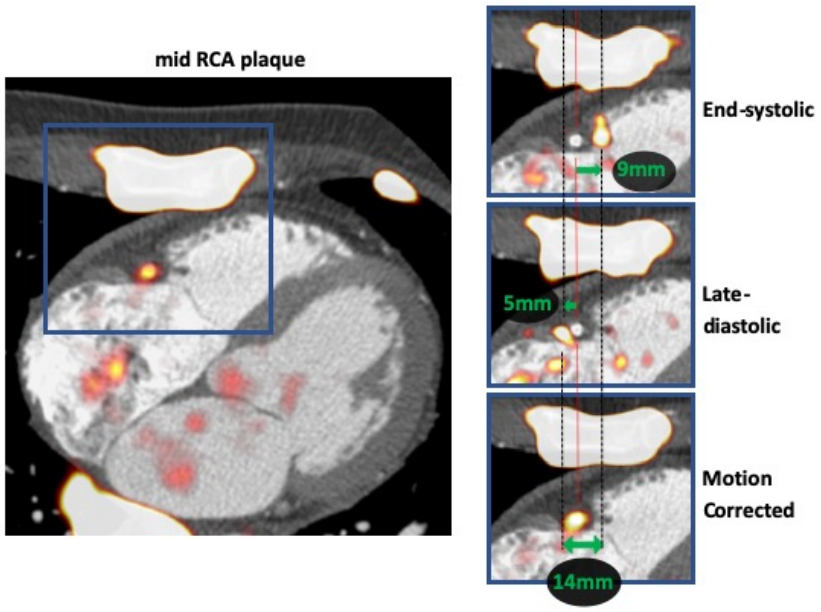

Figure 5.5. Motion correction of physiological mid RCA motion.

In a 60-year-old female the systolic excursion of the tricuspid annular plane led to displacement of the PET signal during the cardiac cycle (zoomed area of interest in blue squares). The difference in the shift of PET from reference is shown on the end-systolic (top-right) and late-diastolic (mid right) images. Green arrows represent the vectors of mid RCA motion. By co-registration of all PET data to the reference end-diastolic gate the final motion corrected image is corrected for the 14mm mid RCA motion (bottom-right).

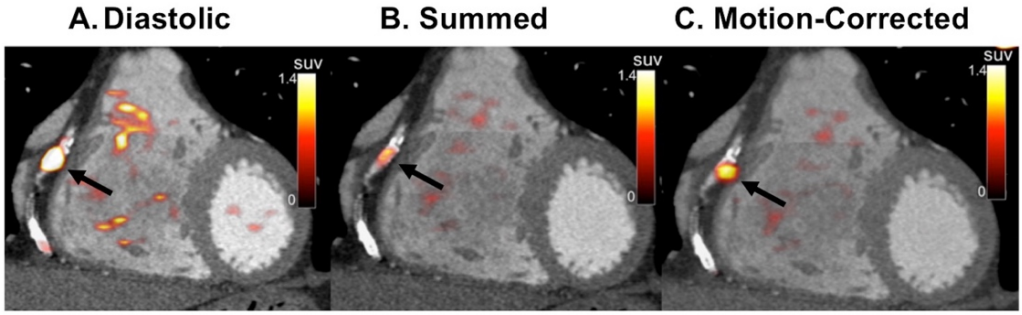

Figure 5.6. Fused PET-CTA images before and after motion-correction.

An example of a PET-positive lesion in the right coronary artery (arrows) using the diastolic (A), summed (B) and motion-corrected (C) PET data.

5.4.4.1 Signal to Noise Ratio.

Motion-correction was performed in all cases using 10 cardiac gates and the optimized reconstruction parameters: time of flight and resolution recovery, 4 iterations, 24 subsets, 5-mm post-filtering and 256x256 matrix size. Compared to the original diastolic gate (15.7 [12.4-18.1]), motion-correction led to a significant improvement in SNR for PET-positive lesions (n=33; 24.5 [19.9-31.5]; p<0.001). Further, motion-correction also increased SNR when compared with the summed data (22.1 [18.9-29.2] versus 24.5 [19.9-31.5], p<0.001).

When analysing PET-negative reference lesions, there was an increase in SNR following motion-correction when compared to the diastolic gate (n=23; diastolic 8.8 [7.2-11.3] versus 13.0 [11.2-15.7] p<0.001), but no significant difference between the summed and MC data (summed 13.3 [10.6-16.7] versus 13.0 [11.2-15.7] p=0.648). Background noise was higher in the diastolic (0.12 [0.10-0.19]) compared to motion-corrected (0.08 [0.06-0.09]; p<0.001) data. There was no significant difference in background noise between the summed (0.07 [0.06-0.10]) and motion-corrected data (0.08 [0.06-0.09]; p=0.59; Figure 5.7). Motion-correction led to an improvement in the absolute difference between PET-positive culprit and PET-negative reference lesions compared to the diastolic gate (10.9 [6.3-12.6] versus 6.2 [3.6-10.3], p<0.001) and summed data (10.9 [6.3-12.6] versus 7.1 [4.8-11.6] p<0.001).

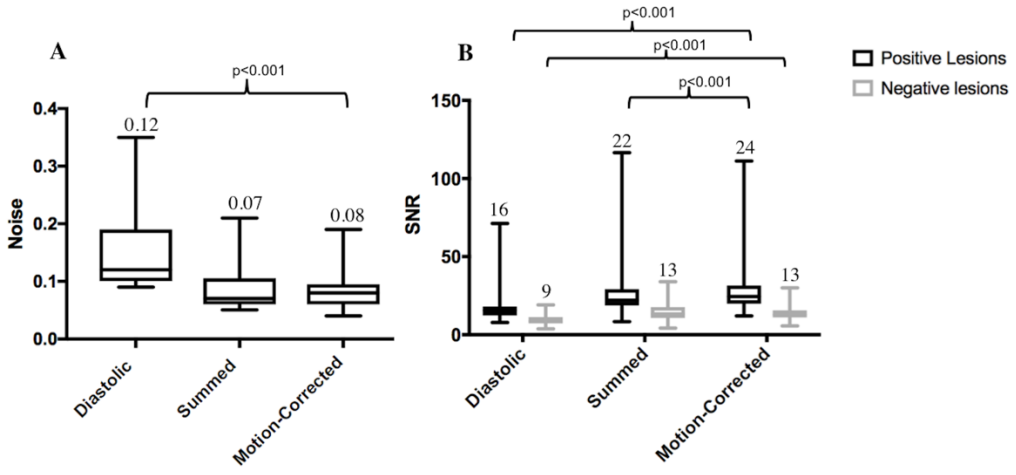

Figure 5.7. Image noise and signal-to-noise ratio (SNR) in diastolic, summed and motion-corrected data.

(A) The median noise improves from 0.12 in the diastolic data to 0.08 following motion correction (median; p<0.001) and (B) Signal-to-Noise Ratio (SNR) before and after motion-correction. Median SNR for the motion-corrected data was highest in the positive lesions (n=33), and similar to SNR of the summed data for negative lesions (n=23).

5.4.4.2 Tissue to Background Ratio.

Tissue-to-background ratios for PET-positive lesions were higher in the original diastolic (2.1 [1.8-2.4]) versus motion-corrected image (1.8 [1.6-2.1]); p<0.001) and higher in the motion-corrected than summed image (1.8 [1.6-2.1] versus 1.6 [1.4-1.9]; p<0.0001). For PET-negative lesions, TBR was also higher in the original diastolic (1.4 [1.1-1.7]) versus motion-corrected image (1.2 [0.9-1.4]; p=0.002) and lower in the summed (1.1 [0.9-1.2]) versus motion-corrected image (1.2 [0.9-1.4]; p=0.014]).

5.4.4.3 Standardized Uptake Value.

For PET-positive lesions, SUVmax was higher in the diastolic image (1.9 [1.7-2.5]) versus motion-corrected (1.8 [1.4-2.1]; p<0.001). When compared to the summed, non-gated data, SUVmax was higher following motion-correction (1.6 [1.3-1.92] versus 1.8 [1.4-2.1]; p<0.001). For PET-negative lesions, SUVmax was higher in the diastolic image (1.40 [1.07-1.79]) versus the motion-corrected image (1.10 [0.89-1.56]; p<0.001). There was no significant difference in SUVmax of negative lesions between the summed and motion-corrected data (1.06 [0.91-1.38] versus 1.10 [0.89-1.56]; p=0.078).

5.5 DISCUSSION

While potentially a promising technique to identify adverse plaque features, coronary PET faces many challenges which must be overcome for this imaging method to reach its full research and clinical potential. An accurate and reproducible method for quantification is necessary to distinguish positive and negative lesions, as well as to allow use in monitoring disease progression and response to therapies. In this study, we have evaluated the effect of a variety of reconstruction methods on quantitative coronary PET and have subsequently demonstrated improved discrimination between positive and negative lesions following the application of cardiac motion-correction.

We have demonstrated that, while more iterations and no post-filtering results in higher SUVmax and TBR values, these images are excessively noisy and difficult to interpret. Similarly, although end-diastolic images may demonstrate higher SUVmax and TBR as compared to summed or motion-corrected images, these images are of poorer visual quality with lower SNR values. Moreover, plaque lesions without visible radiotracer uptake often demonstrate higher SUVmax and TBR values in the end-diastolic images, which likely represents the noisier character of these data rather than a true increase in PET signal. (188, 189) Thus, while TBR is used to provide useful information with regards to biological activity of atherosclerosis within the peripheral, carotid and coronary arteries, (58, 190-193) TBR and SUVmax may not be the most suitable parameters for assessing the optimal method of coronary PET reconstruction. Instead, SNR assessments capture both the signal intensity and the surrounding noise, improving the ability to discriminate between active and inactive disease, thereby potentially improving the overall specificity and reliability of the test. Indeed, while

we also observed a small increase in SNR for negative lesions following motion-correction, the difference between positive and negative lesions in each patient also increased, suggesting improved discrimination between active and inactive plaques. Similar to previous reports, the majority (81%) of patients had evidence of increased ^{18}F-fluoride activity following an acute event, and sites of ^{18}F-fluoride uptake corresponded to regions of severe disease on invasive angiography. (55)

Our study highlights the marked influence of different reconstruction parameters on PET quantification of coronary uptake. A recent report highlighted that details of the reconstruction algorithm used were not documented in one third of published PET studies. (194) As this imaging modality continues to evolve and become more widely adopted, standardization of imaging protocols is of extreme importance in drawing meaningful conclusions from quantitative PET results. Even small changes in imaging protocols may markedly influence results. The choice of the reconstruction algorithm, particularly the number of iterations used as well as post-filtering have the most marked effect on quantification when compared to image analysis methods. Indeed, acquisition protocols have been shown to lead to variations in SUV up to a factor of three. (194) In a recent report, it was highlighted that increasing the number of iterations reduced bias in SUV measurements and OSEM with at least 120 maximization equivalent iterations and no post-filtering was recommended. (194) However, the majority of studies have considered large-calibre stationary vessels such as the aorta and carotid arteries, which are less subject to motion than the coronary arteries. (195) In order to optimize the research and clinical potential of 18F-fluoride PET, there must be a balance between recovering ‘true’ lesion activity while

maintaining image quality for the clinician or researcher interpreting the study. Thus, reducing noise by applying smoothing is necessary to improve visual image quality when interpreting coronary PET. In our results, image noise was lowest and visual quality highest in the reconstruction using 4 iterations (4x24subsets=96 image updates) and 5-mm post-filtering.

We have recently demonstrated that the application of level-set-based nonlinear PET registration improves PET image quality and quantification in a small cohort of patients with acute coronary syndrome. (149) This study adds to these initial findings by focusing on further optimization of image reconstruction and applying a new and improved motion correction approach which produces smoother deformation fields and better noise characteristics compared to our initial study. (150) The refined motion correction method is now integrated within image analysis software, facilitating automation of results within the research and clinical setting.

We recognize that there are limitations to our study. Firstly, we did not apply corrections for partial volume effects in our patient population. The impact of partial volume effects on PET quantification in this study is uncertain without precise quantification of lesion size. It is likely that partial volume effects would decrease with higher resolution provided by increasing number of iterations, however, further increases beyond a maximum resolution would increase noise without improving spatial resolution. (75) Future studies should consider investigating the effects of partial volume correction on PET quantification. Secondly, we did not apply dual cardio-respiratory motion to our patient population. Although the effects of cardiac contraction exceed that of respiration with regards to displacement of the coronaries

(cardiac contraction displaces the coronary arteries 8-26mm during the cardiac cycle, while normal respiration leads to movement of the heart of approximately 6-13mm), (195) the development and integration of novel methods to allow dual cardio-respiratory motion correction will likely lead to further improvements in signal-to-noise ratio in future studies. This will require innovative dual cardio-respiratory gating and dual correction approaches which do not rely upon segmentation of the myocardium (due to low myocardial uptake of ^{18}F-fluoride) and therefore overcome difficulties relating to the lack of anatomical landmarks to reference motion within the vicinity of the heart.

In this study, we investigated the influence of time of flight and resolution recovery in combination and did not measure the incremental effects of each feature in isolation. Prior studies have, however, demonstrated that both parameters in combination provide optimal results when compared to each feature individually. (196, 197)

Moreover, we evaluated performance on only one scanner platform under a fixed acquisition protocol and the optimal reconstruction settings will likely be different for other vendors, injected activities, and scan durations. Further, our study involved only rigid alignment between PET and CTA using a whole heart approach, which may lead to modest inaccuracies in precise PET-CTA fusion. The research software developed at our institution provides the ability to save rigid registration and regions of interest and load the same registration and measurements on multiple studies. This therefore provides an accurate method for quantification and direct comparison between multiple reconstructions, minimizing variation in plaque measurements. Fully automated registration between CTA and PET would further improve this process and

may enable patients to undergo initial clinical coronary CTA before proceeding to PET-CTA, thereby improving clinical workflow.

While the number of patients in our study population is small, we have demonstrated significant differences between different reconstruction parameters and following the application of motion-correction. Although this suggests an improvement in diagnostic capability, results from prospective clinical trials are required to explore the relationship between coronary ^{18}F-fluoride PET activity and future risk of cardiac events, and define thresholds associated with increased risk. While this was not a focus of our study, a large multicentre trial is currently seeking to answer this question (NCT02278211). Finally, although our study focused on ^{18}F-fluoride, this motion-correction method would be applicable to other PET tracers exploring alternative pathophysiological processes within the coronary arterial system.

5.6 CONCLUSION

In conclusion, the number of iterations and extent of post-filtering in ^{18}F-fluoride PET reconstruction has marked effects on quantitation and should be considered when using coronary PET. Motion-correction, using a diffeomorphic mass-preserving registration algorithm driven by anatomical framework from coronary CTA improved signal to noise ratio in active culprit plaques, and improves discrimination between active and reference coronary lesions.

CHAPTER 6

Computed Tomography Aortic Valve Calcium Scoring for the Assessment of Aortic Stenosis Progression

Published in;

Doris MK*, Jenkins WS*, Robson PM, Pawade TA, Andrews JPM, Bing R, Timothy Cartlidge T, Shah A, Pickering A, Williams MC, Fayad ZA, White AC, van Beek EJR, Newby DE *, Dweck MR *. Computed Tomography Aortic Valve Calcium Scoring for the Assessment of Aortic Stenosis Progression. *Heart 2020;106(24):1906-1913*

**Equal contribution*

Chapter 6 Computed Tomography Aortic Valve Calcium Scoring for the Assessment of Aortic Stenosis Progression

6.1 SUMMARY

Background

Computed tomography quantification of aortic valve calcification (CT-AVC) is useful in the assessment of aortic stenosis severity. Our objective was to assess its ability to track aortic stenosis progression compared with echocardiography.

Methods

Subjects were recruited in two cohorts; 1) a reproducibility cohort where patients underwent repeat CT-AVC or echocardiography within four weeks and 2) a disease progression cohort where patients underwent annual CT-AVC and/or echocardiography. Cohen's d statistic was computed from the ratio of annualized progression and measurement repeatability and used to estimate group sizes required to detect annualized changes in CT-AVC and echocardiography.

Results

A total of 33 (age 71±8) and 81 participants (age 72±8) were recruited to the reproducibility and progression cohorts respectively. Ten CT scans (16%) were excluded from the progression cohort due to non-diagnostic image quality. Scan-rescan reproducibility was excellent for CT-AVC (limits of agreement -12-10 %, intraclass correlation [ICC] 0.99), peak velocity (-7-17%; ICC 0.92) mean gradient (-

25-27%, ICC 0.96) and dimensionless index (-11-15%; ICC 0.98). Repeat measurements of aortic valve area (AVA) were less reliable (-44-28%, ICC 0.85).

CT-AVC progressed by 152 [65-375] AU/year. For echocardiography, the median annual change in peak velocity was 0.1 [0.0-0.3] ms-1/year, mean gradient 2 [0–4] mmHg/year and AVA -0.1 [-0.2-0.0] cm2/yr. Cohen's d statistic was more than double for CT-AVC (d=3.12) than each echocardiographic measure (peak velocity d=0.71 ; mean gradient d=0.66; AVA d=0.59, dimensionless index d=1.41).

Conclusion

CT-AVC is reproducible and demonstrates larger increases over time normalized to measurement repeatability compared to echocardiographic measures.

6.2 INTRODUCTION

Aortic stenosis represents a major cause of morbidity and mortality, the burden of which is set to increase. Currently the only definitive treatment is surgical or transcatheter aortic valve replacement in patients with severe symptomatic stenosis. Aortic valve narrowing progresses inexorably but at a variable and unpredictable rate in individual patients. Frequent echocardiographic follow-up is therefore mandated to determine the optimal timing for intervention. (98)

The clinical assessment of aortic stenosis severity is based upon two-dimensional echocardiography and Doppler, with measurement of the peak jet velocity, mean gradient and aortic valve area frequently used to guide severity assessment. (98) However, the measurement of disease progression by echocardiography is challenged by small changes in these markers of haemodynamic severity over time, combined with a relatively high degree of variability between measurements. (103, 198) A complementary imaging technique capable of providing improved reproducibility and sensitivity to change is therefore desirable. This is of importance in the clinical setting for accurate tracking of disease progression, and also in the research arena, where imaging endpoints are increasingly being utilized to assess the effects of novel therapies on aortic stenosis progression.

Quantification of aortic valve calcification by non-contrast computed tomography (CT-AVC) has demonstrated promise in accurately defining the valvular calcification burden, with sex-specific thresholds demonstrating good diagnostic accuracy compared to concordant echocardiography and providing incremental prognostic

information. (107, 199) In this study, our objective was to assess the ability of CT-AVC to monitor aortic stenosis progression compared to echocardiographic assessments. We investigated scan-rescan reproducibility and annual progression of both CT-AVC and echocardiographic measurements in a large prospective cohort of patients with aortic stenosis.

6.3 METHODS

6.3.1 STUDY POPULATION

Participants aged >50 years attending the outpatient department of the Edinburgh Heart Centre with aortic stenosis (peak aortic jet velocity >2 m/s) were recruited into two cohorts as part of a previously reported study (NCT01358513) and an ongoing clinical trial (NCT02132026). (60, 200, 201) In the *reproducibility cohort,* participants underwent repeat echocardiography or CT-AVC scanning within 4 weeks. In the *disease progression cohort*, participants underwent either repeat echocardiography, CT or both after at least one year. The study was approved by the Scottish Research Ethics Committee and performed in accordance with the Declaration of Helsinki. All patients provided written informed consent. This research was undertaken without patient involvement. Patients were not invited to comment on the study design and were not consulted to interpret the results or contribute to writing or editing of this document for readability or accuracy.

6.3.2 BASELINE ASSESSMENT

All participants underwent a comprehensive baseline clinical assessment. Echocardiography was performed by an experienced echocardiographer (AW) using a pre-specified protocol according to European Society of Echocardiography guidelines (202) on the same scanner of a British Society of Echocardiography accredited laboratory. Multiple acoustic windows were assessed with the S51 and D2cwc probes (Philips Medical Systems, the Netherlands). Aortic stenosis severity was assessed on the basis of the peak velocity, mean gradient, aortic valve area (AVA; calculated using the continuity equation) and dimensionless index (DI; defined as left ventricular outflow tract [LVOT] peak velocity divided by aortic peak velocity) according to American Heart Association and American College of Cardiology guidelines. (203)

To measure CT-AVC, an electrocardiogram (ECG)-gated non-contrast CT scan was performed during inspiration on a 128 multidetector scanner (Biograph mCT Siemens, 40 mA/rot tube voltage 100 kV, tube current selected using automatic exposure control). (54, 60) In the absence of contraindications, participants were administered beta-blockade to achieve a resting heart rate ≤65 bpm. Images were reconstructed in the transverse plane with 3 mm slice width and 1.5 mm increment. Valvular calcification was quantified by the Agatston method (31) using dedicated analysis software (Vitrea Advanced, Vital Images, Minnetonka, USA; Supplementary Figure 1). Care was taken to exclude calcium from extra-valvular structures such as the mitral valve annulus and coronary arteries. When confluent calcium extended into the ascending aorta, the origin of the left coronary artery was set as the most rostral slice

beyond which further calcium was excluded. (107, 204) The aortic valve calcium burden was expressed as CT-AVC in Agatston Units (AU).

6.3.3 SCAN RE-SCAN REPRODUCIBILITY

The reproducibility cohort consisted of two groups of participants with aortic stenosis who underwent either repeat CT-AVC scoring or echocardiographic assessment of their valve. In one group, CT was performed at baseline and again within 4 weeks. Scan-rescan reproducibility was determined for CT-AVC measurements. In a second group, patients underwent two echocardiographic assessments during the same visit, using the same scanner on the same bed and in the same room by two accredited echocardiographers (AW, JA) blinded to each other's assessment. Scan-rescan reproducibility was determined for haemodynamic measures of stenosis severity (peak velocity, mean gradient, AVA and DI).

6.3.4 ASSESSMENT OF DISEASE PROGRESSION

Participants in the *disease progression cohort* returned for repeat clinical assessment and echocardiography at 1 and 2 years as well as repeat CT at either 1 or 2-years. (61) The same scanner and imaging protocol was used for all CT scans and echocardiograms were performed by the same echocardiographer (AW) using the same scanner. To assess disease progression, annualized differences in each measure of stenosis severity were calculated. In participants who underwent three echocardiograms (baseline, 1 and 2 years), a line of best fit was used to determine annualized progression. Finally, Cohen's d statistic was calculated for CT-AVC and each echocardiographic assessment (peak velocity, mean gradient, AVA, DI) to

express the magnitude of progression normalized by the uncertainty in the measurement technique. This was calculated by dividing the annualized progression by the measurement repeatability, defined as $(1/\sqrt{2})$ of the standard deviation of the differences between measurements at scan and rescan. (205)

6.3.5 GROUP SIZE ANALYSIS

Power analysis was performed to determine group sizes needed to detect changes in CT-AVC and echocardiographic parameters in a hypothetical clinical trial. To determine the group size needed to detect changes after a therapeutic intervention in a single group, power analyses were based on paired t-tests. The annualized progression and measurement repeatability for each modality were used to compute the effect size and subsequently group sizes required to detect i) disease progression using CT-AVC and each echocardiography measure and ii) sample sizes needed to detect treatment effects on disease progression using the different modalities. Treatment effects of 30, 20 and 10% of the annualized progression values measured in the progression group were considered. Group sizes were estimated for powers of 70, 80 and 90% and an error probability (α) of 0.05. Analysis was carried out using G-power software. (206)

6.3.6 STATISTICAL METHODS

Continuous variables were expressed as either mean ± standard deviation or median [interquartile range] depending on normality. Parametric (unpaired Student's *t*-test) and non-parametric (Mann-Whitney U) tests were used for independent variables as appropriate. Categorical data were presented as n (%) and compared when appropriate using a contingency table and Fisher's or Chi-squared tests. Reproducibility was

assessed using Bland-Altman analysis and intra-class correlation (ICC). Correlation between continuous variables was assessed with linear regression analysis and either Pearson's r or Spearman's Rho subject to normality. Annualized rates of progression were calculated using the difference between two time-points (CT-AVC) or regression analysis over three time-points (echocardiography). Statistical significance was defined as two-sided $p<0.05$.

6.4 RESULTS

6.4.1 STUDY POPULATION

Thirty-three participants comprised the reproducibility cohort (aged 71±8, 68% male). Eighteen participants underwent two echocardiograms (aged 70±8, 67% male, Table 6.1) and fifteen underwent two CT scans (aged 73±7, 67% male, Table 1). A total of 81 participants were enrolled in the disease progression cohort (aged 72±8%, 69% male, Table 6.1). Of these, 71 underwent repeat echocardiography and 61 underwent repeat CT-AVC. Ten CT scans were excluded due to suboptimal image quality, leaving 51 included in the analysis. There was a high prevalence of cardiovascular risk factors, with the majority of patients having co-existing hypertension.

Table 6.1. Baseline characteristics

	Reproducibility Cohort		Disease Progression Cohort		
	Echocardiography	**CT-AVC**	**All**	**Echo Follow-up**	**CT-AVC Follow-up**
Number	18	15	81	71	51
Age (years)	70±8	73±7	72±8	72±8.2	73±7
Male	12 (67)	10 (67)	55 (69)	50 (70)	34 (67)
Body Mass Index (kg/m^2)	30±4	30±6	29±5	28±4	28±4
Systolic Blood Pressure (mmHg)	152±20	151±18	146±20	144±18	143±17
Co-morbidity					
Diabetes Mellitus	4 (22)	4 (27)	15 (18)	13 (18)	9 (18)
Hypertension	13 (72)	11 (73)	60 (74)	50 (70)	36 (70)
Documented CAD	9 (50)	6 (40)	33 (41)	31 (44)	26 (51)
Current smoker	8 (44)	6 (40)	9 (11)	8 (11)	5 (9)
Serum Creatinine (mg/dL)	0.89±0.23	0.70±0.11	1.01±0.31	1.00±0.30	0.98±0.28
Medications					
ACE inhibitors	8 (44)	6 (40)	32 (40)	27 (38)	20 (39)
AIIRB	4 (22)	3 (20)	11 (13)	9 (13)	7 (13)
Beta Blockers	7 (39)	7 (47)	33 (41)	30 (43)	23 (45)
Statins	14 (78)	9 (60)	54 (66)	46 (64)	34 (67)
Baseline Echocardiographic Assessment					
AV jet velocity (m/s)	3.5 [3.2-4.0]	3.3 [3.0-3.8]	3.4 [2.8-4.1]	3.3 [2.7-3.9]	3.0 [2.5-3.6]
AV mean gradient (mmHg)	25 [21-31]	24 [22-30]	25 [16-36]	24 [14-32]	21 [13-25]
AV area (cm^2)	1.1 [0.8-1.3]	1.1 [1.0-1.3)	1.1 [0.9-1.4]	1.2 [0.9-1.5]	1.2 [1.0-1.5]
Dimensionless Index	0.30 [0.23-0.37]	0.32 [0.25-0.40]	0.32 [0.25-0.39]	0.33 [0.26-0.39]	0.36 [0.30-0.40]
CT Assessment					
AV Calcium Score (AU)	989 [497-1708]	1178 [579-2109]	1339 [553-2422]	1190 [505-2182]	874 [459-1792]

Mean±SD, median [IQR] and number (percentage). Abbreviations: ACE, angiotensin converting enzyme; AIIRB, angiotensin 2 receptor antagonists; AS, aortic stenosis; AV, aortic valve; CAD, coronary artery disease; AU, Agatston units; LV, left ventricle; LVH, left ventricular hypertrophy.

6.4.2 REPRODUCIBILITY COHORT

Within the reproducibility cohort (n=33), 15 patients underwent two non-contrast CT scans within 3.9±3.3 weeks. Scan-rescan reproducibility for CT-AVC was excellent, without fixed or proportional bias (mean difference -1% [limits of agreement -12 to 10%], ICC 0.99;Table 6.2, Figure 6.1). Measurement variability for CT-AVC was 49 AU, or 4.2% when normalised to the median CT-AVC at baseline. Intra-observer (median CT-AVC 1178 AU, mean difference 1% [limits of agreement 9 to -11%], ICC 0.99) and inter-observer (median CT-AVC 1207 AU, mean difference 0% [limits of agreement -5 to 6%], ICC 0.99) reproducibility were also excellent. Scan-rescan reproducibility was also assessed with two observers and demonstrated good reproducibility (ICC 1.00 (0.99-1.00) mean difference 2.57% (44 AU) and limits of agreement -27.5- 22.4%.(Figure 6.2).

Eighteen patients underwent two echocardiograms during a single study visit. Scan-rescan reproducibility was excellent for peak velocity (mean difference 5%; limits of agreement -7 to 17%; ICC 0.96; measurement repeatability 4.0%; ICC 0.96) and DI (mean difference -1.7%; limits of agreement -11.1-14.5%; ICC 0.98; measurement repeatability 3.3%). Reproducibility was also good for mean gradient (mean difference 1%; limits of agreement -25-27%; ICC 0.97; measurement repeatability 12.0%; ICC 0.97) but less reliable in the assessment of AVA (mean difference -8%; limits of agreement -44 to 28%;ICC 0.85, measurement repeatability 15.5%;Table 6.2).

Table 6.2 Reproducibility of CT-AVC and echocardiography assessments of aortic stenosis severity.

	Bias, % **(95% limits of agreement)**	**Bias, units** **(SD of difference of scan 1 and scan 2)**	**Measurement repeatability, units (%)**	**Intraclass Correlation** **(95% limit of agreement)**
	CT AVC			
Scan-scan reproducibility, AU	-1 (-12 – 10)	-20 (69)	49 (4.2%)	0.99 (0.99 – 1.00)
Intra-observer reproducibility, AU	-1 (-11 – 7)	-12 (85)	-	1.00 (1.00 – 1.00)
Inter-observer reproducibility, AU	0 (-5 – 6)	11 (65)	-	0.99 (0.99 – 1.00)
	Echocardiography, scan-rescan			
AV max, ms^{-1}	5 (-7 – 17)	0.17 (0.20)	0.14 (4.0%)	0.96 (0.78 – 0.99)
Mean gradient, mmHg	1 (-25 – 27)	0.28 (4.3)	3.0 (12.0%)	0.97 (0.91 – 0.99)
AVA (VTI), cm^2	-8 (-44 – 28)	-0.11 (0.24)	0.17 (15.5%)	0.85 (0.59 – 0.95)
Dimensionless Index	-2(-11-15)	0.01(0.02)	0.01(3.3%)	0.98(0.95-0.99)

Mean±SD, median [IQR]. Abbreviations: AV: aortic valve; AU: Agatston units

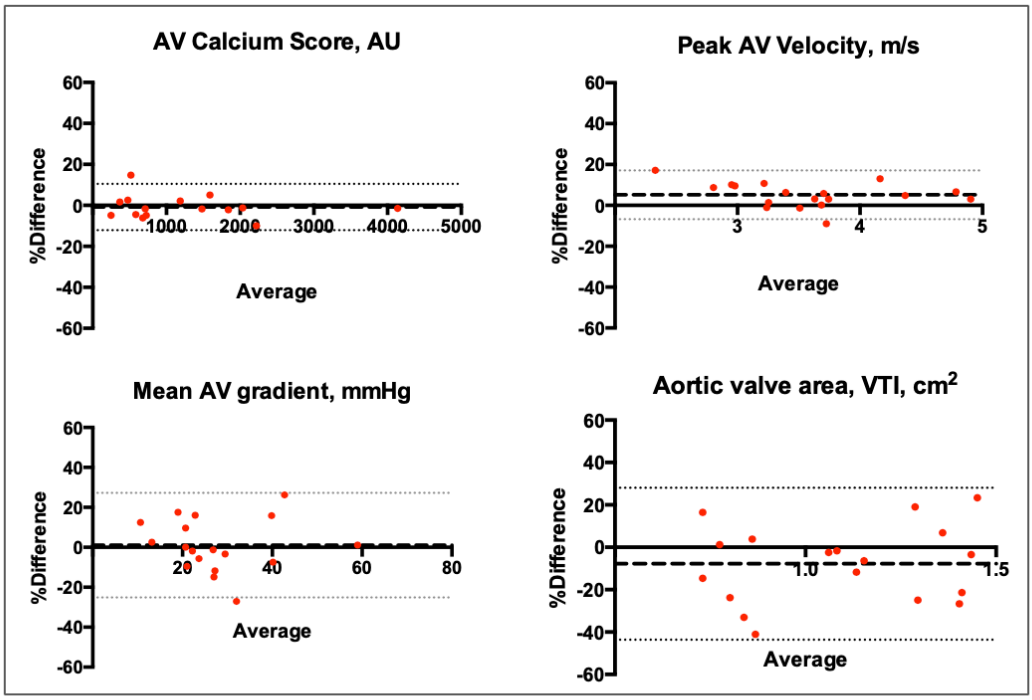

Figure 6.1. Scan-rescan reproducibility of CT-AVC and echocardiography assessments of aortic stenosis severity.

Bland-Altman plots displaying the scan rescan reproducibility of aortic stenosis severity measurements on serial CT-AVC (3.9±3.3 weeks) and echocardiography (1±0 days). VTI, velocity time integral.

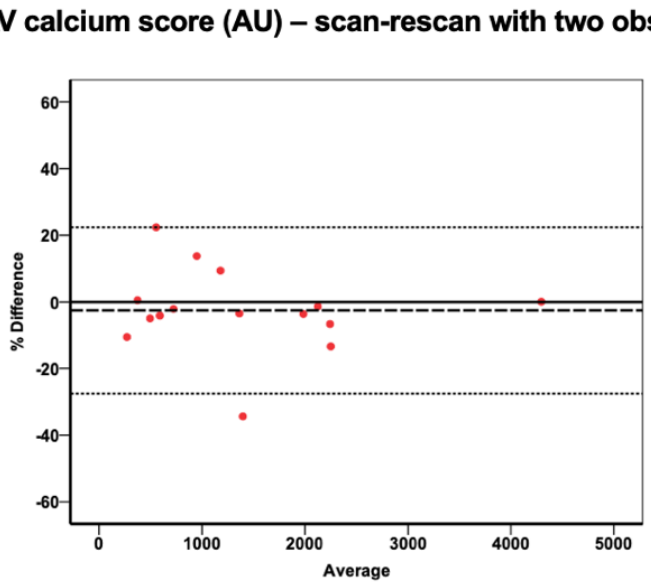

Figure 6.2. Scan-rescan reproducibility of CT-AVC using a different observer for each scan.

Scan-rescan reproducibility was also assessed with two different observers and demonstrated good reproducibility (ICC 1.00 (0.99-1.00) mean difference 2.57% (44 AU) and limits of agreement -27.5- 22.4%.

6.4.3 CT-AVC AND AORTIC STENOSIS SEVERITY

At baseline, CT-AVC correlated with all echocardiographic measures (Table 6.3). The closest associations were observed with peak velocity (r=0.75 [95% CI 0.63 to 0.84], p<0.001) and mean gradient (r=0.75 [0.64 to 0.83], p<0.001) and the weakest with AVA (r=-0.46 [-0.61 to -0.25], p<0.001).

Table 6.3. Correlation between CT-AVC and echocardiographic measures of aortic stenosis severity.

Pearson's correlations between square-root transformed computed tomography calcium scores (CT-AVC) and echocardiographic indices. R values (95% confidence intervals) are shown.

	CT-AVC (AU)	**Peak Aortic Jet Velocity (m/s)**	**Mean Aortic Gradient (mmHg)**	**Aortic Valve Area (cm^2)**
CT-AVC (AU)		0.75 (0.63 to 0.84) P<0.001	0.75 (0.64 to 0.83) P<0.001	-0.46 (-0.61 to -0.25) P<0.001
Peak Aortic Jet Velocity (m/s)	0.75 (0.63 to 0.84) P<0.001		0.97 (0.96 to 0.98) P<0.001	-0.66 (-0.76 to -0.53) P<0.001
Mean Aortic Gradient (mmHg)	0.75 (0.64 to 0.83) P<0.001	0.97 (0.96 to 0.98) P<0.001		-0.71 (-0.79 to -0.59) P<0.001
Aortic Valve Area (cm^2)	-0.46 (-0.61 to 0.25) P<0.001	-0.66 (-0.76 to -0.53) P<0.001	-0.71 (-0.79 - -0.59) P<0.001	

Abbreviations: AVC, aortic valve calcium; CE, continuity equation.

6.4.4 PATIENT FOLLOW-UP

During the 2-year follow-up period, (736 [722–760] days), 61 participants (75%) underwent repeat CT (13 at 1 year and 48 at 2 years). Images were non-interpretable in 10 participants (16%) due to motion artefact and were excluded, predominantly in those in whom beta-blockers were contra-indicated. Follow-up echocardiography was performed in 71 participants at 1 year and 62 at 2 years. No echocardiography scans were excluded from analysis.

6.4.5 AORTIC STENOSIS DISEASE PROGRESSION

Across all patients, modest progression in each echocardiographic measure of severity was observed (Δ peak velocity 0.1 [0.0-0.3] ms^{-1}/year; Δ mean gradient 2 [0–4] mmHg/year; Δ AVA -0.1 [-0.2-0.0), ΔDI 0.02 [-0.04 to -0.01]; Figure 6.3, Table 6.4). When patients were divided into mild, moderate and severe aortic stenosis, those in the moderate group demonstrated the clearest evidence of disease progression (n=30, Δ peak velocity 0.2 [0.1-0.3] ms^{-1}/year; Δ mean gradient 3 [1–5] mmHg/year; Table 6.4).

Across the cohort as a whole, CT-AVC progressed by 152 [65-375] AU/year, with the most rapid rates of progression observed in participants with the most severe disease (Δ CT-AVC; mild AS 64 [48-134] AU/year, moderate AS 289 [106-443] AU/year, severe AS 342 [163-583] AU/year) (Figure 6.3, Table 6.4).

The Cohen's d-statistic (d) was calculated by dividing the overall annualized rate of change in each severity measure by the measurement repeatability (Table 6.4) By this method, CT-AVC displayed a greater progression to measurement repeatability ratio (CT-AVC: d = 3.12) when compared to each echocardiographic parameter (peak velocity: d = 0.71; mean gradient: d = 0.66; AVA: d = 0.59; DI d=1.41). When patients with more advanced disease were considered, the differences between echocardiography and CT-AVC were greater. In participants with severe aortic stenosis, CT-AVC displayed a greater than six-fold higher value (d = 6.98) compared to echocardiographic measures (peak velocity d = 0.71; mean gradient d =1.0; AVA d =0.0; DI d=0.71). In those with moderate and mild disease, the d-statistic for CT-AVC

remained higher when compared with echocardiographic measures of the same severity (Table 6.4).

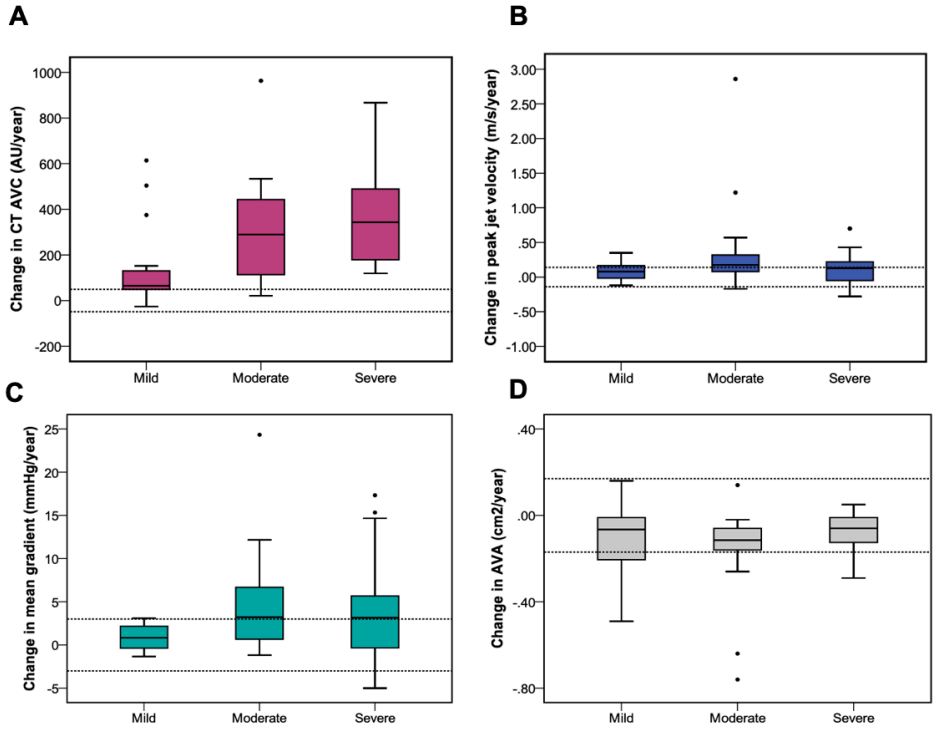

Figure 6.3. Aortic stenosis disease progression measured using CT-AVC and echocardiography.

Annualized disease progression across each cohort using CT calcium scoring (**A**), peak aortic jet velocity (B), mean gradient (C) and aortic valve area (D). Relatively large annualized changes in the CT calcium score are observed compared to smaller changes and wide overlap in the measurements obtained by echocardiography. Dashed lines demonstrate the expected measurement repeatability from scan-rescan measurements.

Table 6.4. Disease progression on echocardiography and CT-AVC in patients with aortic stenosis.

Variable	All patients	Mild Aortic Stenosis	Moderate Aortic Stenosis	Severe Aortic Stenosis
Baseline Echocardiography				
No. of patients	81	25	33	23
Peak aortic-jet velocity, (m/s)	3.4 [2.8-4.1]	2.5 [2.4-2.7]	3.4 [3.2-3.7]	4.5 [4.1-5.1]
Mean gradient (mmHg)	25 [16-36]	13 [11-16]	25 [22-29]	43 [38-58]
Aortic-valve area (cm^2)	1.1 [0.9-1.4]	1.4 [1.2-1.7]	1.1 [1.0-1.3]	0.8 [0.6-0.9]
Follow-up Echocardiography				
No. of patients	71	24	30	17
Δ aortic jet velocity (m/s/year)	0.1 [0.0-0.3]	0.1 [0.0-0.2]	0.2 [0.1-0.3]	0.1 [-0.1-0.2]
Δ aortic jet velocity (%m/s/year)	3.5 [0.0 to 7.8]	3.2 [-0.7 to 6.3]	5.0 [2.3 to 10.2]	3.2 [-1.1 to 5.2]
Cohen's D statistic	0.71	0.71	1.43	0.71
Δ mean gradient (mmHg/year)	2 [0-4]	1 [0-2]	3 [1-5]	3 [0 to 5]
Δ mean gradient (%mmHg/year)	9.5 [-0.5 to 17.0]	7.5 [-2.4 to 14.9]	11.6 [2.4 to 29.5]	7.0 [-1.7 to 13.7]
Cohen's D statistic	0.66	0.33	1.0	1.0
Δ aortic-valve area (cm^2/year)	-0.1 [-0.2 to 0.0]	-0.1 [-0.2 to -0.0]	-0.1 [-0.1 to -0.0]	0.0 [-0.1 to -0.0]
Δ aortic-valve area (%cm^2/year)	-8.7 [-14.4 to -2.9]	-5.2 [-13.3 to -0.6]	-9.9 [-15.6 to -4.8]	-7.7 [-15.0 to 0]
Cohen's D statistic	0.59	0.59	0.59	0.0
Δ Dimensionless Index	-0.02 [-0.04 to -0.01]	-0.02 [-0.04 to 0.00]	-0.02 [-0.04 to -0.01]	-0.01 [-0.02 to 0.00]
Δ Dimensionless Index (%/year)	-5.7 [-11 to -2.0]	-4.4 [10.0 to -0.3]	-6.7 [-13.6 to -2.9]	-5.7 [-10.3 to 2.3]
Cohen's D statistic	1.41	1.41	1.41	0.71
Baseline Computed Tomography				
No. of patients	72	23	30	19
AV Calcium score (AU)	1339 [553 to 2422]	489 [281 to 693]	1427 [777 to 2215]	3386 [1770 to 6211]
Follow-up Computed Tomography				
No. of patients	51	21	24	6
Δ AV calcium score (AU / year)	152 [65-375]	64 [48-134]	289 [106-443]	342 [163-583]
Δ AV calcium score (%AU / year)	20.0 [13.0 to 24.5]	20.3 [17.5 to 31.1]	20.0 [10.8 to 24.5]	16.9 [10.9-24.4]
Cohen's D statistic	3.12	1.30	5.90	6.98

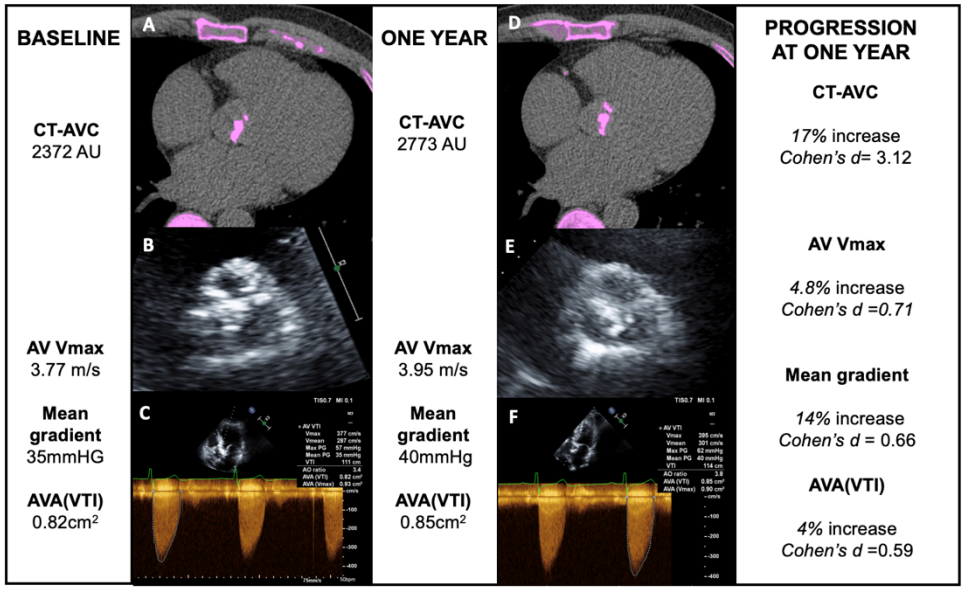

Figure 6.4. Computed tomography calcium scoring and echocardiography to monitor disease progression in aortic stenosis.

CT calcium scoring of the aortic valve and echocardiography in a patient at baseline (A-C) and one year (D-F). Baseline CT calcium scoring demonstrates CT-AVC of 2372 AU (A), transthoracic echocardiography of the aortic valve shows calcified leaflets with a calcium score of 4 (B) and doppler echocardiography demonstrates a peak velocity of 3.77 m/s (C) at baseline. At one year, CT-AVC has increased to 2773 (D), the aortic valve calcium score on echocardiography is graded as 4 (E) and the peak jet velocity has increased to 3.95 m/s (F).

6.4.6 GROUP SIZE ANALYSIS

Using the cohort-averaged progression and measurement repeatability values, the effect size for a matched-pairs t-test was computed for CT-AVC and each echocardiographic measure. The group size required to detect annualised disease progression for CT-AVC was smaller than for echocardiographic measures (CT-AVC: 4, peak velocity: 33, mean gradient: 39, AVA: 48 [$\alpha = 0.05$, power = 80%]). Similarly the group size required to detect a treatment effect of a new therapy (30, 20 and 10%

reduction in the annualized progression) was more than 10-fold smaller for CT-AVC than for echocardiographic measures (CT-AVC: 20, 43, 165 patients respectively; peak velocity: 351, 787, 3142 patients respectively; mean gradient: 403, 910, 3632 patients respectively; AVA: 505, 1134, 4516 patients respectively [$\alpha = 0.05$, power = 80%]) (Figure 6.5).

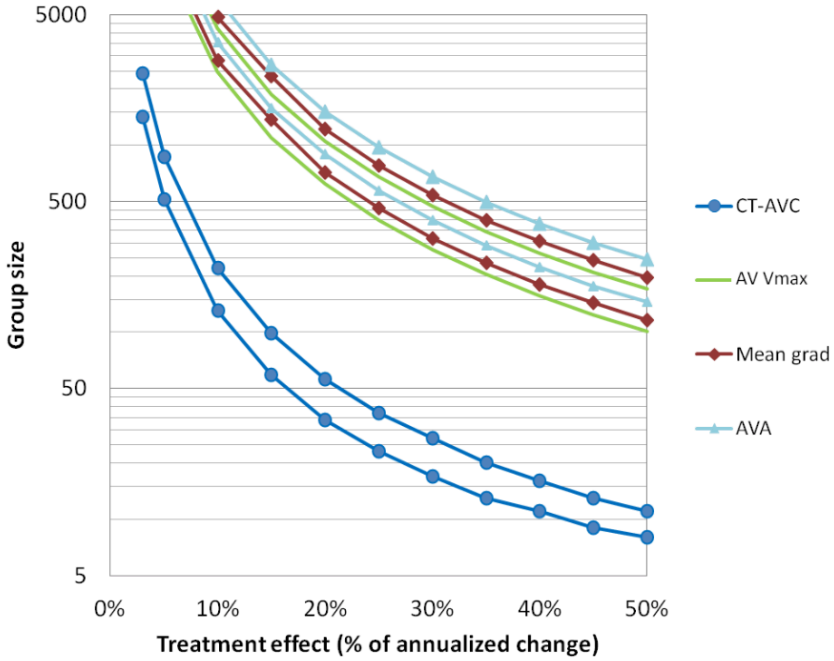

Figure 6.5. Sample sizes needed for studies of novel therapies in aortic stenosis using CT-AVC to assess their effect on disease progression.

The number of participants required in a study to detect a given treatment effect size at different levels of power are plotted. For each modality an upper bound at 90% power and lower bound at 70% are plotted with $\alpha = 0.05$ for all. Nominal treatment effects up to 50% of the measured annualized progression for each modality are considered.

6.5 DISCUSSION

In this study, we have investigated the utility of CT-AVC and echocardiography in assessing disease progression in patients with aortic stenosis. CT-AVC demonstrated excellent scan-rescan reproducibility. Calculation of Cohen's d-statistic demonstrated that CT-AVC had a large annualized change normalized to measurement repeatability compared to echocardiography, with a four-fold higher value for CT-AVC (d=3.12) compared to peak velocity (d=0.71). CT-AVC may therefore be a useful technique both in clinical practice for assessing aortic stenosis progression and as an endpoint in clinical trials assessing the efficacy of novel therapies.

Given the central role of calcification in the progression of aortic stenosis, direct assessments of calcification hold major interest. (79) Quantification of aortic valve calcification has demonstrated considerable promise in a number of studies, discerning the presence of severe stenosis amongst patients with discordant echocardiography and providing powerful prognostic information. (106, 199, 207) In this study, we have demonstrated excellent scan-rescan reproducibility of CT-AVC coupled with relatively large progression in values over time, demonstrating the feasibility and potential advantages of this modality for tracking aortic stenosis progression.

Before an imaging technique can be applied to routine clinical practice, clinicians must be reassured that the technique is robust and reproducible. Measurement of CT-AVC is technically straightforward although can be complicated by motion artefact, particularly in patients with advanced disease, systolic dysfunction or conduction disease in whom administration of beta-blockade is not possible. In this study, this

resulted in exclusion of 16% of scans. This limitation of CT-AVC must be considered when deciding whether to use this test in the clinical or research settings and certain patient characteristics including BMI, tachycardia or contraindications to beta blockade may be used to identify patients in whom CT-AVC may be unreliable. However, when CT-AVC is possible we have demonstrated that excellent reproducibility can be achieved with a consistent and standardized approach. While all echocardiography scans were of diagnostic quality in our study, we acknowledge that there is a selection bias in our patient population since participants were only recruited if they had clear assessments of aortic stenosis severity on clinical echocardiograms. In non-selective cohorts, it is estimated that 10-15% of patients have poor echocardiographic windows, similar to our observations for CT-AVC. Further, variability in echocardiography was minimized by performing two echocardiograms under as consistent conditions as possible, thereby diminishing many sources of error encountered in clinical practice. This approach necessitated two different echocardiographers performing the scan to avoid recall bias.

For echocardiography, while peak velocity and mean gradient both demonstrated good reproducibility, repeatability of AVA was poor, likely reflecting the multiple different measurements required for its calculation. Measurement of the left ventricular outflow tract (LVOT) diameter represents the major source of error in calculation of AVA. By disregarding LVOT diameter and considering a simplified ratio of LVOT to aortic velocity, the dimensionless index (DI), this overcomes discrepancies in LVOT measurements and has proven effective in distinguishing aortic stenosis severity and

predicting adverse outcomes. (101, 208, 209) We have shown that this measure improves reproducibility when compared to AVA.

In order to compare the utility of CT-AVC and echocardiography for tracking disease progression, both the magnitude of change and measurement repeatability must be considered. On this basis, we calculated the Cohen's d-statistic for each modality. This indicated that CT-AVC appears superior to echocardiography for detecting small changes in disease severity over time. Indeed, this marker was four times higher for CT-AVC compared to peak velocity. This may have important clinical implications when tracking disease progression and predicting when patients are likely to require valve intervention. Further research is required to assess how this approach may work in clinical practice, but CT-AVC is likely to be of particular value in patients whose heart rate can be optimised for imaging and who have poor echocardiographic windows or low flow states where mean gradient and peak velocity may underestimate disease severity.

Our data also support a role for CT-AVC as an endpoint in research trials investigating the effects of novel therapies. Imaging end points are increasingly adopted for this purpose, and those with greater reproducibility and sensitivity to detect small changes in progression are likely to minimize cost and sample sizes required (SALTIRE 2 NCT02132026). Indeed, our data suggest that >10-fold fewer patients would be required to detect 10, 20 and 30% treatment effects using CT-AVC (165, 43 and 20 patients respectively) compared to peak velocity (3142, 787 and 351 patients respectively). While this suggests a considerable advantage in using CT-AVC, consideration should be placed on the frequency of non-diagnostic scans and clinical

characteristics for which CT-AVC may not be suitable. Indeed, the proportion of non-interpretable CT scans must be taken into account when considering sample sizes and measurement repeatability. It is also important to consider that CT-AVC does not account for the effects of therapy on non-calcific valve thickening (i.e. fibrosis) and echocardiography remains the first line imaging technique to assess aortic stenosis. Further, another important consideration is the radiation dose associated with CT, although standard imaging techniques enable CT calcium scoring to be performed with low levels of radiation exposure (1-3 mSV). (35)

Our study has several limitations. We acknowledge that our study numbers are small and in the reproducibility cohort different patients underwent repeat CT-AVC to those undergoing repeat echocardiography. While the characteristics of both patient groups were similar, we cannot rule out the possibility of confounding variables and recognise this as a limitation of our study. Our study findings should therefore be confirmed in larger studies with direct comparisons of reproducibility and disease progression for echo and CT-AVC within the same population. Further, we assessed annualised changes in disease severity in all patients who underwent follow-up beyond one year. This assumes linear disease progression and therefore does not take into account a more rapid rise in disease progression as severity increases, although this is consistent with other studies investigating disease progression in aortic stenosis. (110, 210)

6.6 CONCLUSION

CT-AVC is a robust and reproducible imaging technique that holds major promise as a method for tracking disease progression in aortic stenosis.

CHAPTER 7

Motion-Corrected Imaging of the Aortic Valve with ^{18}F-Fluoride PET-CT and PET-MR: A Feasibility Study

Published in:

Doris MK*, Rubeaux M*, Pawade T, Otaki Y, Xie Y, Li D, Tamarappoo BK, Newby DE, Berman DS, Dweck MR, Slomka PJ, Damini D. Motion-corrected imaging of the aortic valve with ^{18}F-NaF PET/CT and PET/MRI: A feasibility study. *J Nucl Med* 2017 Nov;58(11):1811-1814

**Equal contribution as first author*

Chapter 7 Motion-Corrected Imaging of the Aortic Valve with ^{18}F-fluoride PET-CT and PET-MR: A Feasibility Study.

7.1 SUMMARY

Introduction

We investigated whether motion correction of gated ^{18}F-fluoride PET-CT and PET-MR of the aortic valve could improve PET quantitation and image quality.

Methods

A diffeomorphic, mass-preserving, anatomy-guided registration algorithm was used to align PET images from 4 cardiac gates, preserving all counts, and applied to PET-MR and PET-CT data of six patients with aortic stenosis. Measured Signal-to-Noise Ratios (SNRs) and Tissue-to-Background Ratios (TBRs) were compared with the standard method of utilizing only the diastolic gate.

Results

High-intensity ^{18}F-fluoride uptake was observed in the aortic valve of all 6 patients. Following motion correction, SNR and TBR increased compared to the diastolic gate (SNR 51.61 vs 21.0; TBR 2.85 vs 2.22) and summed data (SNR 51.61 vs 34.10, p=0.028; TBR 2.85 vs 1.95, median, p=0.028 for all). Furthermore, noise decreased from 0.105 (median, diastolic) to 0.042 (median, motion-corrected [p=0.028]).

Conclusion

Motion-corrected ^{18}F-fluoride PET-CT and PET-MR imaging markedly improves SNR, resulting in improved image quality.

7.2 INTRODUCTION

Aortic stenosis is the commonest form of valve disease in the western world and is set to increase rapidly with an aging population. (79, 80) Recently, interest has developed in the potential role of ^{18}F-fluoride Positron Emission Tomography (PET) for the assessment of disease activity, the prediction of disease progression and as an end point in clinical trials investigating novel therapies. (61, 79)

Combined PET Computed Tomography (PET-CT) and PET Magnetic Resonance (PET-MR) each possess unique attributes suited to the assessment of aortic stenosis. PET-CT provides detailed anatomical information with respect to valve morphology and calcification, whilst PET-MR informs about the hypertrophic response of the left ventricle, myocardial fibrosis and the transition to heart failure. (211)

A major challenge faced in PET-CT and PET-MR imaging of the heart is the impact of cardiac, respiratory and gross patient movement on PET image quality. Prior 18F-fluoride PET-CT studies have utilized data reconstructed from the diastolic gate (25% of the cardiac cycle) to avoid blurring from cardiac motion, but at the expense of increased image noise. (55, 120)We have developed a novel software cardiac motion correction method which allows the use of data from the full cardiac cycle. This enhances image quality and quantitation in the coronary arteries while reducing noise. (149) To our knowledge, this approach has not yet been applied to patients with valvular heart disease nor PET-MR imaging. In this dual centre study, we report the use of multimodality motion correction in hybrid PET-CT and PET-MR in a group of patients with aortic stenosis.

7.3 METHODS

7.3.1 STUDY POPULATION

7.3.1.1 PET-CT

Patients with aortic stenosis were recruited prospectively from outpatient clinics at the Edinburgh Heart Centre as part of the ongoing SALTIRE 2 clinical trial (NCT02132026). The study was approved by the local research ethics committee in accordance with the declaration of Helsinki and all patients provided written informed consent.

7.3.1.2 PET-MR

A 60-year-old asymptomatic male was prospectively recruited as part of an ongoing research study. The study was approved by the IRB and the patient provided written informed consent for use of the data.

7.3.2 IMAGE ACQUISITION AND ANALYSIS

7.3.2.1 PET-MR

The PET-MR protocol involved PET acquisition in list mode for 40-60 min, with concurrent MR acquisitions to assess the myocardium comprehensively (Biograph mMR scanner, Siemens). These included standard cine views to evaluate left ventricular function, contrast-enhanced MR angiography (MRA) acquired in diastole, late gadolinium enhancement for assessment of midwall fibrosis or infarction (212, 213) and a new interleaved T1-weighted sequence ('CATCH'). (214) The pre-contrast CATCH sequence facilitates acquisition of a dark-blood T1-weighted image in one heartbeat followed by an anatomical bright-blood reference in the next; post-

reconstruction, a hyper-intense signal has been shown to correspond to potential intra-plaque haemorrhage. (214)

For PET-MR imaging, 212 MBq of 18F-fluoride was injected and MR image acquisition began 20 min later. PET acquisition began one hour post injection and was performed in list mode for over 60 min. Dixon-based MR images for water and fat were used for attenuation correction using the standard method provided on the scanner.

7.3.2.2 PET-CT

125 MBq of 18F-fluoride was administered intravenously and patients were subsequently rested in a quiet environment. After 60 min, image acquisition was performed using a hybrid PET-CT scanner (Biograph mCT; Siemens). Attenuation-correction CT scans were performed before acquisition of PET data in list mode using a single 30-min bed position centred on the valve in 3-dimensional mode. Finally, prospectively ECG-gated contrast-enhanced CT angiography was performed in end-expiration. Patients were given 25 mg of oral metoprolol if their resting heart rate was >65 beats/min.

For both PET-MR and PET-CT, PET images were reconstructed using a standard iterative Ordered Subsets Expectation Maximization (OSEM) algorithm with High Definition resolution recovery (215), using 4 cardiac gates.

7.3.3 CARDIAC MOTION CORRECTION

Cardiac motion correction was performed using an anatomically guided automated registration algorithm, similar to our method previously described. (74, 149) First, a

three-dimensional sphere was drawn to define the aortic valve region. A non-linear registration algorithm used was a diffeomorphic mass-preserving, anatomy-guided Demons method which optimises the global energy between PET frames; with built-in optimisation for anatomical data. (150, 186, 216) The motion corrected gates were then summed to form a motion-free image (74) containing all the PET counts. The motion correction procedure required approximately 10 min per patient. PET quantification was performed by delimiting 3-dimensional regions-of-interest on fused PET-MR angiography and PET-CT angiography using FusionQuant software (Cedars-Sinai Medical Center, Los Angeles, CA). For each PET-CT subject, rigid registration was performed between the PET data and CTA on the transverse, sagittal and coronal planes using CTA data from the most optimal diastolic phase. For the PET-MR subject, MR angiography was acquired during a single diastolic phase and this image was similarly fused and manually registered with the PET data. Background blood pool activity was measured in the right atrium using mean standardised uptake values from 3-dimensional spherical volumes. Maximum uptake in the aortic valve was computed by creating a sphere-shaped volume of interest through the aortic valve after re-orientation of the image into the aortic valve plane. (120) Signal to noise ratio (defined as the maximum uptake in the aortic valve divided by the image noise; SNR) and Tissue-to-Background Ratio (defined as the maximum uptake in the aortic valve divided by the mean standardised uptake value of the blood pool; TBR) were computed in the motion-corrected image, summed image and in the original diastolic gate. PET image noise was calculated as the standard deviation of the blood pool measurement.

7.3.4 STATISTICAL ANALYSIS

Statistical analyses were performed with SPSS (SPSS version 22, IBM corp). Continuous variables are expressed as mean ± standard deviation. The Shapiro-Wilk test was used to assess normality for continuous data. Non-parametric data are expressed as median and interquartile range. Two-sample *t*-test or Wilcoxon rank-sum test were applied to compare groups for continuous variables. A two-sided $p<0.05$ was taken as statistically significant.

7.4 RESULTS

Increased ^{18}F-fluoride uptake in the aortic valve was observed in all six patients (Table 7.1 and Figure 7.1 and Figure 7.2). Following motion correction, there was an increase in SNR and TBR when compared to the diastolic gate (SNR 51.61[32.79-61.15] vs 21.0 [16.37-25.25]; TBR 2.85[2.45-3.84] vs 2.22 [1.94-3.29], median [IQR], p=0.028 for all) and summed data (SNR 51.61[32.79-61.15] vs 34.10[24.36-42.54]; TBR 2.85[2.45-3.84] vs 1.95[1.75-2.66], median[IQR], p=0.028 for all) (Figure 7.3**).** Further, there was a reduction in noise in the motion corrected image when compared to both the summed data 0.042[0.037-0.076] vs 0.052[0.051-0.104]) and original diastolic gate (0.042[0.037-0.076] vs 0.105[0.096-0.160], median[IQR] p=0.028 for all) (Figure 7.4). On the PET-MR scan, detailed CMR investigation of the left ventricle was possible including measurements of the left ventricle mass volumes (45 g/m^2) and ejection fraction (53%) as well as late gadolinium enhancement imaging. The CATCH sequence was also well tolerated by the patient but did not reveal evidence of haemorrhage in either the valve or the coronary arteries.

Table 7.1. Baseline characteristics.

Baseline Characteristics	
Age in years, mean (SD)	74 (9)
Men, n (%)	4 (67)
Body Mass Index (kg/m^2), mean (SD)	27 (5)
Past Medical History	
CABG/PCI, n (%)	2 (33)
Previous MI, n (%)	0
Hypercholesterolemia, n (%)	4 (67)
Hypertension, n (%)	2 (33)
Renal Disease, n (%)	0
Diabetes, n (%)	2 (33)
Medications	
ACE inhibitors/AIIRB, n (%)	3 (50)
Beta blockers, n (%)	3 (50)
Statin, n (%)	4 (67)
Echocardiography	
AV jet velocity (m/sec), mean (SD)	3.23 (0.37)
AV mean gradient (mmHg), mean (SD)	24 (6.72)

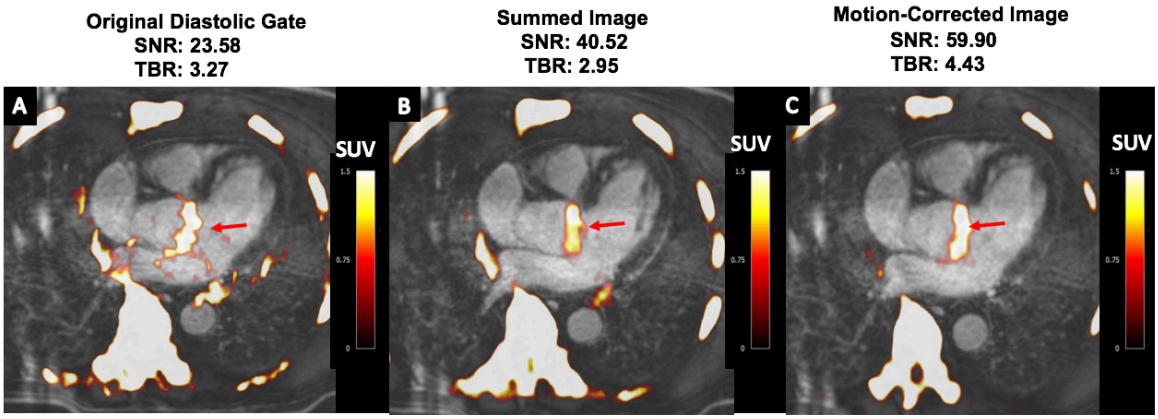

Figure 7.1. Fused ^{18}F-fluoride PET and contrast-enhanced MRA of the aortic valve in a 60-year-old male with aortic stenosis.

Images display the original diastolic gate (A), summed image (B) and motion-corrected image (C) with focal ^{18}F-fluoride uptake (red arrows).

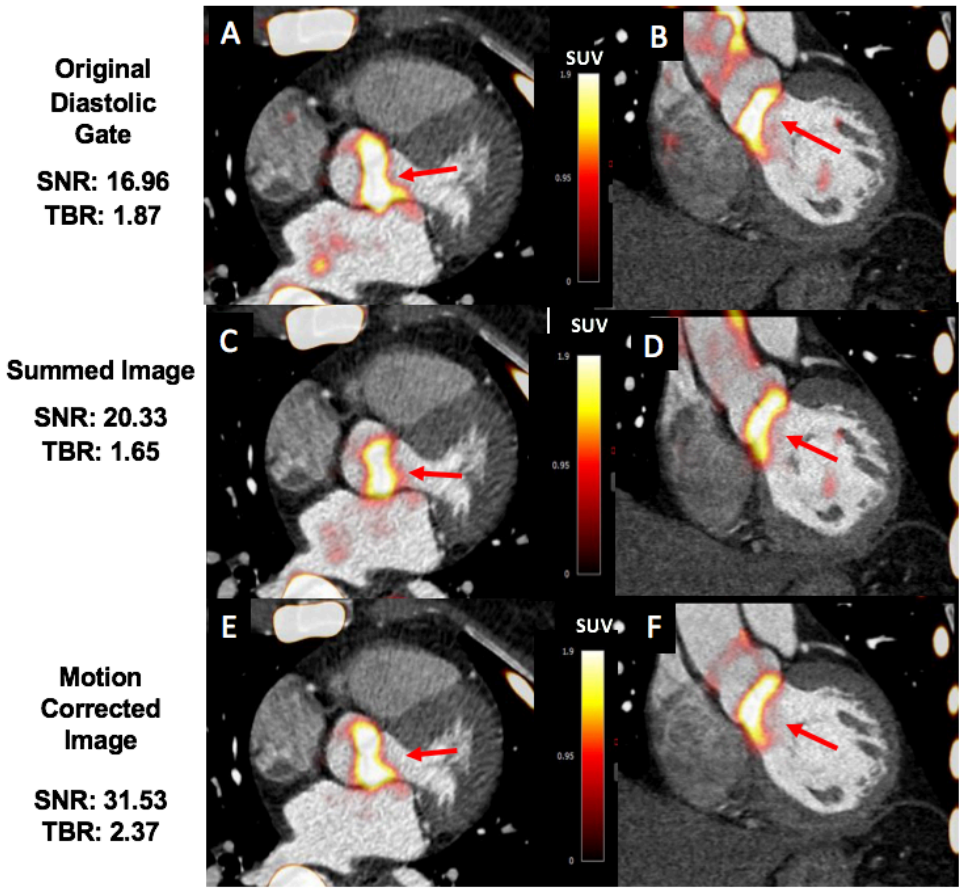

Figure 7.2. Fused PET-CTA images in a 79-year-old female with aortic stenosis.

Images display the original diastolic gate (A&B), summed image (C&D) and motion-corrected image (E&F) demonstrating focal 18F-fluoride uptake (red arrows).

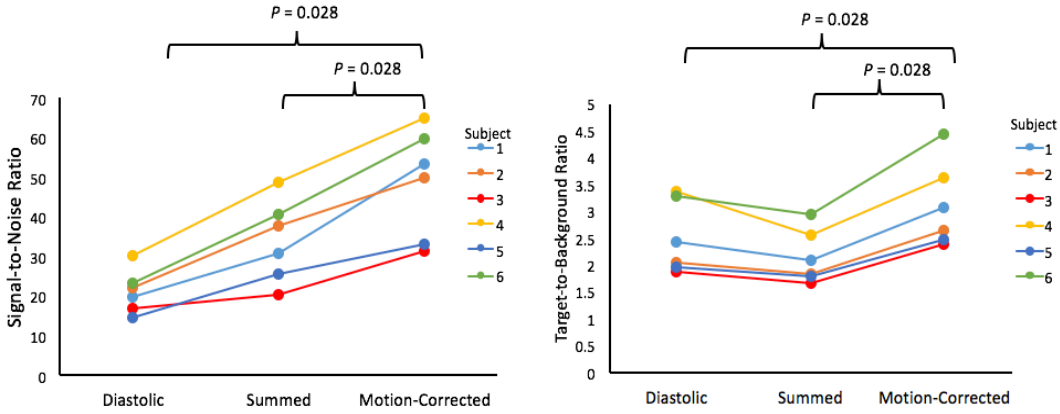

Figure 7.3. Signal-to-noise ratios (A) and tissue-to-background ratios (B) in original gate, summed and motion corrected data.

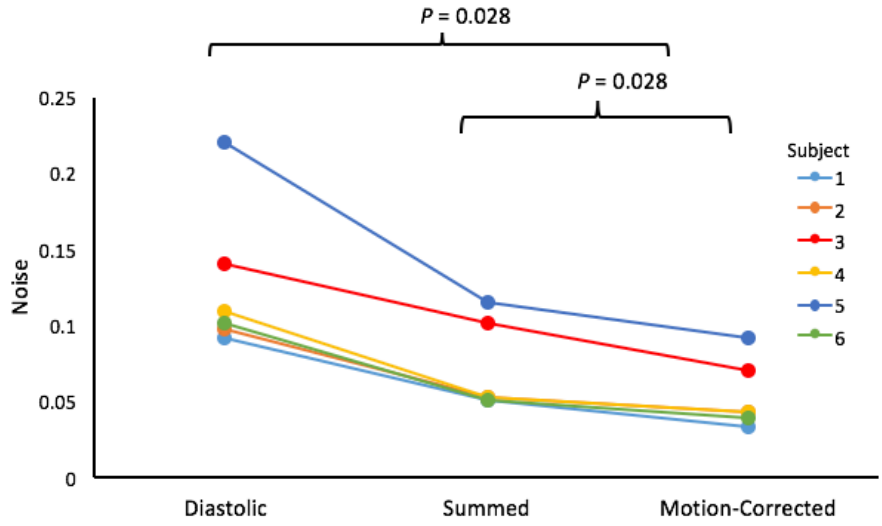

Figure 7.4. Difference in noise between motion corrected image, original diastolic gate and summed image.

While noise was higher in subjects 1 and 3, likely due to an increased body weight, the same trend was observed.

7.5 DISCUSSION

This feasibility study represents the first analysis of multimodality cardiac motion correction guided by anatomical data from ^{18}F-fluoride PET-MR and PET-CT. It also represents the first demonstration of hybrid PET-MR imaging in aortic stenosis which allows simultaneous imaging of calcification activity in the aortic valve using ^{18}F-fluoride PET alongside the detailed myocardial assessments provided by MR.

In the future, this sophisticated imaging method has great clinical potential in assessing native aortic valve disease alongside markers of myocardial decompensation including midwall late gadolinium enhancement (212) and T1 mapping. (217, 218) However, a limitation of PET-MR is the inability to accurately assess prosthetic valve disease due to the influence of metal artefact on PET attenuation and MR image quality. With the increasing use of Transcatheter Aortic Valve Replacement (TAVR), PET-CT is likely to play an important role in the assessment of aortic valve bioprostheses. Indeed, the role of ^{18}F-fluoride PET-CT in assessing the longevity of TAVR valves is currently under investigation (NCT02304276). Here, we describe how these imaging techniques may be optimized with motion-corrected imaging of the aortic valve to maximize the research and clinical potential of hybrid cardiac imaging.

Our study is limited by data from only a small number of patients. While this was sufficient to demonstrate the clear improvements in SNR and TBR values offered by motion correction techniques, larger studies are required for confirmation.

7.6 CONCLUSION

Simultaneous motion-corrected PET imaging of the aortic valve is feasible with both hybrid ^{18}F-fluoride PET-MR and PET-CT. Motion correction, using a diffeomorphic mass-preserving image registration algorithm improved quantitative SNR and TBR, while significantly reducing image noise.

CHAPTER 8

Conclusions and Future Directions

Including extracts and adaptations from**:**

Doris MK, Dweck MR, Fayad ZA. The future of imaging in CVD intervention trials: 2017 and beyond. Curr Opin Lipidol. 2016;27:605-614

Chapter 8 Conclusions and Future Directions

8.1 SUMMARY OF THESIS FINDINGS

Despite innovative advances in investigation and management strategies, cardiovascular disease remains a leading cause of death worldwide. In order to improve outcomes, more individualised care with improved identification of those at greatest risk of disease progression and future events is crucial. Technological advances in the non-invasive investigation of cardiovascular disease provide the opportunity to identify detailed features of disease burden, activity and progression and potentially those who may benefit from tailored therapies. Further, they provide a platform on which to investigate the effects of novel therapeutic interventions.

The principal aim of this thesis was to investigate whether complementary non-invasive imaging strategies could improve the assessment of disease burden, activity and progression in two leading forms of cardiovascular disease; coronary artery disease and aortic stenosis.

8.1.1 NON-INVASIVE FRACTIONAL FLOW RESERVE AND CORONARY PLAQUE BURDEN

Non-invasive fractional flow reserve derived from computed tomography (FFRCT) can provide a surrogate measure of the haemodynamic effects of coronary stenosis. To investigate the effects of diffuse non-obstructive atherosclerosis, the relationship between whole vessel FFRCT (V-FFRCT) and quantitative plaque features on coronary CTA was assessed in 155 participants undergoing coronary CTA.

Total, calcified and non-calcified plaque volume, as well as low-density plaque volume were each greater in vessels with an abnormal V-FFRCT. Quantitative plaque measures predicted an abnormal V-FFRCT, independent of the degree of arterial stenosis. This suggests non-invasive fractional flow reserve may provide a marker of diffuse non-obstructive atherosclerosis.

8.1.2 CORONARY ^{18}F-FLUORIDE UPTAKE AND PROGRESSION OF CORONARY ARTERY CALCIFICATION

Combined PET-CT imaging of the coronary arteries has been demonstrated to identify microcalcification beyond the resolution of computed tomography, providing important insights into calcification activity within the vasculature. In this sub-study of the Dual Antiplatelet to Reduce Myocardial Injury (DIAMOND) trial, I investigated whether ^{18}F-fluoride activity at baseline could predict the progression of coronary calcium score at one year.

Participants with increased ^{18}F-fluoride activity demonstrated greater progression of coronary calcification at one year compared to those without evidence of increased ^{18}F-fluoride activity. When individual coronary plaques were examined, those with increased ^{18}F-fluoride uptake exhibited progressive calcium deposition at one year, whilst plaques without ^{18}F-fluoride activity had no increase in calcium score at one year. At the individual segment level, baseline ^{18}F-fluoride activity predicted change in calcification at one year. However, at the patient level, these associations were not independent of age, sex and baseline calcium score. These findings confirm the role of ^{18}F-fluoride as a marker of disease activity in coronary atherosclerosis.

8.1.3 Optimisation of reconstruction and quantification of coronary PET-CT

The application of positron emission tomography to the coronary arteries remains challenging as a consequence of cardiorespiratory motion and limits of spatial and temporal resolution. This leads to signal blurring which may impair the ability to distinguish 'active' from 'inactive' lesions. In a study of patients with acute coronary syndrome, I evaluated quantitative coronary PET by applying different reconstruction algorithms to PET data. A novel motion correction method was applied to correct for cardiac motion.

The signal-to-noise ratio was affected by small changes in reconstruction. The application of a novel cardiac motion correction method in which the entire PET dataset was utilised led to a reduction in noise and an improvement in discrimination

between positive culprit and negative reference lesions when compared to the technique utilised in previous studies.

8.1.4 COMPUTED TOMOGRAPHY AORTIC VALVE CALCIUM SCORING FOR THE ASSESSMENT OF AORTIC STENOSIS PROGRESSION

Aortic stenosis remains an important cause of morbidity and mortality worldwide and, in an ageing population, its burden is set to increase. Two-dimensional echocardiography is currently the gold standard imaging modality to define and track changes in disease severity over time. Computed tomography has recently emerged as a useful modality to quantify valvular calcification burden in aortic stenosis.

In a study of patients with aortic stenosis, quantification of aortic valve calcification burden by computed tomography (CT-AVC) was reproducible and able to detect smaller changes over time when compared to haemodynamic markers of aortic stenosis severity measured on echocardiography. Measurement variability between scans was lower for CT-AVC compared to echocardiography, suggesting that this modality may be of value in clinical trials investigating the effects of novel therapies on disease progression, and in monitoring disease progression in the clinical setting. Important limitations of CT-AVC remain, however, and further work is required to improve feasibility of this modality in patients with a raised body-mass index or in whom rate control is contra-indicated.

8.1.5 MOTION-CORRECTED IMAGING OF THE AORTIC VALVE WITH ^{18}F-FLUORIDE PET-CT AND PET-MR: A FEASIBILITY STUDY

Similar to imaging of the coronary arteries, utilising PET for imaging of the aortic valve is subject to challenges secondary to cardiorespiratory motion. In a cohort of seven patients with aortic stenosis undergoing hybrid imaging with ^{18}F-fluoride PET, I investigated the application of a novel cardiac motion-correction technique. ^{18}F-Fluoride PET-CT was performed in six participants and one participant underwent ^{18}F-fluoride PET-MR. The application of a novel cardiac motion correction technique led to a reduction in noise and an increase in the measured PET activity in the aortic valve of all patients, demonstrating the feasibility of this motion correction technique in aortic valve imaging and, for the first time, in PET-MR imaging.

8.2 FUTURE DIRECTIONS

The findings of this thesis lay important groundwork for future studies investigating novel advanced imaging techniques in coronary heart disease and aortic valve disease.

With an expanding catalogue of novel therapies targeting multiple different aspects of the atherosclerotic disease process, early indicators of therapeutic efficacy and safety are of critical importance prior to the initiation of phase III outcome studies. Non-invasive imaging modalities have already played a valuable role in our understanding of drug effects and with the advent of hybrid imaging offer comprehensive multi-parametric assessments of drug efficacy. These approaches are likely to play an expanding role in the testing and development of novel therapies targeted against atherosclerosis and aortic stenosis.

8.2.1 PREDICTING RECURRENT CORONARY EVENTS USING ^{18}F-FLUORIDE (PREFFIR)

Despite optimal medical therapy, one in five patients will suffer a recurrent cardiac event following myocardial infarction. (219) Predicting subsequent events is challenging and these events may arise from vessels with only mild disease at the time of the index event. Events arise in non-culprit vessels which had previously mild disease just as frequently as recurring in the original culprit vessel. (219)

Hybrid imaging provides useful insight into biological disease activity and we have shown that ^{18}F-fluoride PET-CT can detect plaques which demonstrate more rapid progression of calcification. However, the relationship between ^{18}F-fluoride uptake and coronary heart disease outcomes is yet unknown. Whilst attractive in the research setting for monitoring disease activity and progression, the clinical utility of PET-CT will be guided by its prognostic impact. In a recent post-hoc analysis of observational studies which included patients with established stable and unstable coronary artery disease, increased ^{18}F-fluoride activity was associated with an increased risk of subsequent myocardial infarction. Using a novel measure to quantify ^{18}F-fluoride activity throughout the coronary vasculature, coronary microcalcification activity (CMA), this study showed that participants with an elevated CMA were seven times more likely to suffer fatal or non-fatal myocardial infarction. ^{18}F-fluoride activity, measured by TBR or CMA, was a powerful predictor of future myocardial infarction independent of age, comorbidities, number of coronary stents, the presence of multivessel disease and calcium score. (220) While promising, these initial findings should be confirmed in larger prospective studies.

The Prediction of Recurrent events with ^{18}F-fluoride to Predict Ruptured and High Risk Plaques in Patients with Myocardial Infarction (PREFFIR NCT02278211) aims to determine whether ^{18}F-Fluoride activity can predict recurrent events in patients with multivessel coronary disease following myocardial infarction. This prospective International study will recruit over 700 participants with follow-up over five years and will include repeat CTCA to measure plaque progression at two years.

8.2.2 INVESTIGATING THE ROLE OF ANTI-CALCIFIC THERAPY IN AORTIC STENOSIS (SALTIRE 2)

CT-AVC has been shown to be a reproducible imaging modality with the capability of detecting small changes in aortic valve calcification burden over time. This attribute is attractive for research trials seeking to investigate the effect of novel therapies for aortic stenosis, in which fewer patients and shorter follow-up periods are likely to be required to demonstrate a positive effect of therapies on disease progression. Similarly, ^{18}F-Fluoride PET may provide early indications of disease activity. Indeed, a number of studies have employed CT-AVC and ^{18}F-Fluoride PET as endpoints in the investigation of novel treatments for aortic stenosis. (136) The Study Investigating the effect of Drugs used to Treat Osteoporosis on the Progression of Calcific Osteoporosis (SALTIRE 2 NCT 02132026) is a randomised double-blind clinical trial of bisphosphonate and RANK-L inhibition in which participants are randomised to alendronic acid, denosumab or matched placebo. The study involves clinical and imaging follow up over a two-year period with the primary end point being change in CT-AVC at two years. ^{18}F-Fluoride PET-CT is also employed by the study design and change in disease activity as measured by ^{18}F-fluoride PET at one year is an

exploratory endpoint. Recruitment and clinical follow-up of 150 participants is now complete and results of this study will be publicly available this year.

8.2.3 NOVEL PET TRACERS

While coronary PET has demonstrated the successful translation of radiotracers with recognised safety profiles and widespread use in oncological imaging, the feasibility of coronary imaging now sets the stage for the application of novel PET tracers. A number of tracers targeted to a variety of different features of atherosclerosis are currently under investigation. (Table 8.1)

Table 8.1 Applications of novel PET tracers in cardiovascular disease

Target Process	Radiotracer	Action	Applications
Microcalcification	^{18}F-fluoride	Binds to hydroxyapatite	Coronary and carotid atherosclerosis, aortic aneurysm, aortic stenosis. (55, 58, 61, 221)
Inflammation	^{18}F-FDG	Uptake by metabolically active cells	Carotid and coronary atherosclerosis, aortic stenosis (56, 191)
	G68-DOTATATE	Binds to somatostatin receptor subtype 2	Carotid and coronary atherosclerosis (222-224)
	^{18}F-Choline	Metabolised to phosphatidylcholine and incorporated into cell membrane	Large vessel and carotid atherosclerosis (225, 226)
	^{11}CK-11195	Binds to translocator protein 18-kDa	Carotid atherosclerosis (227)
Thrombus	^{18}F-GP1	Binds to GPIIb/IIIa receptors on activated platelets	Acute arterial thrombosis including aortic aneurysm and carotid disease (228)
Hypoxia	^{18}F-FMISO	Reduction to amine derivative in hypoxic environment	Aortic and carotid atherosclerosis (229, 230)
Angiogenesis	^{18}F-fluciclatide	Binds to $a_v ß_3$ and $a_v ß_5$ integrin	Aortic atherosclerosis (231)
	^{18}F-RGD-K5	Binds to $a_v ß_3$ integrin	Carotid atherosclerosis (232)
Apoptosis	^{68}Ga-annexin A5	Binds to phosphatidylserine on plasma membrane of apoptotic cells	Carotid atherosclerosis, heart failure, myocardial infarction. (233, 234)

Refining PET and overcoming challenges faced by motion will also be of benefit in the application of novel PET tracers to coronary imaging. 18F-Glycoprotein I (18F-GP1) is one promising novel tracer and binds with high affinity to the glycoprotein IIb/IIa receptor on activated platelets, representing a key target for direct imaging of thrombosis. First in-human studies have demonstrated the ability of this tracer to localise to acute arterial thrombosis and venous thromboembolism with high tissue-to-background ratios and a favourable safety and pharmacodynamic profile. (228, 235)

The In-vivo Thrombus Imaging with 18F-GP1, a Novel Platelet PET Radiotracer (iThrombus NCT03943966) will investigate whether this radiotracer can identify arterial and venous thrombosis in a spectrum of cardiovascular conditions including myocardial infarction, aortic valve replacement and acute stroke and transient ischaemic attack.

8.2.4 COMBINED POSITRON EMISSION TOMOGRAPHY AND MAGNETIC RESONANCE IMAGING

Following the demonstration of feasibility of a novel cardiac motion-correction applied to PET-MR, this may be further utilised in the investigation of both aortic stenosis and coronary artery disease. Further refinement of PET with combined respiratory gating and advanced techniques for correction of respiratory motion as well as gross patient motion will further enhance this technique. (236, 237) With the added advantages of superior soft tissue resolution and ability to provide detailed information about the myocardial response to aortic stenosis (238), this imaging modality will be particularly useful in research studies investigating the role of novel therapies in aortic

stenosis. (136) A further advantage of hybrid PET-MR imaging is the lower radiation dose associated with this modality, potentially enabling imaging at many different time points or the use of multiple PET tracers while incurring lower radiation doses than PET-CT.

8.3 CLINICAL PERSPECTIVE

In this thesis, it has been demonstrated that advanced non-invasive imaging technologies can provide novel and complementary measures of disease burden and disease progression in coronary heart disease and aortic valve disease.

It has been demonstrated that quantification of plaque burden and composition can relate to non-invasive measures of fractional flow reserve in coronary atherosclerosis. It has also been demonstrated that measures of disease activity by positron emission tomography can provide an indication of progressive calcification in coronary atherosclerosis. In the study of aortic stenosis, aortic valve calcification quantified by computed tomography can provide a reproducible and sensitive measure of disease progression. Finally, application of advanced cardiac motion-correction techniques provides the ability to refine imaging of both the coronary arteries and aortic valve, improving image quality and thereby aiding future research and clinical applications of hybrid imaging.

Advanced non-invasive imaging techniques can provide a safe, efficient means of monitoring response to therapies – highlighting any positive effect in trials which may be designed with fewer patients and shorter follow-up durations than clinical outcome trials. Further, as well as providing early indicators of drug efficacy, imaging-based

end points can provide early indicators of safety of novel therapies. This can in turn provide evidence to inform the planning of larger clinical outcomes-based trials. Further research is now needed to utilise these methods to improve risk stratification and targeting of treatments against these important cardiovascular diseases.

REFERENCES

1. Virmani R, Kolodgie FD, Burke AP, Farb A, Schwartz SM. Lessons from sudden coronary death: a comprehensive morphological classification scheme for atherosclerotic lesions. Arteriosclerosis, thrombosis, and vascular biology. 2000;20(5):1262-75.
2. Virmani R, Burke AP, Farb A, Kolodgie FD. Pathology of the vulnerable plaque. Journal of the American College of Cardiology. 2006;47(8 Suppl):C13-8.
3. Narula J, Nakano M, Virmani R, Kolodgie FD, Petersen R, Newcomb R, et al. Histopathologic characteristics of atherosclerotic coronary disease and implications of the findings for the invasive and noninvasive detection of vulnerable plaques. Journal of the American College of Cardiology. 2013;61(10):1041-51.
4. Ehara S, Kobayashi Y, Yoshiyama M, Shimada K, Shimada Y, Fukuda D, et al. Spotty calcification typifies the culprit plaque in patients with acute myocardial infarction: an intravascular ultrasound study. Circulation. 2004;110(22):3424-9.
5. Vergallo R, Ren X, Yonetsu T, Kato K, Uemura S, Yu B, et al. Pancoronary plaque vulnerability in patients with acute coronary syndrome and ruptured culprit plaque: a 3-vessel optical coherence tomography study. American heart journal. 2014;167(1):59-67.
6. Arbab-Zadeh A, Fuster V. The myth of the "vulnerable plaque": transitioning from a focus on individual lesions to atherosclerotic disease burden for coronary artery disease risk assessment. Journal of the American College of Cardiology. 2015;65(8):846-55.
7. Kubo T, Maehara A, Mintz GS, Doi H, Tsujita K, Choi S-Y, et al. The dynamic nature of coronary artery lesion morphology assessed by serial virtual histology intravascular ultrasound tissue characterization. Journal of the American College of Cardiology. 2010;55(15):1590-7.
8. Hoffmann U, Moselewski F, Nieman K, Jang I-K, Ferencik M, Rahman AM, et al. Noninvasive assessment of plaque morphology and composition in culprit and stable lesions in acute coronary syndrome and stable lesions in stable angina by multidetector computed tomography. Journal of the American College of Cardiology. 2006;47(8):1655-62.
9. Wexler L, Brundage B, Crouse J, Detrano R, Fuster V, Maddahi J, et al. Coronary artery calcification: pathophysiology, epidemiology, imaging methods, and clinical implications. A statement for health professionals from the American Heart Association. Writing Group. Circulation. 1996;94(5):1175-92.
10. Allison MA, Criqui MH, Wright CM. Patterns and risk factors for systemic calcified atherosclerosis. Arteriosclerosis, thrombosis, and vascular biology. 2004;24(2):331-6.
11. Goodman WG, Goldin J, Kuizon BD, Yoon C, Gales B, Sider D, et al. Coronary-artery calcification in young adults with end-stage renal disease who are undergoing dialysis. New England Journal of Medicine. 2000;342(20):1478-83.
12. Kronmal RA, McClelland RL, Detrano R, Shea S, Lima JA, Cushman M, et al. Risk factors for the progression of coronary artery calcification in asymptomatic subjects: results from the Multi-Ethnic Study of Atherosclerosis (MESA). Circulation. 2007;115(21):2722-30.

13. Sangiorgi G, Rumberger JA, Severson A, Edwards WD, Gregoire J, Fitzpatrick LA, et al. Arterial calcification and not lumen stenosis is highly correlated with atherosclerotic plaque burden in humans: a histologic study of 723 coronary artery segments using nondecalcifying methodology. JAC. 1998;31(1):126-33.
14. Budoff MJ, Hokanson JE, Nasir K, Shaw LJ, Kinney GL, Chow D, et al. Progression of coronary artery calcium predicts all-cause mortality. JACC: Cardiovascular Imaging. 2010;3(12):1229-36.
15. Budoff MJ, Young R, Lopez VA, Kronmal RA, Nasir K, Blumenthal RS, et al. Progression of coronary calcium and incident coronary heart disease events: MESA (Multi-Ethnic Study of Atherosclerosis). Journal of the American College of Cardiology. 2013;61(12):1231-9.
16. Demer LL, Tintut Y. Mechanisms linking osteoporosis with cardiovascular calcification. Current Osteoporosis Reports. 2009;7(2):42-6.
17. Aikawa E, Nahrendorf M, Figueiredo J-L, Swirski FK, Shtatland T, Kohler RH, et al. Osteogenesis associates with inflammation in early-stage atherosclerosis evaluated by molecular imaging in vivo. Circulation. 2007;116(24):2841-50.
18. New SEP, Aikawa E. Cardiovascular calcification: an inflammatory disease. Circulation journal : official journal of the Japanese Circulation Society. 2011;75(6):1305-13.
19. Ewence AE, Bootman M, Roderick HL, Skepper JN, McCarthy G, Epple M, et al. Calcium phosphate crystals induce cell death in human vascular smooth muscle cells: a potential mechanism in atherosclerotic plaque destabilization. Circulation research. 2008;103(5):e28-34.
20. Abedin M, Tintut Y, Demer LL. Vascular calcification: mechanisms and clinical ramifications. Arteriosclerosis, thrombosis, and vascular biology. 2004;24(7):1161-70.
21. Vengrenyuk Y, Carlier S, Xanthos S, Cardoso L, Ganatos P, Virmani R, et al. A hypothesis for vulnerable plaque rupture due to stress-induced debonding around cellular microcalcifications in thin fibrous caps. Proceedings of the National Academy of Sciences. 2006;103(40):14678-83.
22. Hutcheson JD, Goettsch C, Bertazzo S, Maldonado N, Ruiz JL, Goh W, et al. Genesis and growth of extracellular-vesicle-derived microcalcification in atherosclerotic plaques. Nature materials. 2016.
23. New SEP, Goettsch C, Aikawa M, Marchini JF, Shibasaki M, Yabusaki K, et al. Macrophage-derived matrix vesicles: an alternative novel mechanism for microcalcification in atherosclerotic plaques. Circulation research. 2013;113(1):72-7.
24. New SEP, Aikawa E. Molecular imaging insights into early inflammatory stages of arterial and aortic valve calcification. Circulation research. 2011;108(11):1381-91.
25. Shao J-S, Cheng S-L, Sadhu J, Towler DA. Inflammation and the osteogenic regulation of vascular calcification: a review and perspective. Hypertension. 2010;55(3):579-92.
26. Shemesh J, Apter S, Itzchak Y, Motro M. Coronary calcification compared in patients with acute versus in those with chronic coronary events by using dual-sector spiral CT. Radiology. 2003;226(2):483-8.

27. Topol EJ, Nissen SE. Our preoccupation with coronary luminology. The dissociation between clinical and angiographic findings in ischemic heart disease. Circulation. 1995;92(8):2333-42.
28. Motoyama S, Ito H, Sarai M, Kondo T, Kawai H, Nagahara Y, et al. Plaque Characterization by Coronary Computed Tomography Angiography and the Likelihood of Acute Coronary Events in Mid-Term Follow-Up. Journal of the American College of Cardiology. 2015;66(4):337-46.
29. Williams MC, Kwiecinski J, Doris M, McElhinney P, D'Souza MS, Cadet S, et al. Low-Attenuation Noncalcified Plaque on Coronary Computed Tomography Angiography Predicts Myocardial Infarction: Results From the Multicenter SCOT-HEART Trial (Scottish Computed Tomography of the HEART). Circulation. 2020.
30. Dweck MR, Doris MK, Motwani M, Adamson PD, Slomka P, Dey D, et al. Imaging of coronary atherosclerosis - evolution towards new treatment strategies. Nature reviews Cardiology. 2016.
31. Agatston AS, Janowitz WR, Hildner FJ, Zusmer NR, Viamonte M, Detrano R. Quantification of coronary artery calcium using ultrafast computed tomography. JAC. 1990;15(4):827-32.
32. Detrano R, Guerci AD, Carr JJ, Bild DE, Burke G, Folsom AR, et al. Coronary calcium as a predictor of coronary events in four racial or ethnic groups. New England Journal of Medicine. 2008;358(13):1336-45.
33. Hoffmann U, Massaro JM, D'Agostino RB, Kathiresan S, Fox CS, O'Donnell CJ. Cardiovascular Event Prediction and Risk Reclassification by Coronary, Aortic, and Valvular Calcification in the Framingham Heart Study. J Am Heart Assoc. 2016;5(2).
34. Berman DS, Arnson Y, Rozanski A. Coronary Artery Calcium Scanning: The Agatston Score and Beyond. JACC Cardiovasc Imaging. 2016;9(12):1417-9.
35. Voros S, Rivera JJ, Berman DS, Blankstein R, Budoff MJ, Cury RC, et al. Guideline for minimizing radiation exposure during acquisition of coronary artery calcium scans with the use of multidetector computed tomography: a report by the Society for Atherosclerosis Imaging and Prevention Tomographic Imaging and Prevention Councils in collaboration with the Society of Cardiovascular Computed Tomography. J Cardiovasc Comput Tomogr. 2011;5(2):75-83.
36. Miller JM, Rochitte CE, Dewey M, Arbab-Zadeh A, Niinuma H, Gottlieb I, et al. Diagnostic performance of coronary angiography by 64-row CT. New England Journal of Medicine. 2008;359(22):2324-36.
37. Budoff MJ, Dowe D, Jollis JG, Gitter M, Sutherland J, Halamert E, et al. Diagnostic performance of 64-multidetector row coronary computed tomographic angiography for evaluation of coronary artery stenosis in individuals without known coronary artery disease: results from the prospective multicenter ACCURACY (Assessment by Coronary Computed Tomographic Angiography of Individuals Undergoing Invasive Coronary Angiography) trial. Journal of the American College of Cardiology. 2008;52(21):1724-32.
38. investigators S-H. CT coronary angiography in patients with suspected angina due to coronary heart disease (SCOT-HEART): an open-label, parallel-group, multicentre trial. Lancet. 2015;385(9985):2383-91.

39. Newby DE, Adamson PD, Berry C, Boon NA, Dweck MR, Flather M, et al. Coronary CT Angiography and 5-Year Risk of Myocardial Infarction. N Engl J Med. 2018;379(10):924-33.
40. Motoyama S, Sarai M, Harigaya H, Anno H, Inoue K, Hara T, et al. Computed tomographic angiography characteristics of atherosclerotic plaques subsequently resulting in acute coronary syndrome. Journal of the American College of Cardiology. 2009;54(1):49-57.
41. Williams MC, Moss AJ, Dweck M, Adamson PD, Alam S, Hunter A, et al. Coronary Artery Plaque Characteristics Associated With Adverse Outcomes in the SCOT-HEART Study. Journal of the American College of Cardiology. 2019;73(3):291-301.
42. Maroules CD, Hamilton-Craig C, Branch K, Lee J, Cury RC, Maurovich-Horvat P, et al. Coronary artery disease reporting and data system (CAD-RADS. J Cardiovasc Comput Tomogr. 2018;12(2):125-30.
43. Dey D, Cheng VY, Slomka PJ, Nakazato R, Ramesh A, Gurudevan S, et al. Automated 3-dimensional quantification of noncalcified and calcified coronary plaque from coronary CT angiography. Journal of cardiovascular computed tomography. 2009;3(6):372-82.
44. Øvrehus KA, Schuhbaeck A, Marwan M, Achenbach S, Nørgaard BL, Bøtker HE, et al. Reproducibility of semi-automatic coronary plaque quantification in coronary CT angiography with sub-mSv radiation dose. J Cardiovasc Comput Tomogr. 2016;10(2):114-20.
45. Dey D, Schepis T, Marwan M, Slomka PJ, Berman DS, Achenbach S. Automated three-dimensional quantification of noncalcified coronary plaque from coronary CT angiography: comparison with intravascular US. Radiology. 2010;257(2):516-22.
46. Nørgaard BL, Leipsic J, Gaur S, Seneviratne S, Ko BS, Ito H, et al. Diagnostic performance of noninvasive fractional flow reserve derived from coronary computed tomography angiography in suspected coronary artery disease: the NXT trial (Analysis of Coronary Blood Flow Using CT Angiography: Next Steps). J Am Coll Cardiol. 2014;63(12):1145-55.
47. Koo BK, Erglis A, Doh JH, Daniels DV, Jegere S, Kim HS, et al. Diagnosis of ischemia-causing coronary stenoses by noninvasive fractional flow reserve computed from coronary computed tomographic angiograms. Results from the prospective multicenter DISCOVER-FLOW (Diagnosis of Ischemia-Causing Stenoses Obtained Via Noninvasive Fractional Flow Reserve) study. J Am Coll Cardiol. 2011;58(19):1989-97.
48. Min JK, Leipsic J, Pencina MJ, Berman DS, Koo BK, van Mieghem C, et al. Diagnostic accuracy of fractional flow reserve from anatomic CT angiography. JAMA. 2012;308(12):1237-45.
49. Li S, Tang X, Peng L, Luo Y, Dong R, Liu J. The diagnostic performance of CT-derived fractional flow reserve for evaluation of myocardial ischaemia confirmed by invasive fractional flow reserve: a meta-analysis. Clin Radiol. 2015;70(5):476-86.
50. Nakazato R, Park H-B, Berman DS, Gransar H, Koo BK, Erglis A, et al. Noninvasive fractional flow reserve derived from computed tomography angiography for coronary lesions of intermediate stenosis severity: results from the DeFACTO study. Circulation: Cardiovascular Imaging. 2013;6(6):881-9.

51. Douglas PS, Pontone G, Hlatky MA, Patel MR, Nørgaard BL, Byrne RA, et al. Clinical outcomes of fractional flow reserve by computed tomographic angiography-guided diagnostic strategies vs. usual care in patients with suspected coronary artery disease: the prospective longitudinal trial of FFR(CT): outcome and resource impacts study. European heart journal. 2015;36(47):3359-67.
52. Rominger A, Saam T, Wolpers S, Cyran CC, Schmidt M, Foerster S, et al. 18F-FDG PET/CT identifies patients at risk for future vascular events in an otherwise asymptomatic cohort with neoplastic disease. Journal of nuclear medicine : official publication, Society of Nuclear Medicine. 2009;50(10):1611-20.
53. Derlin T, Richter U, Bannas P, Begemann P, Buchert R, Mester J, et al. Feasibility of 18F-sodium fluoride PET/CT for imaging of atherosclerotic plaque. Journal of nuclear medicine : official publication, Society of Nuclear Medicine. 2010;51(6):862-5.
54. Dweck MR, Chow MWL, Joshi NV, Williams MC, Jones C, Fletcher AM, et al. Coronary Arterial 18F-Sodium Fluoride Uptake. JAC. 2012;59(17):1539-48.
55. Joshi NV, Vesey AT, Williams MC, Shah ASV, Calvert PA, Craighead FHM, et al. 18F-fluoride positron emission tomography for identification of ruptured and high-risk coronary atherosclerotic plaques: a prospective clinical trial. The Lancet. 2014;383(9918):705-13.
56. Rudd JHF, Warburton EA, Fryer TD, Jones HA, Clark JC, Antoun N, et al. Imaging atherosclerotic plaque inflammation with [18F]-fluorodeoxyglucose positron emission tomography. Circulation. 2002;105(23):2708-11.
57. Derlin T, Wisotzki C, Richter U, Apostolova I, Bannas P, Weber C, et al. In vivo imaging of mineral deposition in carotid plaque using 18F-sodium fluoride PET/CT: correlation with atherogenic risk factors. Journal of nuclear medicine : official publication, Society of Nuclear Medicine. 2011;52(3):362-8.
58. Vesey AT, Jenkins WSA, Irkle A, Moss A, Sng G, Forsythe RO, et al. 18F-Fluoride and 18F-Fluorodeoxyglucose Positron Emission Tomography After Transient Ischemic Attack or Minor Ischemic Stroke: Case-Control Study. Circulation: Cardiovascular Imaging. 2017;10(3):e004976.
59. Chin CWL, Khaw HJ, Luo E, Tan S, White AC, Newby DE, et al. Echocardiography underestimates stroke volume and aortic valve area: implications for patients with small-area low-gradient aortic stenosis. The Canadian journal of cardiology. 2014;30(9):1064-72.
60. Dweck MR, Jones C, Joshi NV, Fletcher AM, Richardson H, White A, et al. Assessment of valvular calcification and inflammation by positron emission tomography in patients with aortic stenosis. Circulation. 2012;125(1):76-86.
61. Dweck MR, Jenkins WSA, Vesey AT, Pringle MAH, Chin CWL, Malley TS, et al. 18F-sodium fluoride uptake is a marker of active calcification and disease progression in patients with aortic stenosis. Circulation: Cardiovascular Imaging. 2014;7(2):371-8.
62. Irkle A, Vesey AT, Lewis DY, Skepper JN, Bird JLE, Dweck MR, et al. Identifying active vascular microcalcification by (18)F-sodium fluoride positron emission tomography. Nature communications. 2015;6:7495.
63. Blau M, Nagler W, Bender MA. Fluorine-18: a new isotope for bone scanning. Journal of nuclear medicine : official publication, Society of Nuclear Medicine. 1962;3:332-4.

64. Even-Sapir E, Metser U, Mishani E, Lievshitz G, Lerman H, Leibovitch I. The detection of bone metastases in patients with high-risk prostate cancer: 99mTc-MDP Planar bone scintigraphy, single- and multi-field-of-view SPECT, 18F-fluoride PET, and 18F-fluoride PET/CT. Journal of nuclear medicine : official publication, Society of Nuclear Medicine. 2006;47(2):287-97.
65. Cook GJR, Blake GM, Marsden PK, Cronin B, Fogelman I. Quantification of Skeletal Kinetic Indices in Paget's Disease Using Dynamic18F-Fluoride Positron Emission Tomography. Journal of Bone and Mineral Research. 2002;17(5):854-9.
66. Cook GJR, Fogelman I. The role of positron emission tomography in skeletal disease. Seminars in nuclear medicine. 2001;31(1):50-61.
67. Blake GM, Siddique M, Frost ML, Moore AEB, Fogelman I. Imaging of Site Specific Bone Turnover in Osteoporosis Using Positron Emission Tomography. Current Osteoporosis Reports. 2014;12(4):475-85.
68. Drubach LA, Johnston PR, Newton AW, Perez-Rossello JM, Grant FD, Kleinman PK. Skeletal Trauma in Child Abuse: Detection with 18F-NaF PET1. Radiology. 2010;255(1):173-81.
69. Czernin J, Satyamurthy N, Schiepers C. Molecular mechanisms of bone 18F-NaF deposition. Journal of nuclear medicine : official publication, Society of Nuclear Medicine. 2010;51(12):1826-9.
70. Kurdziel KA, Shih JH, Apolo AB, Lindenberg L, Mena E, McKinney YY, et al. The kinetics and reproducibility of 18F-sodium fluoride for oncology using current PET camera technology. Journal of nuclear medicine : official publication, Society of Nuclear Medicine. 2012;53(8):1175-84.
71. Derlin T, Tóth Z, Papp L, Wisotzki C, Apostolova I, Habermann CR, et al. Correlation of inflammation assessed by 18F-FDG PET, active mineral deposition assessed by 18F-fluoride PET, and vascular calcification in atherosclerotic plaque: a dual-tracer PET/CT study. Journal of nuclear medicine : official publication, Society of Nuclear Medicine. 2011;52(7):1020-7.
72. Fiz F, Morbelli S, Piccardo A, Bauckneht M, Ferrarazzo G, Pestarino E, et al. ^{18}F-NaF Uptake by Atherosclerotic Plaque on PET/CT Imaging: Inverse Correlation Between Calcification Density and Mineral Metabolic Activity. Journal of nuclear medicine : official publication, Society of Nuclear Medicine. 2015;56(7):1019-23.
73. Saam T, Yuan C, Chu B, Takaya N, Underhill H, Cai J, et al. Predictors of carotid atherosclerotic plaque progression as measured by noninvasive magnetic resonance imaging. Atherosclerosis. 2007;194(2):e34-42.
74. Rubeaux M, Pawade T, Cartlidge T, Otaki Y, Dweck M, Dey D, et al. Cardiac motion compensation improves reproducibility of 18F-sodium fluoride PET uptake quantification in the aortic valve. Journal of nuclear medicine : official publication, Society of Nuclear Medicine. 2016;57(supplement 2):506-.
75. Soret M, Bacharach SL, Buvat I. Partial-volume effect in PET tumor imaging. Journal of nuclear medicine : official publication, Society of Nuclear Medicine. 2007;48(6):932-45.
76. Iung B, Baron G, Butchart EG, Delahaye F, Gohlke-Bärwolf C, Levang OW, et al. A prospective survey of patients with valvular heart disease in Europe: The Euro Heart Survey on Valvular Heart Disease. European heart journal. 2003;24(13):1231-43.

77. Nkomo VT, Gardin JM, Skelton TN, Gottdiener JS, Scott CG, Enriquez-Sarano M. Burden of valvular heart diseases: a population-based study. Lancet (London, England). 2006;368(9540):1005-11.
78. Marquis-Gravel G, Redfors B, Leon MB, Généreux P. Medical Treatment of Aortic Stenosis. Circulation. 2016;134(22):1766-84.
79. Pawade TA, Newby DE, Dweck MR. Calcification in Aortic Stenosis: The Skeleton Key. Journal of the American College of Cardiology. 2015;66(5):561-77.
80. Dweck MR, Boon NA, Newby DE. Calcific aortic stenosis: a disease of the valve and the myocardium. Journal of the American College of Cardiology. 2012;60(19):1854-63.
81. Kaden JJ, Dempfle C-E, Grobholz R, Fischer CS, Vocke DC, Kiliç R, et al. Inflammatory regulation of extracellular matrix remodeling in calcific aortic valve stenosis. Cardiovascular pathology : the official journal of the Society for Cardiovascular Pathology. 2005;14(2):80-7.
82. Rajamannan NM. Bicuspid aortic valve disease: the role of oxidative stress in Lrp5 bone formation. Cardiovascular pathology : the official journal of the Society for Cardiovascular Pathology. 2011;20(3):168-76.
83. Freeman RV, Otto CM. Spectrum of calcific aortic valve disease: pathogenesis, disease progression, and treatment strategies. Circulation. 2005;111(24):3316-26.
84. Olsson M, Dalsgaard CJ, Haegerstrand A, Rosenqvist M, Rydén L, Nilsson J. Accumulation of T lymphocytes and expression of interleukin-2 receptors in nonrheumatic stenotic aortic valves. JAC. 1994;23(5):1162-70.
85. Olsson M, Thyberg J, Nilsson J. Presence of oxidized low density lipoprotein in nonrheumatic stenotic aortic valves. Arteriosclerosis, thrombosis, and vascular biology. 1999;19(5):1218-22.
86. Min H, Morony S, Sarosi I, Dunstan CR, Capparelli C, Scully S, et al. Osteoprotegerin reverses osteoporosis by inhibiting endosteal osteoclasts and prevents vascular calcification by blocking a process resembling osteoclastogenesis. The Journal of experimental medicine. 2000;192(4):463-74.
87. Kaden JJ, Bickelhaupt S, Grobholz R, Haase KK, Sarikoç A, Kiliç R, et al. Receptor activator of nuclear factor kappaB ligand and osteoprotegerin regulate aortic valve calcification. Journal of molecular and cellular cardiology. 2004;36(1):57-66.
88. Dweck MR, Pawade TA, Newby DE. Aortic stenosis begets aortic stenosis: between a rock and a hard place? Heart (British Cardiac Society). 2015;101(12):919-20.
89. Schultz JEJ, Witt SA, Glascock BJ, Nieman ML, Reiser PJ, Nix SL, et al. TGF-beta1 mediates the hypertrophic cardiomyocyte growth induced by angiotensin II. The Journal of clinical investigation. 2002;109(6):787-96.
90. Hein S, Arnon E, Kostin S, Schönburg M, Elsässer A, Polyakova V, et al. Progression from compensated hypertrophy to failure in the pressure-overloaded human heart: structural deterioration and compensatory mechanisms. Circulation. 2003;107(7):984-91.
91. Heymans S, Schroen B, Vermeersch P, Milting H, Gao F, Kassner A, et al. Increased cardiac expression of tissue inhibitor of metalloproteinase-1 and tissue inhibitor of metalloproteinase-2 is related to cardiac fibrosis and dysfunction in the chronic pressure-overloaded human heart. Circulation. 2005;112(8):1136-44.

92. Brubakk AO, Angelsen BA, Hatle L. Diagnosis of valvular heart disease using transcutaneous Doppler ultrasound. Cardiovascular research. 1977;11(5):461-9.
93. Hatle L, Angelsen BA, Tromsdal A. Non-invasive assessment of aortic stenosis by Doppler ultrasound. British heart journal. 1980;43(3):284-92.
94. Hatle L. Noninvasive assessment of valve lesions with Doppler ultrasound. Herz. 1984;9(4):213-21.
95. Holen J, Aaslid R, Landmark K, Simonsen S. Determination of pressure gradient in mitral stenosis with a non-invasive ultrasound Doppler technique. Acta medica Scandinavica. 1976;199(6):455-60.
96. Otto CM, Burwash IG, Legget ME, Munt BI, Fujioka M, Healy NL, et al. Prospective study of asymptomatic valvular aortic stenosis. Clinical, echocardiographic, and exercise predictors of outcome. Circulation. 1997;95(9):2262-70.
97. Leon MB, Smith CR, Mack M, Miller DC, Moses JW, Svensson LG, et al. Transcatheter aortic-valve implantation for aortic stenosis in patients who cannot undergo surgery. New England Journal of Medicine. 2010;363(17):1597-607.
98. Baumgartner H, Falk V, Bax JJ, De Bonis M, Hamm C, Holm PJ, et al. 2017 ESC/EACTS Guidelines for the management of valvular heart disease. European heart journal. 2017;38(36):2739-91.
99. Rusinaru D, Malaquin D, Maréchaux S, Debry N, Tribouilloy C. Relation of Dimensionless Index to Long-Term Outcome in Aortic Stenosis With Preserved LVEF. JACC Cardiovasc Imaging. 2015;8(7):766-75.
100. Bohbot Y, Kowalski C, Rusinaru D, Ringle A, Maréchaux S, Tribouilloy C. Impact of Mean Transaortic Pressure Gradient on Long-Term Outcome in Patients With Severe Aortic Stenosis and Preserved Left Ventricular Ejection Fraction. Journal of the American Heart Association. 2017;6(6):e005850.
101. Otto CM, Pearlman AS, Comess KA, Reamer RP, Janko CL, Huntsman LL. Determination of the stenotic aortic valve area in adults using Doppler echocardiography. JAC. 1986;7(3):509-17.
102. Sacchi S, Dhutia NM, Shun-Shin MJ, Zolgharni M, Sutaria N, Francis DP, et al. Doppler assessment of aortic stenosis: a 25-operator study demonstrating why reading the peak velocity is superior to velocity time integral. Eur Heart J Cardiovasc Imaging. 2018;19(12):1380-9.
103. Moura LM, Ramos SF, Pinto FJ, Barros IM, Rocha-Gonçalves F. Analysis of variability and reproducibility of echocardiography measurements in valvular aortic valve stenosis. Revista portuguesa de cardiologia : orgao oficial da Sociedade Portuguesa de Cardiologia = Portuguese journal of cardiology : an official journal of the Portuguese Society of Cardiology. 2011;30(1):25-33.
104. Galderisi M, Henein MY, D'Hooge J, Sicari R, Badano LP, Zamorano JL, et al. Recommendations of the European Association of Echocardiography: how to use echo-Doppler in clinical trials: different modalities for different purposes. European journal of echocardiography : the journal of the Working Group on Echocardiography of the European Society of Cardiology. 2011;12(5):339-53.
105. Otto CM, Pearlman AS, Gardner CL. Hemodynamic progression of aortic stenosis in adults assessed by Doppler echocardiography. JAC. 1989;13(3):545-50.
106. Clavel M-A, Messika-Zeitoun D, Pibarot P, Aggarwal SR, Malouf J, Araoz PA, et al. The complex nature of discordant severe calcified aortic valve disease

grading: new insights from combined Doppler echocardiographic and computed tomographic study. Journal of the American College of Cardiology. 2013;62(24):2329-38.
107. Pawade T, Clavel M-A, Tribouilloy C, Dreyfus J, Mathieu T, Tastet L, et al. Computed Tomography Aortic Valve Calcium Scoring in Patients With Aortic Stenosis. Circulation: Cardiovascular Imaging. 2018;11(3):e007146.
108. Annabi M-S, Touboul E, Dahou A, Burwash IG, Bergler-Klein J, Enriquez-Sarano M, et al. Dobutamine Stress Echocardiography for Management of Low-Flow, Low-Gradient Aortic Stenosis. Journal of the American College of Cardiology. 2018;71(5):475-85.
109. Monin JL, Monchi M, Gest V, Duval-Moulin AM, Dubois-Rande JL, Gueret P. Aortic stenosis with severe left ventricular dysfunction and low transvalvular pressure gradients: risk stratification by low-dose dobutamine echocardiography. JAC. 2001;37(8):2101-7.
110. Rosenhek R, Binder T, Porenta G, Lang I, Christ G, Schemper M, et al. Predictors of outcome in severe, asymptomatic aortic stenosis. New England Journal of Medicine. 2000;343(9):611-7.
111. Rosenhek R, Klaar U, Schemper M, Scholten C, Heger M, Gabriel H, et al. Mild and moderate aortic stenosis. Natural history and risk stratification by echocardiography. European heart journal. 2004;25(3):199-205.
112. Messika-Zeitoun D, Aubry M-C, Detaint D, Bielak LF, Peyser PA, Sheedy PF, et al. Evaluation and clinical implications of aortic valve calcification measured by electron-beam computed tomography. Circulation. 2004;110(3):356-62.
113. Cueff C, Serfaty J-M, Cimadevilla C, Laissy J-P, Himbert D, Tubach F, et al. Measurement of aortic valve calcification using multislice computed tomography: correlation with haemodynamic severity of aortic stenosis and clinical implication for patients with low ejection fraction. Heart (British Cardiac Society). 2011;97(9):721-6.
114. Aggarwal SR, Clavel M-A, Messika-Zeitoun D, Cueff C, Malouf J, Araoz PA, et al. Sex differences in aortic valve calcification measured by multidetector computed tomography in aortic stenosis. Circulation: Cardiovascular Imaging. 2013;6(1):40-7.
115. Nguyen V, Cimadevilla C, Estellat C, Codogno I, Huart V, Benessiano J, et al. Haemodynamic and anatomic progression of aortic stenosis. Heart (British Cardiac Society). 2015;101(12):943-7.
116. Owens DS, Katz R, Takasu J, Kronmal R, Budoff MJ, O'Brien KD. Incidence and progression of aortic valve calcium in the Multi-ethnic Study of Atherosclerosis (MESA). The American journal of cardiology. 2010;105(5):701-8.
117. Tastet L, Enriquez-Sarano M, Capoulade R, Malouf J, Araoz PA, Shen M, et al. Impact of Aortic Valve Calcification and Sex on Hemodynamic Progression and Clinical Outcomes in AS. Journal of the American College of Cardiology. 2017;69(16):2096-8.
118. Messika-Zeitoun D, Bielak LF, Peyser PA, Sheedy PF, Turner ST, Nkomo VT, et al. Aortic valve calcification: determinants and progression in the population. Arteriosclerosis, thrombosis, and vascular biology. 2007;27(3):642-8.
119. Jenkins WSA, Vesey AT, Shah ASV, Pawade TA, Chin CWL, White AC, et al. Valvular (18)F-Fluoride and (18)F-Fluorodeoxyglucose Uptake Predict Disease Progression and Clinical Outcome in Patients With Aortic Stenosis. Journal of the American College of Cardiology. 2015;66(10):1200-1.

120. Pawade TA, Cartlidge TRG, Jenkins WSA, Adamson PD, Robson P, Lucatelli C, et al. Optimization and Reproducibility of Aortic Valve 18F-Fluoride Positron Emission Tomography in Patients With Aortic Stenosis. Circulation: Cardiovascular Imaging. 2016;9(10):e005131.
121. Installé J, Nzeusseu A, Bol A, Depresseux G, Devogelaer J-P, Lonneux M. (18)F-fluoride PET for monitoring therapeutic response in Paget's disease of bone. Journal of nuclear medicine : official publication, Society of Nuclear Medicine. 2005;46(10):1650-8.
122. Robson PM, Dey D, Newby DE, Berman D, Li D, Fayad ZA, et al. MR/PET Imaging of the Cardiovascular System. JACC: Cardiovascular Imaging. 2017;10(10 Pt A):1165-79.
123. Cowell SJ, Newby DE, Prescott RJ, Bloomfield P, Reid J, Northridge DB, et al. A randomized trial of intensive lipid-lowering therapy in calcific aortic stenosis. New England Journal of Medicine. 2005;352(23):2389-97.
124. Chan KL, Teo K, Dumesnil JG, Ni A, Tam J, Investigators A. Effect of Lipid lowering with rosuvastatin on progression of aortic stenosis: results of the aortic stenosis progression observation: measuring effects of rosuvastatin (ASTRONOMER) trial. Circulation. 2010;121(2):306-14.
125. Rossebø AB, Pedersen TR, Boman K, Brudi P, Chambers JB, Egstrup K, et al. Intensive lipid lowering with simvastatin and ezetimibe in aortic stenosis. New England Journal of Medicine. 2008;359(13):1343-56.
126. Nordestgaard BG, Chapman MJ, Ray K, Borén J, Andreotti F, Watts GF, et al., editors. Lipoprotein(a) as a cardiovascular risk factor: current status. European heart journal; 2010/12/01.
127. Thanassoulis G, Campbell CY, Owens DS, Smith JG, Smith AV, Peloso GM, et al. Genetic associations with valvular calcification and aortic stenosis. New England Journal of Medicine. 2013;368(6):503-12.
128. Capoulade R, Chan KL, Yeang C, Mathieu P, Bossé Y, Dumesnil JG, et al. Oxidized Phospholipids, Lipoprotein(a), and Progression of Calcific Aortic Valve Stenosis. Journal of the American College of Cardiology. 2015;66(11):1236-46.
129. Thanassoulis G. Lipoprotein (a) in calcific aortic valve disease: from genomics to novel drug target for aortic stenosis. Journal of lipid research. 2016;57(6):917-24.
130. Helas S, Goettsch C, Schoppet M, Zeitz U, Hempel U, Morawietz H, et al. Inhibition of receptor activator of NF-kappaB ligand by denosumab attenuates vascular calcium deposition in mice. The American journal of pathology. 2009;175(2):473-8.
131. Lai T-j, Hsu S-f, Li T-m, Hsu H-c, Lin J-g, Hsu C-j, et al. Alendronate inhibits cell invasion and MMP-2 secretion in human chondrosarcoma cell line. Acta pharmacologica Sinica. 2007;28(8):1231-5.
132. Corrado A, Santoro N, Cantatore FP. Extra-skeletal effects of bisphosphonates. Joint, bone, spine : revue du rhumatisme. 2007;74(1):32-8.
133. Price PA, Faus SA, Williamson MK. Bisphosphonates alendronate and ibandronate inhibit artery calcification at doses comparable to those that inhibit bone resorption. Arteriosclerosis, thrombosis, and vascular biology. 2001;21(5):817-24.
134. Synetos A, Toutouzas K, Benetos G, Drakopoulou M, Trantalis G, Kotronias R, et al. Catheter based inhibition of arterial calcification by bisphosphonates in an

experimental atherosclerotic rabbit animal model. International journal of cardiology. 2014;176(1):177-81.
135. Study Investigating the Effect of Drugs Used to Treat Osteoporosis on the Progression of Calcific Aortic Stenosis. (SALTIRE II). 2018:1-8.
136. Peeters FECM, van Mourik MJW, Meex SJR, Bucerius J, Schalla SM, Gerretsen SC, et al. Bicuspid Aortic Valve Stenosis and the Effect of Vitamin K2 on Calcification Using 18F-Sodium Fluoride Positron Emission Tomography/Magnetic Resonance: The BASIK2 Rationale and Trial Design. Nutrients. 2018;10(4):386.
137. Venardos N, Bennett D, Weyant MJ, Reece TB, Meng X, Fullerton DA. Matrix Gla protein regulates calcification of the aortic valve. The Journal of surgical research. 2015;199(1):1-6.
138. Stewart RAH, Kerr AJ, Cowan BR, Young AA, Occleshaw C, Richards AM, et al. A randomized trial of the aldosterone-receptor antagonist eplerenone in asymptomatic moderate-severe aortic stenosis. American heart journal. 2008;156(2):348-55.
139. Bull S, Loudon M, Francis JM, Joseph J, Gerry S, Karamitsos TD, et al. A prospective, double-blind, randomized controlled trial of the angiotensin-converting enzyme inhibitor Ramipril In Aortic Stenosis (RIAS trial). European heart journal cardiovascular Imaging. 2015;16(8):834-41.
140. Capoulade R, Clavel M-A, Mathieu P, Côté N, Dumesnil JG, Arsenault M, et al. Impact of hypertension and renin-angiotensin system inhibitors in aortic stenosis. European journal of clinical investigation. 2013;43(12):1262-72.
141. Côté N, Couture C, Pibarot P, Després J-P, Mathieu P. Angiotensin receptor blockers are associated with a lower remodelling score of stenotic aortic valves. European journal of clinical investigation. 2011;41(11):1172-9.
142. McVicker BL, Bennett RG. Novel Anti-fibrotic Therapies. Frontiers in pharmacology. 2017;8:318.
143. Moss AJ, Dweck MR, Doris MK, Andrews JPM, Bing R, Forsythe RO, et al. Ticagrelor to Reduce Myocardial Injury in Patients With High-Risk Coronary Artery Plaque. JACC Cardiovasc Imaging. 2019.
144. Baumgartner H, Hung J, Bermejo J, Chambers JB, Edvardsen T, Goldstein S, et al. Recommendations on the Echocardiographic Assessment of Aortic Valve Stenosis: A Focused Update from the European Association of Cardiovascular Imaging and the American Society of Echocardiography. Journal of the American Society of Echocardiography : official publication of the American Society of Echocardiography. 2017;30(4):372-92.
145. Smith LA, Cowell SJ, White AC, Boon NA, Newby DE, Northridge DB. Contrast agent increases Doppler velocities and improves reproducibility of aortic valve area measurements in patients with aortic stenosis. J Am Soc Echocardiogr. 2004;17(3):247-52.
146. Taylor CA, Fonte TA, Min JK. Computational fluid dynamics applied to cardiac computed tomography for noninvasive quantification of fractional flow reserve: scientific basis. Journal of the American College of Cardiology. 2013;61(22):2233-41.
147. Budoff MJ, McClelland RL, Chung H, Wong ND, Carr JJ, McNitt-Gray M, et al. Reproducibility of coronary artery calcified plaque with cardiac 64-MDCT: the Multi-Ethnic Study of Atherosclerosis. AJR Am J Roentgenol. 2009;192(3):613-7.

148. Detrano RC, Anderson M, Nelson J, Wong ND, Carr JJ, McNitt-Gray M, et al. Coronary calcium measurements: effect of CT scanner type and calcium measure on rescan reproducibility--MESA study. Radiology. 2005;236(2):477-84.
149. Rubeaux M, Joshi N, Dweck MR, Fletcher A, Motwani M, Thomson LE, et al. Motion correction of 18F-sodium fluoride PET for imaging coronary atherosclerotic plaques. Journal of nuclear medicine : official publication, Society of Nuclear Medicine. 2015:jnumed.115.162990.
150. Rubeaux M, Joshi N, Dweck MR, Fletcher A, Motwani M, Thomson LE, et al. Demons versus Level-Set motion registration for coronary (18)F-sodium fluoride PET. Proceedings of SPIE--the International Society for Optical Engineering. 2016;9784:97843Y-Y-7.
151. Nakazato R, Shalev A, Doh J-H, Koo BK, Gransar H, Gomez MJ, et al. Aggregate plaque volume by coronary computed tomography angiography is superior and incremental to luminal narrowing for diagnosis of ischemic lesions of intermediate stenosis severity. Journal of the American College of Cardiology. 2013;62(5):460-7.
152. Diaz Zamudio M, Dey D, Schuhbaeck A, Nakazato R, Gransar H, Slomka PJ, et al. Automated Quantitative Plaque Burden from Coronary CT Angiography Noninvasively Predicts Hemodynamic Significance by using Fractional Flow Reserve in Intermediate Coronary Lesions. Radiology. 2015;276(2):408-15.
153. Shmilovich H, Cheng VY, Tamarappoo BK, Dey D, Nakazato R, Gransar H, et al. Vulnerable plaque features on coronary CT angiography as markers of inducible regional myocardial hypoperfusion from severe coronary artery stenoses. Atherosclerosis. 2011;219(2):588-95.
154. Gutstein A, Wolak A, Lee C, Dey D, Ohba M, Suzuki Y, et al. Predicting success of prospective and retrospective gating with dual-source coronary computed tomography angiography: development of selection criteria and initial experience. Journal of cardiovascular computed tomography. 2008;2(2):81-90.
155. Achenbach S, Ropers D, Hoffmann U, MacNeill B, Baum U, Pohle K, et al. Assessment of coronary remodeling in stenotic and nonstenotic coronary atherosclerotic lesions by multidetector spiral computed tomography. JAC. 2004;43(5):842-7.
156. Steigner ML, Mitsouras D, Whitmore AG, Otero HJ, Wang C, Buckley O, et al. Iodinated contrast opacification gradients in normal coronary arteries imaged with prospectively ECG-gated single heart beat 320-detector row computed tomography. Circulation: Cardiovascular Imaging. 2010;3(2):179-86.
157. Chiribiri A, Hautvast GLTF, Lockie T, Schuster A, Bigalke B, Olivotti L, et al. Assessment of coronary artery stenosis severity and location: quantitative analysis of transmural perfusion gradients by high-resolution MRI versus FFR. JACC: Cardiovascular Imaging. 2013;6(5):600-9.
158. Williams RL. A note on robust variance estimation for cluster-correlated data. Biometrics. 2000;56(2):645-6.
159. De Bruyne B, Hersbach F, Pijls NH, Bartunek J, Bech JW, Heyndrickx GR, et al. Abnormal epicardial coronary resistance in patients with diffuse atherosclerosis but "Normal" coronary angiography. Circulation. 2001;104(20):2401-6.
160. Gaur S, Øvrehus KA, Dey D, Leipsic J, Bøtker HE, Jensen JM, et al. Coronary plaque quantification and fractional flow reserve by coronary computed tomography

angiography identify ischaemia-causing lesions. European heart journal. 2016;37(15):1220-7.
161. Park H-B, Heo R, ó Hartaigh B, Cho I, Gransar H, Nakazato R, et al. Atherosclerotic plaque characteristics by CT angiography identify coronary lesions that cause ischemia: a direct comparison to fractional flow reserve. JACC: Cardiovascular Imaging. 2015;8(1):1-10.
162. Lavi S, Bae JH, Rihal CS, Prasad A, Barsness GW, Lennon RJ, et al. Segmental coronary endothelial dysfunction in patients with minimal atherosclerosis is associated with necrotic core plaques. Heart (British Cardiac Society). 2009;95(18):1525-30.
163. Lavi S, Yang EH, Prasad A, Mathew V, Barsness GW, Rihal CS, et al. The interaction between coronary endothelial dysfunction, local oxidative stress, and endogenous nitric oxide in humans. Hypertension. 2008;51(1):127-33.
164. Deanfield JE, Halcox JP, Rabelink TJ. Endothelial function and dysfunction: testing and clinical relevance. Circulation. 2007;115(10):1285-95.
165. Rizvi A, Hartaigh BÓ, Danad I, Han D, Lee JH, Gransar H, et al. Diffuse coronary artery disease among other atherosclerotic plaque characteristics by coronary computed tomography angiography for predicting coronary vessel-specific ischemia by fractional flow reserve. Atherosclerosis. 2017;258:145-51.
166. Tonino PAL, Fearon WF, De Bruyne B, Oldroyd KG, Leesar MA, Ver Lee PN, et al. Angiographic versus functional severity of coronary artery stenoses in the FAME study fractional flow reserve versus angiography in multivessel evaluation. Journal of the American College of Cardiology. 2010;55(25):2816-21.
167. Pijls NH, Van Gelder B, Van der Voort P, Peels K, Bracke FA, Bonnier HJ, et al. Fractional flow reserve. A useful index to evaluate the influence of an epicardial coronary stenosis on myocardial blood flow. Circulation. 1995;92(11):3183-93.
168. Hou ZH, Lu B, Gao Y, Jiang SL, Wang Y, Li W, et al. Prognostic value of coronary CT angiography and calcium score for major adverse cardiac events in outpatients. JACC Cardiovasc Imaging. 2012;5(10):990-9.
169. Arad Y, Spadaro LA, Goodman K, Newstein D, Guerci AD. Prediction of coronary events with electron beam computed tomography. JAC. 2000;36(4):1253-60.
170. Raggi P, Callister TQ, Shaw LJ. Progression of coronary artery calcium and risk of first myocardial infarction in patients receiving cholesterol-lowering therapy. Arterioscler Thromb Vasc Biol. 2004;24(7):1272-7.
171. Hoegerle S, Juengling F, Otte A, Altehoefer C, Moser EA, Nitzsche EU. Combined FDG and [F-18]fluoride whole-body PET: a feasible two-in-one approach to cancer imaging? Radiology. 1998;209(1):253-8.
172. Creager MD, Hohl T, Hutcheson JD, Moss AJ, Schlotter F, Blaser MC, et al. F-Fluoride Signal Amplification Identifies Microcalcifications Associated With Atherosclerotic Plaque Instability in Positron Emission Tomography/Computed Tomography Images. Circ Cardiovasc Imaging. 2019;12(1):e007835.
173. Moss A, Doris M, Andrews J, Bing R, Daghem M, van Beek E, et al. Molecular coronary plaque imaging using 18F-fluoride. . *Circ Cardiovasc Imaging* 2019; in press.
174. Menke J. Comparison of different body size parameters for individual dose adaptation in body CT of adults. Radiology. 2005;236(2):565-71.
175. Austen WG, Edwards JE, Frye RL, Gensini GG, Gott VL, Griffith LS, et al. A reporting system on patients evaluated for coronary artery disease. Report of the Ad

Hoc Committee for Grading of Coronary Artery Disease, Council on Cardiovascular Surgery, American Heart Association. Circulation. 1975;51(4 Suppl):5-40.
176. Motoyama S, Kondo T, Anno H, Sugiura A, Ito Y, Mori K, et al. Atherosclerotic plaque characterization by 0.5-mm-slice multislice computed tomographic imaging. Circ J. 2007;71(3):363-6.
177. Maurovich-Horvat P, Schlett CL, Alkadhi H, Nakano M, Otsuka F, Stolzmann P, et al. The napkin-ring sign indicates advanced atherosclerotic lesions in coronary CT angiography. JACC Cardiovasc Imaging. 2012;5(12):1243-52.
178. Hutcheson JD, Maldonado N, Aikawa E. Small entities with large impact: microcalcifications and atherosclerotic plaque vulnerability. Curr Opin Lipidol. 2014;25(5):327-32.
179. Richardson PD, Davies MJ, Born GV. Influence of plaque configuration and stress distribution on fissuring of coronary atherosclerotic plaques. Lancet. 1989;2(8669):941-4.
180. Johnson RC, Leopold JA, Loscalzo J. Vascular calcification: pathobiological mechanisms and clinical implications. Circ Res. 2006;99(10):1044-59.
181. Massera D, Trivieri MG, Andrews JPM, Sartori S, Abgral R, Chapman AR, et al. Disease Activity in Mitral Annular Calcification. Circ Cardiovasc Imaging. 2019;12(2):e008513.
182. Kwiecinski J, Tzolos E, Adamson PD, Cadet S, Moss AJ, Joshi N, et al. Coronary ¹⁸F-Sodium Fluoride Uptake Predicts Outcomes in Patients With Coronary Artery Disease. Journal of the American College of Cardiology. 2020;75(24):3061-74.
183. Lee JM, Bang J-I, Koo BK, Hwang D, Park J, Zhang J, et al. Clinical Relevance of 18F-Sodium Fluoride Positron-Emission Tomography in Noninvasive Identification of High-Risk Plaque in Patients With Coronary Artery Disease. Circulation: Cardiovascular Imaging. 2017;10(11):e006704.
184. Kitagawa T, Yamamoto H, Toshimitsu S, Sasaki K, Senoo A, Kubo Y, et al. Data on analysis of coronary atherosclerosis on computed tomography and 18F-sodium fluoride positron emission tomography. Data in brief. 2017;13:341-5.
185. Kitagawa T, Yamamoto H, Toshimitsu S, Sasaki K, Senoo A, Kubo Y, et al. 18F-sodium fluoride positron emission tomography for molecular imaging of coronary atherosclerosis based on computed tomography analysis. Atherosclerosis. 2017;263:385-92.
186. Vercauteren T, Pennec X, Perchant A, Ayache N. Symmetric log-domain diffeomorphic Registration: a demons-based approach. Medical image computing and computer-assisted intervention : MICCAI International Conference on Medical Image Computing and Computer-Assisted Intervention. 2008;11(Pt 1):754-61.
187. An ITK Implementation of the Symmetric Log-Domain Diffeomorphic Demons Algorithm. 2017:1-11.
188. Thie JA. Understanding the standardized uptake value, its methods, and implications for usage. Journal of nuclear medicine : official publication, Society of Nuclear Medicine. 2004;45(9):1431-4.
189. Boellaard R, Krak NC, Hoekstra OS, Lammertsma AA. Effects of noise, image resolution, and ROI definition on the accuracy of standard uptake values: a simulation study. Journal of nuclear medicine : official publication, Society of Nuclear Medicine. 2004;45(9):1519-27.

190. Tawakol A, Migrino RQ, Bashian GG. In vivo 18F-fluorodeoxyglucose positron emission tomography imaging provides a noninvasive measure of carotid plaque inflammation in patients. Journal of the …. 2006.
191. Rudd JHF, Myers KS, Bansilal S, Machac J, Rafique A, Farkouh M, et al. (18)Fluorodeoxyglucose positron emission tomography imaging of atherosclerotic plaque inflammation is highly reproducible: implications for atherosclerosis therapy trials. Journal of the American College of Cardiology. 2007;50(9):892-6.
192. Asabella AN, Ciccone MM, Cortese F, Pietro S, Gesualdo M, Zito A, et al. Higher reliability of 18F-FDG target background ratio compared to standardized uptake value in vulnerable carotid plaque detection: a pilot study. Annals of Nuclear Medicine. 2014;28(6):571-9.
193. Rudd JHF, Myers KS, Bansilal S, Machac J, Pinto CA, Tong C, et al. Atherosclerosis inflammation imaging with 18F-FDG PET: carotid, iliac, and femoral uptake reproducibility, quantification methods, and recommendations. Journal of nuclear medicine : official publication, Society of Nuclear Medicine. 2008;49(6):871-8.
194. Huet P, Burg S, Le Guludec D, Hyafil F, Buvat I. Variability and uncertainty of 18F-FDG PET imaging protocols for assessing inflammation in atherosclerosis: suggestions for improvement. Journal of nuclear medicine : official publication, Society of Nuclear Medicine. 2015;56(4):552-9.
195. Shechter G, Resar JR, McVeigh ER. Displacement and velocity of the coronary arteries: cardiac and respiratory motion. IEEE transactions on medical imaging. 2006;25(3):369-75.
196. Akamatsu G, Ishikawa K, Mitsumoto K, Taniguchi T, Ohya N, Baba S, et al. Improvement in PET/CT image quality with a combination of point-spread function and time-of-flight in relation to reconstruction parameters. Journal of nuclear medicine : official publication, Society of Nuclear Medicine. 2012;53(11):1716-22.
197. Schaefferkoetter J, Casey M, Townsend D, El Fakhri G. Clinical impact of time-of-flight and point response modeling in PET reconstructions: a lesion detection study. Physics in medicine and biology. 2013;58(5):1465-78.
198. Sacchi S, Dhutia NM, Shun-Shin MJ, Zolgharni M, Sutaria N, Francis DP, et al. Doppler assessment of aortic stenosis: a 25-operator study demonstrating why reading the peak velocity is superior to velocity time integral. European heart journal cardiovascular Imaging. 2018;56:565.
199. Clavel M-A, Pibarot P, Messika-Zeitoun D, Capoulade R, Malouf J, Aggarval S, et al. Impact of aortic valve calcification, as measured by MDCT, on survival in patients with aortic stenosis: results of an international registry study. Journal of the American College of Cardiology. 2014;64(12):1202-13.
200. Dweck MR, Khaw HJ, Sng GKZ, Luo ELC, Baird A, Williams MC, et al. Aortic stenosis, atherosclerosis, and skeletal bone: is there a common link with calcification and inflammation? European heart journal. 2013;34(21):1567-74.
201. Dweck MR, Joshi NV, Rudd JHF, Newby DE. Imaging of Inflammation and Calcification in Aortic Stenosis. Current Cardiology Reports. 2013;15(1):1-7.
202. Baumgartner H, Hung J, Bermejo J, Chambers JB, Evangelista A, Griffin BP, et al. Echocardiographic assessment of valve stenosis: EAE/ASE recommendations for clinical practice. European journal of echocardiography : the journal of the

Working Group on Echocardiography of the European Society of Cardiology2009. p. 1-25.
203. Bonow RO, Carabello BA, Chatterjee K, de Leon AC, Faxon DP, Freed MD, et al. 2008 focused update incorporated into the ACC/AHA 2006 guidelines for the management of patients with valvular heart disease: a report of the American College of Cardiology/American Heart Association Task Force on Practice Guidelines (Writing Committee to revise the 1998 guidelines for the management of patients with valvular heart disease). Endorsed by the Society of Cardiovascular Anesthesiologists, Society for Cardiovascular Angiography and Interventions, and Society of Thoracic Surgeons. J Am Coll Cardiol. 2008;52(13):e1-142.
204. Pawade T, Sheth T, Guzzetti E, Dweck MR, Clavel MA. Why and How to Measure Aortic Valve Calcification in Patients With Aortic Stenosis. JACC Cardiovasc Imaging. 2019;12(9):1835-48.
205. Martin B. An Introduction To Medical Statistics. Third ed: Oxford University Press; 2000.
206. Faul F, Erdfelder E, Buchner A, Lang AG. Statistical power analyses using G*Power 3.1: tests for correlation and regression analyses. Behav Res Methods. 2009;41(4):1149-60.
207. Utsunomiya H, Yamamoto H, Kitagawa T, Kunita E, Urabe Y, Tsushima H, et al. Incremental prognostic value of cardiac computed tomography angiography in asymptomatic aortic stenosis: significance of aortic valve calcium score. International journal of cardiology. 2013;168(6):5205-11.
208. Rusinaru D, Malaquin D, Maréchaux S, Debry N, Tribouilloy C. Relation of Dimensionless Index to Long-Term Outcome in Aortic Stenosis With Preserved LVEF. JACC: Cardiovascular Imaging. 2015;8(7):766-75.
209. Oh JK, Taliercio CP, Holmes DR, Reeder GS, Bailey KR, Seward JB, et al. Prediction of the severity of aortic stenosis by Doppler aortic valve area determination: prospective Doppler-catheterization correlation in 100 patients. J Am Coll Cardiol. 1988;11(6):1227-34.
210. Bahler RC, Desser DR, Finkelhor RS, Brener SJ, Youssefi M. Factors leading to progression of valvular aortic stenosis. Am J Cardiol. 1999;84(9):1044-8.
211. Chin CWL, Pawade TA, Newby DE, Dweck MR. Risk Stratification in Patients With Aortic Stenosis Using Novel Imaging Approaches. Circulation: Cardiovascular Imaging. 2015;8(8):e003421.
212. Dweck MR, Joshi S, Murigu T, Alpendurada F, Jabbour A, Melina G, et al. Midwall fibrosis is an independent predictor of mortality in patients with aortic stenosis. Journal of the American College of Cardiology. 2011;58(12):1271-9.
213. Vassiliou VS, Perperoglou A, Raphael CE, Joshi S, Malley T, Everett R, et al. Midwall Fibrosis and 5-Year Outcome in Moderate and Severe Aortic Stenosis. Journal of the American College of Cardiology. 2017;69(13):1755-6.
214. Xie Y, Kim Y-J, Pang J, Kim J-S, Yang Q, Wei J, et al. Coronary Atherosclerosis T1-Weighed Characterization With Integrated Anatomical Reference: Comparison With High-Risk Plaque Features Detected by Invasive Coronary Imaging. JACC: Cardiovascular Imaging. 2016.
215. Le Meunier L, Slomka PJ, Dey D, Ramesh A, Thomson LEJ, Hayes SW, et al. Enhanced definition PET for cardiac imaging. Journal of Nuclear Cardiology. 2010;17(3):414-26.

216. Gigengack F, Ruthotto L, Burger M, Wolters CH, Jiang X, Schäfers KP. Motion correction in dual gated cardiac PET using mass-preserving image registration. IEEE transactions on medical imaging. 2012;31(3):698-712.
217. Chin CWL, Everett RJ, Kwiecinski J, Vesey AT, Yeung E, Esson G, et al. Myocardial Fibrosis and Cardiac Decompensation in Aortic Stenosis. JACC: Cardiovascular Imaging. 2016.
218. Everett RJ, Stirrat CG, Semple SIR, Newby DE, Dweck MR, Mirsadraee S. Assessment of myocardial fibrosis with T1 mapping MRI. Clinical radiology. 2016;71(8):768-78.
219. Stone GW, Maehara A, Lansky AJ, De Bruyne B, Cristea E, Mintz GS, et al. A Prospective Natural-History Study of Coronary Atherosclerosis. New England Journal of Medicine. 2011;364(3):226-35.
220. Kwiecinski J, Tzolos E, Adamson PD, Cadet S, Moss AJ, Joshi N, et al. Coronary ¹⁸F-Sodium Fluoride Uptake Predicts Outcomes in Patients With Coronary Artery Disease. Journal of the American College of Cardiology. 2020;75(24):3061.
221. Forsythe RO, Dweck MR, McBride OMB, Vesey AT, Semple SI, Shah ASV, et al. 18F-Sodium Fluoride Uptake in Abdominal Aortic Aneurysms: The SoFIA3 Study. Journal of the American College of Cardiology. 2018;71(5):513-23.
222. Rominger A, Saam T, Vogl E, Ubleis C, la Fougère C, Förster S, et al. In vivo imaging of macrophage activity in the coronary arteries using 68Ga-DOTATATE PET/CT: correlation with coronary calcium burden and risk factors. Journal of nuclear medicine : official publication, Society of Nuclear Medicine. 2010;51(2):193-7.
223. Mojtahedi A, Alavi A, Thamake S, Amerinia R, Ranganathan D, Tworowska I, et al. Assessment of vulnerable atherosclerotic and fibrotic plaques in coronary arteries using (68)Ga-DOTATATE PET/CT. Am J Nucl Med Mol Imaging. 2015;5(1):65-71.
224. Tarkin JM, Joshi FR, Evans NR, Chowdhury MM, Figg NL, Shah AV, et al. Detection of Atherosclerotic Inflammation by. J Am Coll Cardiol. 2017;69(14):1774-91.
225. Kato K, Schober O, Ikeda M, Schäfers M, Ishigaki T, Kies P, et al. Evaluation and comparison of 11C-choline uptake and calcification in aortic and common carotid arterial walls with combined PET/CT. Eur J Nucl Med Mol Imaging. 2009;36(10):1622-8.
226. Bucerius J, Schmaljohann J, Böhm I, Palmedo H, Guhlke S, Tiemann K, et al. Feasibility of 18F-fluoromethylcholine PET/CT for imaging of vessel wall alterations in humans--first results. Eur J Nucl Med Mol Imaging. 2008;35(4):815-20.
227. Gaemperli O, Shalhoub J, Owen DRJ, Lamare F, Johansson S, Fouladi N, et al. Imaging intraplaque inflammation in carotid atherosclerosis with 11C-PK11195 positron emission tomography/computed tomography. European heart journal. 2012;33(15):1902-10.
228. Chae SY, Kwon TW, Jin S, Kwon SU, Sung C, Oh SJ, et al. A phase 1, first-in-human study of. EJNMMI Res. 2019;9(1):3.
229. Joshi FR, Manavaki R, Fryer TD, Figg NL, Sluimer JC, Aigbirhio FI, et al. Vascular Imaging With. J Am Coll Cardiol. 2017;69(14):1873-4.
230. Mateo J, Izquierdo-Garcia D, Badimon JJ, Fayad ZA, Fuster V. Noninvasive assessment of hypoxia in rabbit advanced atherosclerosis using ^{18}F-

fluoromisonidazole positron emission tomographic imaging. Circ Cardiovasc Imaging. 2014;7(2):312-20.
231. Tarkin JM, Mason JC, Fayad ZA. Imaging at the inter-face of inflammation and angiogenesis by. Heart. 2019;105(24):1845-7.
232. Golestani R, Mirfeizi L, Zeebregts CJ, Westra J, de Haas HJ, Glaudemans AW, et al. Feasibility of [18F]-RGD for ex vivo imaging of atherosclerosis in detection of αvβ3 integrin expression. J Nucl Cardiol. 2015;22(6):1179-86.
233. Wang X, Feng H, Zhao S, Xu J, Wu X, Cui J, et al. SPECT and PET radiopharmaceuticals for molecular imaging of apoptosis: from bench to clinic. Oncotarget. 2017;8(12):20476-95.
234. Kietselaer BL, Reutelingsperger CP, Heidendal GA, Daemen MJ, Mess WH, Hofstra L, et al. Noninvasive detection of plaque instability with use of radiolabeled annexin A5 in patients with carotid-artery atherosclerosis. N Engl J Med. 2004;350(14):1472-3.
235. Kim C, Lee JS, Han Y, Chae SY, Jin S, Sung C, et al. Glycoprotein IIb/IIIa receptor imaging with. J Nucl Med. 2018.
236. Munoz C, Neji R, Cruz G, Mallia A, Jeljeli S, Reader AJ, et al. Motion-corrected simultaneous cardiac positron emission tomography and coronary MR angiography with high acquisition efficiency. Magn Reson Med. 2018;79(1):339-50.
237. Munoz C, Neji R, Kunze KP, Nekolla SG, Botnar RM, Prieto C. Respiratory- and cardiac motion-corrected simultaneous whole-heart PET and dual phase coronary MR angiography. Magn Reson Med. 2019;81(3):1671-84.
238. Everett RJ, Tastet L, Clavel M-A, Chin CWL, Capoulade R, Vassiliou VS, et al. Progression of Hypertrophy and Myocardial Fibrosis in Aortic Stenosis: A Multicenter Cardiac Magnetic Resonance Study. Circulation: Cardiovascular Imaging. 2018;11(6):e007451.

APPENDIX

PUBLICATIONS ARISING FROM THIS THESIS

Doris MK, Otaki Y, Arnson Y, Tamarappoo B, Goeller M, Gransar H, Wang F, Hayes S, Friedman J, Thomson L, Slomka P, Dey D, Berman D. Non-invasive fractional flow reserve in vessels without severe obstructive stenosis is associated with coronary plaque burden. J Cardiovasc Comput Tomogr. 2018 Sep - Oct;12(5):379-384.

Doris MK, Meah MN, Moss AJ, Andrews JPM, Bing R, Gillen R, Weir N, Syed M, Daghem M, Shah A, Williams MC, Beek EJR, Forsyth L, Dweck MR, Newby DE, Adamson PD. Coronary 18F-Fluoride Uptake and Progression of Coronary Artery Calcification. Circ Cardiovasc Imaging, 2020 (in press)

Doris MK, Otaki Y, Krishnan SK, Kwiecinski J, Rubeaux M, Alessio A, Pan T, Cadet S, Dey D, Dweck MR, Newby DE, Berman DS, Slomka PJ. Optimization of reconstruction and quantification of motion-corrected coronary PET-CT. J Nucl Cardiol. 2018 Jun 11. doi: 10.1007/s12350-018-1317-5. [Epub ahead of print].

Doris MK, Jenkins W, Robson P, Pawade T, Andrews JP, Bing R, Cartlidge T, Shah A, Pickering A, Williams MC, Fayad ZA, White A, van Beek EJ, Newby DE, Dweck MR. Computed tomography aortic valve calcium scoring for the assessment of aortic stenosis progression. Heart. 2020 Dec;106(24):1906-1913.

Doris MK, Rubeaux M, Pawade T, Otaki Y, Xie Y, Li D, Tamarappoo BK, Newby D, Berman DS, Dweck MR, Slomka PJ, Dey D. Motion-corrected imaging of the aortic valve with 18F-NaF PET/CT and PET/MR: a feasibility study. *Journal of Nuclear Medicine*, 2017; doi: 10.2967/jnumed.117.194597. [Epub ahead of print].

Doris MK, Everett RJ, Shun-Shin M, Clavel MA, Dweck MR. The Role of Imaging in Measuring Disease Progression and Assessing Novel Therapies in Aortic Stenosis. JACC Cardiovasc Imaging. 2019 Jan;12(1):185-197.

Doris MK, Newby DE. Identification of Early Vascular Calcification with 18F-Sodium Fluoride: Potential Clinical Application. *Expert Review of Cardiovascular Therapy*. 2016;14(6):691-701.

Doris M, Newby DE. How should CT coronary angiography be integrated into the management of patients with chest pain and how does this affect outcomes? *European Heart Journal – Quality of Care and Clinical Outcomes*. 2015 DOI: http://dx.doi.org/10.1093/ehjqcco/qcv027.

Doris M, Newby DE. Coronary CT angiograph as a Diagnostic and Prognostic Tool: Perspectives from the SCOTHEART trial. *Current Cardiology Reports*. 2016:18(2):18.

Doris MK, Dweck MR, Fayad ZA. The future of imaging in cardiovascular disease intervention trials:2017 and beyond. *Current Opinion in Lipidology*. 2016;27(6):605-614.

Dweck MR, **Doris MK**, Motwani M, Adamson PD, Slomka P, Dey D, Fayad ZA, Newby DE, Berman D. Imaging of coronary atherosclerosis- evolution towards new treatment strategies. *Nature Reviews Cardiology*. 2016;13(9):533-48.

Rubeaux M, **Doris MK**, Alessio A, Slomka PJ. Enhancing cardiac PET by motion correction techniques. *Current Cardiology Reports*. 2017;19(2)14

Moss AJ, **Doris MK**, Andrews JPM, Bing R, Daghem M, van Beek EJR, Forsyth L, Shah ASV, Williams MC, Sellers S, Leipsic J, Dweck MR, Parker RA, Newby DE, Adamson PD. Molecular coronary plaque imaging using 18F-fluoride. Circ Cardiovasc Imaging 2019;12(8):e008574

Williams MC, Kwiecinski J, **Doris M**, McElhinney P, D'Souza MS, Cadet S, Adamson PD, Moss AJ, Alam S, Hunter A, Shah ASV, Mills NL, Pawade T, Wang C, Weir McCall J, Bonnici-Mallia M, Murrills C, Roditi G, van Beek EJR, Shaw LJ, Nicol ED, Berman DS, Slomka PJ, Newby DE, Dweck MR, Dey D. Low-Attenuation noncalcified plaque on coronary computed tomography angiography predicts myocardial infarction; Results from the multicentre SCOT-HEART Trial (Scottish Computed Tomography of the HEART). Circulation 2020;141(18):1452-1462.

Andrews JPM, MacNaught G, Moss AJ, **Doris MK**, Pawade T, Adamson PD, van Beek EJR, Lucatelli C, Lassen ML, Robson PM, Fayad ZA, Kwiecinski J, Slomka PJ, Berman DS, Newby DE, Dweck MR. Cardiovascular 18F-Fluoride positron emission tomography-magnetic resonance imaging: A comparison study. J Nucl Cardiol 2019;2. Doi: 10.1007/s12350-019-01962-y.

Moss AJ, Dweck MR, **Doris MK**, Andrews JPM, Bing R, Forsythe RO, Cartlidge TR, Pawade TA, Daghem M, Raftis JB, Williams MC, van Beek EJR, Forsyth L, Lewis SC, Lee RJ, Shah ASV, Mills NL, Newby DE, Adamson PD. Ticagrelor to reduce myocardial injury in patients with high-risk coronary artery plaque. JACC Cardiovasc Imaging. 2019; S1936-878X(19)30557-1.

Massera D, Trivieri MG, Andrews JPM, Sartori S, Abgral R, Chapman AR, Jenkins WSA, Vesey AT, **Doris MK**, Pawade TA, Zheng KH, Kizer JR, Newby DE, Dweck MR. Disease Activity in Mitral Annular Calcification. Circ Cardiovasc Imaging. 2019 Feb;12(2):e008513.

Kwiecinski J, Adamson PD, Lassen ML, **Doris MK**, Moss AJ, Cadet S, Jansen MA, Dey D, Lee SE, Yun M, Chang HJ, Dweck MR, Newby DE, Berman DS, Slomka PJ. Feasibility of coronary ^{18}F-sodium fluoride Positron-Emission Tomography assessment with the utilization of previously acquired Computed Tomography Angiography. Circ Cardiovasc Imaging. 2018 Dec;11(12):e008325.

Cartlidge TRG, **Doris MK**, Sellers SL, Pawade TA, White AC, Pessotto R, Kwiecinski J, Fletcher A, Alcaide C, Lucatelli C, Densem C, Rudd JHF, van Beek EJR, Tavares A, Virmani R, Berman D, Leipsic JA, Newby DE, Dweck MR. Detection and Prediction of Bioprosthetic Aortic Valve Degeneration. J Am Coll Cardiol. 2019 Mar 19;73(10):1107-1119.

Massera D, **Doris MK**, Cadet S, Kwiecinski J, Pawade TA, Peeters FECM, Dey D, Newby DE, Dweck MR, Slomka PJ. Analytical quantification of aortic valve 18F-sodium fluoride PET uptake. J Nucl Cardiol. 2018 Nov 29. doi: 10.1007/s12350-018-01542-6. [Epub ahead of print]

Tamarappoo B, Otaki Y, **Doris M**, Arnson Y, Gransar H, Hayes S, Friedman J, Thomson L, Wang F, Rozanski A, Slomka P, Dey D, Berman D. Improvement in LDL is associated with decrease in non-calcified plaque volume on coronary CTA as measured by automated quantitative software. J Cardiovasc Comput Tomogr. 2018 Sep - Oct;12(5):385-390.

Krishnan S, Otaki Y, **Doris M**, Slipczuk L, Arnson Y, Rubeaux M, Dey D, Slomka P, Berman DS, Tamarappoo B. Molecular imaging of vulnerable coronary plaque: a pathophysiologic perspective. *Journal of Nuclear Medicine.* 2017;58(3):359-364